In Situ UV-vis Spectroelectrochemical Study of Reduction of Organic Molecules on Transparent Carbon Electrodes

A Thesis

Presented in Partial Fulfillment of the Requirements for

the Degree Master of Science

in the Graduate School of The Ohio State University

By

Hong Tian

*****

The Ohio State University
2005

Master's Examination Committee:

Professor Richard L. McCreery, Advisor

Professor Heather C. Allen

Approved by

R A Mc Creery

Advisor
Department of Chemistry

ABSTRACT

Transparent PPF (pyrolyzed photoresist films) were fabricated by pyrolysis of diluted photoresist solution on quartz. The optical transmission of transparent PPF varies with the concentration of photoresist. The transparent PPF prepared by 5% (volume concentration) photoresist solution is optically transparent with the transmission of 0.5-0.8 in the 200-800 nm regions. The AFM image and Raman spectra indicate that the transparent PPF has a uniform and nearly atomically flat surface with a carbon sp^2 structure.

Diazonium salts of 4-nitroazobenzene (NAB), azobenzene (AB) and 4-nitrobiphenyl (NBP) are capable of forming monolayer or multilayer on transparent PPF electrodes by electrochemical reduction, which is confirmed by AFM "scratching". Covalent carbon-carbon bonds are formed between the organic molecules and the PPF surfaces.

The first example of UV-vis absorption of chemisorbed organic molecules on an optically transparent carbon has been demonstrated. The covalent carbon-carbon bond between organic molecules and PPF electrode has been confirmed by UV-vis spectroscopy. The red shift of chemisorbed organic molecules relative to the solution and solid state is considered as the indication of the extension of the conjugated system.

In situ UV-vis spectroelectrochemical experiments successfully monitored the structure changes of both free molecules in solution and covalently bonded organic molecules on PPF electrodes under applied electrochemical potentials. The reduction of free NAB, AB and NBP in solutions generates their corresponding radical anions. The UV-vis absorption spectra of reduced free NAB, AB and NBP are in agreement with the electronic transitions of their corresponding radical anions calculated by Gaussian, Density Functional Theory. The electronic transitions of reduced chemisorbed NAB, AB and NBP have longer wavelengths than those of their native unreduced forms. A possible mechanism of electron transfer from the electrode surface to chemisorbed molecules is proposed.

Dedicated to my parents

ACKNOWLEDGMENTS

First of all, I would like to express my gratitude to my adviser, Dr. Richard L. McCreery, for his guidance, encouragement and patience. This thesis would not have been possible without his assistance and direction. I would like to thank Dr. Marc D. Porter (Iowa State University), he provided the procedure of preparation of transparent PPF. I would also like to thank my lab mate Jing Wu, she did all the AFM experiments.

I am indebted to all McCreery group members for their kind help, useful discussions, and friendship. I would like to extend my appreciation to all my friends, for continual willingness to lend a hand. My years at Ohio State were enjoyable by their company.

Finally, I am most thankful to my parents and sister for their unwavering love and support.

VITA

1978, May, 16. . . . . Born – Xinxiang, China

1998, July. . . . . .B.S., Zhengzhou University

2001, July. . . . . .M.S., Lanzhou Institute of Chemical Physics, Chinese Academy of Science

2002 – present . . . . . .Graduate Teaching and Research Associate, The Ohio State University.

FIELDS OF STUDY

Major Field: Chemistry

TABLE OF CONTENTS

LIST OF TABLES

LIST OF FIGURES

LIST OF ABBREVIATIONS

AB	azobenzene
AC	activated carbon
AFM	atomic force microscopy
CPZ	Chlorpromazine
ET	electron transfer
HOMO	highest occupied molecular orbital
HOPG	highly ordered pyrolysis graphite
HT	heat treated
IPA	isopropyl alcohol
LUMO	lowest unoccupied molecular orbital
MB	methylene blue
MO	molecular orbital
NAB	4-nitroazobenzene
NBP	4-nitrobiphenyl
NP	nitrophenyl
PPF	pyrolyzed photoresist films
rms	root-mean-square

SEM	scanning electron microscopy
TBATFB	*n*-tetrabutylammonium tetrafluoroborate
UV	ultraviolet
XPS	X-ray photoelectron spectroscopy

CHAPTER 1

INTRODUCTION

Combining an electrochemical method with a spectroscopic technique, spectroelectrochemistry provides a method for probing unique reaction intermediates and products generated at electrode surfaces during redox reactions. In many cases, electrochemical intermediates and products are synthetically inaccessible. Providing spectroscopic information concurrently with redox reactions, spectroelectrochemical methods open a window for exploring the kinetics and mechanism of electrochemical reactions.

The objective of this thesis is to develop an optically transparent carbon film on quartz which can be used as an electrode to investigate the electrochemical intermediates and products on the carbon surfaces by UV-vis absorption spectroscopy. The motivation of this project derives from several fields. First, carbon materials have been used extensively in electroanalysis, electrosynthesis and energy conversion[1-5]. Second, covalently modified carbon surfaces can be used as catalysis surfaces for certain electrochemical reactions[6,7] and sensing surfaces[8,9]. Third, covalently modified carbon surfaces have been employed to investigate the surface structure effect on electron

transfer mechanisms[10,11]. Fourth, molecular electronics incorporate molecules into electronic circuits, the electronic properties of molecules bonded to surfaces play an important role in molecular electronics devices. UV-vis is a probe of electronic structures (e.g. HOMO-LUMO gap) and that is crucial to electron transfer through molecules. A correlation between molecular structure and applied potential provides strong evidence that molecular layer rearrange in response to an applied bias[12]. In addition, the conduction mechanism is revealed to some extent.

The purpose of this introductory chapter is to provide sufficient background information on the subjects of pyrolyzed photoresist films (PPF) and in situ UV-vis spectroelectrochemistry in the context of the investigation presented in this thesis. Chapter 1 commences with the background information on pyrolyzed photoresist films (PPF), which includes its preparation, structure, surface roughness and atomic composition. After that, it describes the electrochemical characteristics of PPF material. The sheet resistance and electron transfer kinetics in different redox systems of PPF electrodes are presented. Surface modification of PPF by diazonium ion reduction, the resulted monolayer or multilayer thickness and the conductance switching property of the modified carbon surfaces are described. The chapter continues with a brief introduction on the transmission mode of UV/vis. Then, a brief review of in situ UV-vis spectroelectrochemistry and its applications are presented. Finally, an outline of the research objectives of this dissertation is provided.

1.1 Surface properties of pyrolyzed photoresist films (PPF)

Carbon materials have been widely used in electroanalytical chemistry, electrosynthesis and energy conversion due to their wide potential window, mechanical stability and low cost[1-5]. Photoresists are commonly used in the integrated circuit industry and exhibit reproducible behavior. Used as a starting material for making carbon films, photoresists can be patterned by photolithography to desired shapes and sizes prior to pyrolysis.

Pyrolyzed photoresist films are prepared by spin-coating a positive photoresist (AZ P4330) on a clean and polished substrate, such as quartz, silicon , or silicon nitride, followed by pyrolysis in a reducing atmosphere (95% N_2 + 5% H_2) at 1000 °C. Conducting carbon films formed from the pyrolysis of photoresist have some special surface properties compared to other carbon electrodes. Several techniques, including microscopy, Raman spectroscopy and X-ray photoelectron spectroscopy (XPS) have been used to characterize the surface properties of PPF[13].

Scanning electron microscopy (SEM) images of PPF show no visible porosity or defects at the PPF surface. Tapping mode atomic force microscopy (AFM) images indicate that PPF has a nearly atomically smooth surface. The root-mean-square (rms) roughness is less than 0.5 nm, and the peak-to-valley distance is 1.5 nm. It is likely that the uniformity of the spin-coated photoresist influences the smoothness of the PPF surface[13].

The pyrolysis of photoresist results in a carbon film which is analogous to a smooth glassy carbon. The characteristic carbon bands at ~1360 cm^{-1} (disorder

band, D) and ~1600 cm^{-1} (graphitic band, E_{2g}) were observed by Raman spectroscopy [13-15]. The peak area ratio of D/E_{2g} was correlated with the degree of disorder of carbon substance. Higher D/E_{2g} intensity ratio is attributed to smaller graphite crystallite size, which indicates greater disorder. Higher temperature treatment resulted in smaller D/E_{2g} ratio, thus less disordered carbon film. The constant D/E_{2g} intensity ratios along a 900 μm line of PPF imply a smooth and uniform surface[13].

Surface oxygen is an important factor which influences the adsorption properties and electrochemical reactivity of carbon films. X-ray photoelectron spectroscopy (XPS) was used to measure the surface oxygen/carbon (O/C) atomic ratio of PPF. The surface oxygen/carbon (O/C) atomic ratio of heat-treated glassy carbon and 2-propanol polished glassy carbon are 1.6% and 6.7% respectively. In comparison, the surface oxygen/carbon (O/C) atomic ratio of a fresh PPF surface is 2.3%. The hydrogen in the pyrolysis atmosphere may react with the oxygen and terminate the carbon surface with hydrogen, which results in low O/C ratio. The PPF surface is relatively stable toward air oxidation. In comparison to heat-treated glassy carbon, the low O/C ratio of PPF extends for a longer period of time[16].

1.2 Electrochemical characteristics of pyrolyzed photoresist films (PPF)

The sheet resistivity of PPF varies with the heat-treatment temperature, ranging from a semiconductor to a conductor from 600 to 1100 °C. The sheet resistance of PPF heat-treated at 1100 °C is 51.2 Ω/square, i.e. 5.1×10^{-3} Ω-cm

for 1.0 μm thick carbon film, which is comparable to that of a heat-treated glassy carbon ((4.0-4.5) × 10^{-3} Ω-cm)[13].

The capacitances of PPF and glassy carbon are calculated from the voltammetric background current in 1 M KCl. Compared to glassy carbon under the same treatment, PPF has lower capacitance. Under the heat-treatment at 1000 °C in forming gas, the capacitances of PPF and glassy carbon are 8 μF/cm^2 and 35 μF/cm^2 respectively. The low capacitance of PPF is due to the smoothness and the low O/C ratio of the surface[13,16].

Methylene blue (MB) has strong physisorption to carbon surfaces, and the cyclic voltammetry of carbon electrodes in methylene blue (MB) solution has been used to measure the surface coverage of adsorbed MB. MB shows a two-electron, surface-confined redox couple in aqueous electrolyte[10]. The adsorption has the same trend as the capacitance: the AC/IPA-treated (AC/IPA is a suspension of activated carbon in 2-propanol) glassy carbon and oxidized PPF has the highest adsorption of MB, and the AC/IPA-treated PPF has the lowest[16].

Electron-transfer (ET) kinetics of PPF surface and heat-treated glassy carbon (HT GC) has been studied for various redox systems. For outer-sphere systems, such as $Ru(NH_3)_6^{3+/2+}$, $Fe(CN)_6^{3-/4-}$ and Chlorpromazine (CPZ), the differences of rate constant between PPF and HT GC are less than a factor of 3. For redox system $Fe^{3+/2+}$, electron transfer is catalyzed by surface carbonyl groups[17,18], and the rate constant of PPF is much slower than that of HT GC by a factor of 32. For inner-sphere systems, such as Dopamine oxidation and O_2 reduction, reactant adsorption on the electrode surface is a prerequisite, the

kinetics of such systems on PPF are slower than those on HT GC, the lower capacitance and slower kinetics of PPF compared to GC are consistent with the weaker MB adsorption[19-23].

Chemical modification of carbon surfaces, which include glassy carbon (GC), highly ordered pyrolytic graphite (HOPG), and pyrolyzed photoresist films (PPF), can be achieved by electrochemical reduction of aromatic diazonium salts[24-26]. Reduction of the diazonium salts can be carried out by cyclic voltammetry or controlled potential electrolysis in a medium of acetonitrile or aqueous acid (H_2SO_4 or HCl, PH < 2)[27,28]. The mechanism of this process is as follows:

$$R\text{-}C_6H_4N_2^+ + e^- \rightarrow N_2 + R\text{-}C_6H_4^{\bullet} \quad (1)$$

$$\text{carbon surface} + R\text{-}C_6H_4^{\bullet} \rightarrow \text{carbon surface}\text{-}C_6H_4\text{-}R \quad (2)$$

Where R is a para substituent[29]. Electrochemical reduction of a diazonium ion salt produces free N_2 and a phenyl radical, which irreversibly binds to carbon surfaces by a carbon-carbon bond. These chemisorbed reactions have been confirmed by voltammetry[19,21], XPS[25,29] and Raman spectroscopy[16,25,29].

The medium of the electrochemical system may influence the surface coverage and thickness of the resulting film. Downard, et al. demonstrated that the 4-nitrophenyl (NP) and 4-(4-nitrophenylazo) benzene (NAB) diazonium ions formed thinner films with lower surface coverage in aqueous acid than in acetonitrile, when the other conditions are the same. Therefore, the author inferred that electron transfer from a monolayer film to diazonium ion in aqueous

solution is inherently blocked, thus impeding multilayer film growth[30]. Multilayers may be formed during the electrochemical reduction process if large over-potentials or more concentrated reagents are used. Diazonium radicals may react with the organic groups already on the surface and coupled products may form. Several researchers have found evidence for such multilayer formation[26,31,32].

Conductance switching behavior of several organic molecules on carbon surfaces have been reported recently[33-36]. The switching behaviors of nitroazobenzene, biphenyl and nitrobiphenyl molecular junctions have been observed, which can persist for many repetitions[33,34]. The conductance switching behavior of organic molecules has also been examined in an electrochemical context, in which covalently modified carbon electrodes are immersed in electrolyte solution. Cyclic voltammetry[35] and Raman spectroscopy[36] have been applied to investigate the mechanism of the conductance switching behavior of organic molecules. Electron injection into the organic molecules causes a structural rearrangement, and the resulting products can be considered as a "methide", which has a smaller HOMO-LUMO gap (Figure 1.1[36]).

1.3 Transmission UV-vis spectroscopy

Molecules which absorb photons of wavelength in the range of 190 nm to 1000 nm undergo promotion of electrons from a ground electronic state to an excited electronic state, thus exhibiting UV/VIS absorption. Absorption of ultraviolet and visible radiation in organic molecules involves the transition of

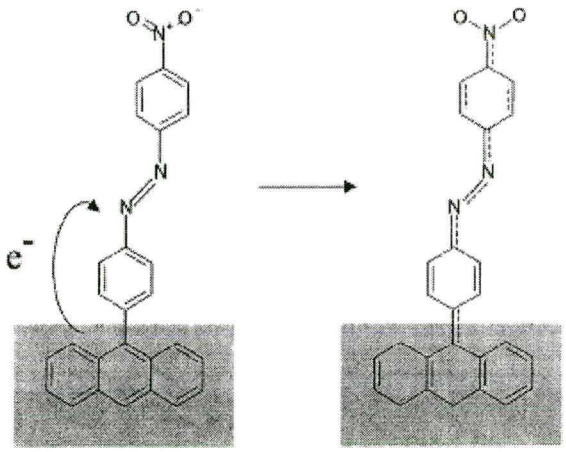

Figure 1.1 Electron transfer from GC to NAB accompanying with a structural change from NAB to NAB 4'-methide[36]. The HOMO-LUMO gaps of NAB and NAB 4'-methide are 3.549 eV and 2.109 eV respectively.

electrons between different orbitals (Figure 1.2). For organic molecules, orbitals are classified as lone pair n-orbitals, σ-orbitals and π-orbitals, and the corresponding excited states are denoted by an asterisk. The energy required for σ-σ^* transition is large (< 200 nm), and is not normally observable in typical UV/VIS spectra (200-800 nm). n-σ^* transitions required less energy than σ-σ^* transitions, and can be promoted by light with wavelength in the range of 150-250 nm. Saturated organic molecules with lone pair (non-bonding) electrons are capable of such transitions. Absorption spectra caused by n-π^* or π-π^* transitions in unsaturated organic molecules fall in the UV/VIS region of the spectrum (200-800 nm). n-π^* transitions are initiated from the plane of the molecule to the plane which is perpendicular to the molecular plane, such transitions are "symmetry forbidden" or "overlap forbidden" , which result in low molar absorptivities, range

form 10 to 100 L mol^{-1} cm^{-1}. π-π^* transitions are allowed transitions, which have more intense molar absorptivities between 1000 and 10,000 L mol^{-1} cm^{-1}.

Absorptions of UV-vis light result in electronic transitions within molecules with chromophore. The electronic transition involves promotion of electrons from an electronic ground state to an excited state. Generally, energetically favored electronic transition is from the highest occupied molecular orbital (HOMO) to the lowest unoccupied molecular orbital (LUMO), originating from valence electrons in a chromophore, such as the nonbonding (*n*) or π electrons in unsaturated groups. UV-vis spectroscopy measures the probability and energy of electron promotion from ground state to excited state. A more highly conjugated system corresponds to a smaller HOMO-LUMO gap, and therefore a longer wavelength transition.

The wavelength of the maximum absorption and the intensity of the absorption depend on molecular structure. π-π^* transitions of isolated groups in a molecule generate low intensity absorptions. If unsaturated groups are conjugated in a molecule, the maximum absorption shifts to a longer wavelength and the absorption intensity often increases.

Molecular structure has an important influence on the degree of conjugation. Trans and cis isomers are different in their spectra. For example, the all-trans linear polyene isomers have the longer conjugated systems compared to the all-cis or mixed isomers, which results in a longer wavelength of the maximum absorption and higher molar absorptivity. Steric hindrance also affects the degree of conjugation. Molecular orbitals conjugate best when molecule is in

a planar configuration. For example, compared to biphenyl itself, the spectra of biphenyls with m- and p- methyl groups change only slightly. However, the methyl groups in the o-positions prevent the substituted biphenyl from being planar, resulting in large effects on the spectra (Figure 1.3)[37].

Transmission spectroscopy is based on the decrease of the intensity of a light which interacts with the measured compounds. When light interacts with a material, absorption, reflectance and scattering may happen at the same time (Figure 1.4). According to the conservation of energy, absorption $\alpha = I_{abs}/I_0$, transmittance $\tau = I_{tr}/I_0$, reflectance $\rho = I_{refl}/I_0$ and scattering $\sigma = I_{scat}/I_0$ amount to unity: $\alpha + \tau + \rho + \sigma = 1$. If the intensities of reflected and scattered light are negligible compared to the intensity of the absorbed light, the absorptance is $\alpha = 1 - \tau$. The experimentally convenient measurement is the absorbance, $A = -\log T$[38].

Traditionally, UV-vis spectroscopy has been employed to determine organic and inorganic compounds in solution and solid states. Recently, it has been used to characterize thin films, monitor photoswitching, investigate molecular interaction and measure molecular orientation. It was employed to characterize the formation self assembled monolayers[40], polymers[41] and ion-coordination films[42]. Using ultrathin gold films on mica or quartz as substrates, transmission UV-vis spectroscopy provides information on the adsorption and binding of self-assembled monolayers[40,43]. Photoswitching of azobenzene based self-assembled monolayers was monitored by the transmission mode[44,45]. The positions of UV-vis absorption peaks reflect the intermolecular interactions, were

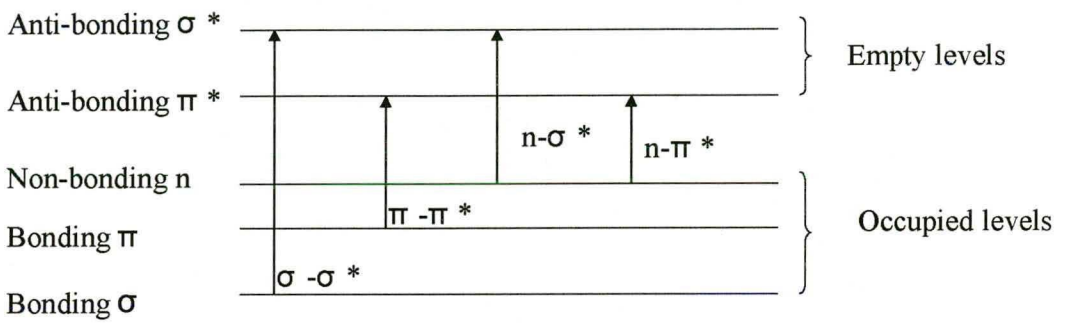

Figure 1.2 Types of electronic transitions.

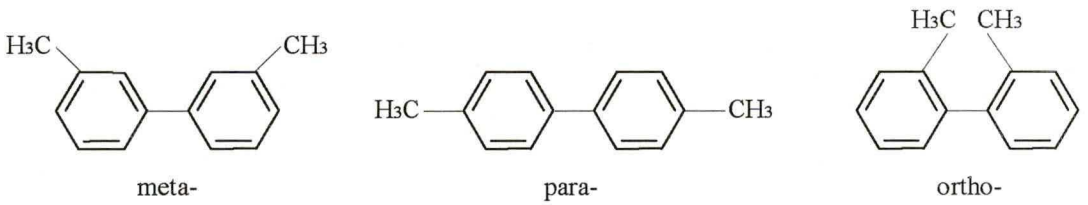

Figure 1.3 Structures of meta-, para-, and ortho- substituted biphenyl[37].

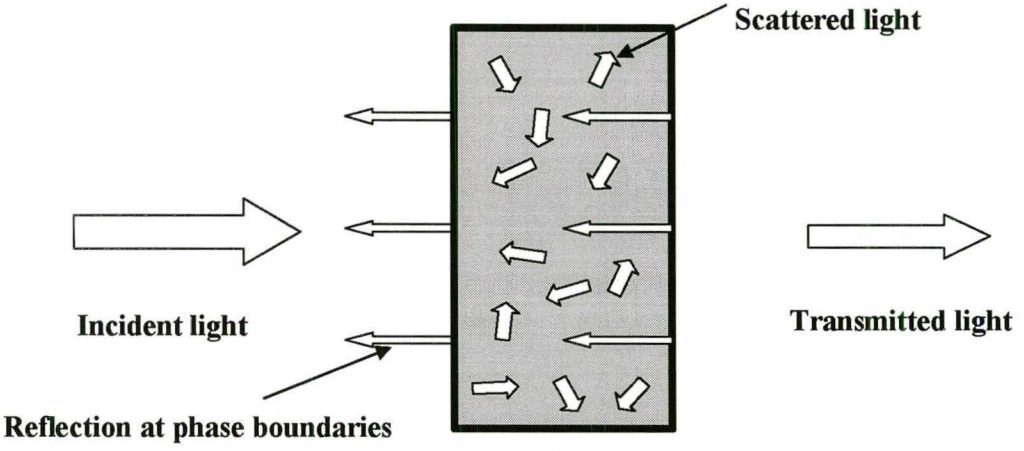

Figure 1.4 Interaction of light with sample[39].

investigated to provide information on packing order and interactions between molecules[46-49]. Both reflection and transmission UV-vis spectroscopy were applied to study the molecular orientation on surfaces[50,51].

1.4 UV/vis spectroelectrochemistry

Spectroelectrochemical methods couple an electrochemical experiment with a spectroscopic technique, obtaining spectroscopic information about electrochemical reactions simultaneously under the same experimental conditions. Compared to the usual electrochemical methods, spectroelectrochemistry is capable of probing the detailed structural information of the intermediate species which were generated in situ during redox reactions at the electrode. These intermediate species could exist both in the solution close to the electrode surface and directly at the surface of the electrode[51].

Successful spectroelectrochemical experiments in transmission mode depend on: (a) optically transparent electrodes (OTE) in the spectrum range being studied; (b) good electrochemical cell design (uniform potential distribution over the whole working electrode surface being studied, low iR_U drop, high counter electrode area); (c) a stable potentiostat system which can supply required output current and voltage without signal distortion[51].

UV/vis spectroelectrochemistry combines UV/vis spectroscopy with electrochemical experiments, which can be achieved in transmission mode with an optically transparent electrode (OTE) used as the working electrode. The optically transparent electrode could be: (a) a transparent substrate covered with

a thin metal film less than 100 nm; (b) a glass plate coated with a thin film of conductive and optically transparent indium-doped tin oxide (ITO); (c) metal grid or mesh electrode[37].

Spectroelectrochemistry provides new routes in characterization of electrochemically generated intermediates and reaction mechanisms. In situ UV/vis spectroelectrochemistry was employed to study the poly (para-phenyleneethynylene) (PPE) films on ITO transparent electrodes during an anodic sweep. Neutral polymer, polaron species, bipolaron species, and species formed by further bipolaron reaction were identified during the reaction process[52]. Using optically transparent ITO-coated glass and gold mesh as electrodes, the quantitative time dependences of neutral, mono- and di-charged segments during redox cycling of polypyrrole was detected by in situ EPR/UV-vis spectroscopy[53]. In situ fluorescence and UV/Vis spectroscopy were used to study the electrochemical reduction mechanism of ethidium bromide, which has been proved to be two one-electron transfer steps[54]. UV-vis spectroelectrochemical experiments of oligothiophenes films on transparent gold electrodes proved that, these oligothiophenes undergo reversible morphology changes on various redox states due to π-stacks formation[55].

1.5 Research objectives

The motivation of this research is to prepare optically transparent carbon electrodes and study the structural changes of organic molecules by electrochemical potentials using in situ UV-vis spectroelectrochemistry. Most in

situ UV/vis spectroelectrochemistry was based on metal and indium doped tin oxide electrodes. Transparent carbon electrodes were barely used in this field. In this research, carbon OTEs have been firstly attempted to investigate the structural changes of chemisorbed organic monolayers and multilayers with potential.

The transparent carbon film is made from positive photoresist AZ P4330, pyrolyzed photoresist films (PPF) are formed on the quartz substrates, and this transparent PPF would be expected to have special physical, optical and electrical properties. The characterization and application of this transparent PPF have been conducted.

Chapter 2 presents a comprehensive investigation of the properties of the transparent PPF. Its optical property has been examined by UV/vis spectroscopy. The morphology of the transparent PPF has been investigated by AFM. Raman spectroscopy has been applied to study the structure of this transparent PPF. Finally, surface modification of these transparent PPF electrodes has been carried out.

The UV/Vis spectroscopic exploration of solution and chemisorbed molecules is described in chapter 3. Chemisorbed 4-nitroazobenzene (NAB), azobenzene (AB) and 4-nitrobiphenyl (NBP) on transparent PPF electrodes were investigated with UV/vis spectroscopy. The structural changes of NAB, AB and NBP, both as free molecules in solutions and chemisorbed on transparent PPF electrodes, under electrochemical reductions, have been investigated.

References

(1) McCreery, R. L.; Cline, K. K.; McDermott, C. A.; McDermott, M. T. *Colloids Surf.* **1994**, *93*, 211-219.

(2) Kinoshita, K. *Carbon: Electrochemical and Physicochemical Properties.* Wiley: New York, **1988**.

(3) McCreery, R. L. *Interfacial Electrochemistry*, Wieckowski, A., Ed.; Dekker: New York, **1999**; Chapter 35.

(4) McCreery, R. L. *Electroanalytical Chemistry*, Bard, A. J., Ed.; Dekker: New York, **1991**; Vol. 17, 221-374.

(5) McCreery, R. L. *Laboratory Techniques in Electroanalytical Chemistry,* 2nd ed..; Kissinger, P. T., Heineman, W. R., Eds.; Dekker: New York, **1996**; Chapter 10.

(6) Antoniadou, S.; Jannakoudakis, A. D.; Jannakoudakis, P. D.; Theodoridou, E. *J. Appl. Electrochem.* **1992**, 22, 1060-1064.

(7) Tanaka, H.; Aramata, A. *J. Electroanal. Chem.* **1997**, *437*, 29-35.

(8) Nowall, W. B.; Wipf, D. O.; Kuhr, W. G. *Anal. Chem.* **1998**, 70, 2601-2606.

(9) Hayes, M. A.; Kuhr, W. G. *Anal. Chem.* **1999**, *71*, 1720-1727.

(10) Chen, P.; McCreery, R. L. *Anal. Chem.* **1996**, *68,* 3958-3965.

(11) Yang, H.-H.; McCreery, R. L. *Anal. Chem.* **1999**, *71*, 4081-4087.

(12) Nowak, A. M.; McCreery, R. L. *J. Am. Chem. Soc.* **2004**, *126*, 16621-16631.

(13) Ranganathan, S.; McCreery, R. L.; Majji, S. M.; Madou, M. *J. Electrochem. Soc.* **2000**, *147*, 277 – 282.

(14) Wang, Y.; Alsmeyer, D.; McCreery, R. L. *Chem. Mater.* **1990**, *2*, 557-563.

(15) Dresselhaus M. S.; Dresselhaus G.; Sugihara K.; Spain I. L.; Goldberg M. A. *Graphite Fibers and Filaments, 98,* Springer-Verlag, New York, 1988.

(16) Ranganathan, S.; McCreery, R. L. *Anal. Chem.* **2001**, *73*, 893-900.

(17) McDermott, C. A.; Kneten, K. R.; McCreery, R. L. *J. Electrochem. Soc.* **1993**, *140*, 2593-2599.

(18) Chen, P.; Fryling, M. A.; McCreery, R. L. *Anal. Chem.* **1995**, *67*, 3115-3122.

(19) Duvall, S. H.; McCreery, R. L. *J. Am. Chem. Soc.* **2000**, *122*, 6759-6764.

(20) Xu, J.; Granger, M. C.; Chen, Q.; Strojek, J. W.; Lister, T. E.; Swain, G. M. *Anal. Chem.* **1997**, *69*, 591A-597A.

(21) Duvall, S. H.; McCreery, R. L. *Anal. Chem.* **1999**, *71*, 4594-4602.

(22) Xu, J.; Huang, W.; McCreery, R. L. *J. Electrochem. Chem.* **1996**, *410*, 235-242.

(23) Yang, H.-H.; McCreery, R. L. *J. Electrochem. Soc.* **2000**, *147*, 3420-3428.

(24) Delamar, M.; Hitmi, R.; Pinson J.; Saveant, J. M. *J. Am. Chem. Soc.* **1992**, *114*, 5883-5884.

(25) Liu. Y.-C., McCreery, R. L. *Anal. Chem.* **1997**, *69*, 2091-2097.

(26) Allongue, P.; Delamar, M.; Desbat, B.; Fagebaume, O.; Hitmi, R.; Pinson J.; Saveant, J. M. *J. Am. Chem. Soc.* **1997**, *119*, 201-207.

(27) Dequaire, M.; Degrand, C.; Limoges, B. *J. Am. Chem. Soc.* **1992**, *121*, 6946-6947.

(28) Delamar, M.; Desarmot, G.; Fagebaume, O.; Hitmi, R.; Pinson, J.; Saveant, J.-M. *Carbon* **1997**, *35*, 801-807.

(29) Liu, Y.-C.; McCreery, R. L. *J. Am. Chem. Soc.* **1995**, *117*, 11254-11259.

(30) Brooksby, P. A.; Downard, A. *Langmuir* **2004**, A-H.

(31) Anariba, F.; DuVall, S. H.; McCreery, R. L. *Anal. Chem.* **2003**, *75*, 3837-3844.

(32) Kariuki, J. K.; McDermott, M. T. *Langmuir* **2001**, *17*, 5947-5951.

(33) Ranganathan, S.; Steidel, I.; Anariba, F.; McCreery, R. L. *Nano Lett.* **2001**, *1*, 491-494.

(34) Solak, A. O.; Ranganathan, S.; Itoh, T.; McCreery, R. L. *Electrochem. Solid State Lett.* **2002**, *5*, E43-E46.

(35) Solak, A. O.; Eichorst, L. R.; Clark, W. J.; McCreery, R. L. *Anal. Chem.* **2003**, *75*, 296-305.

(36) Itoh, T.; McCreery, R. L. *J. Am. Chem. Soc.* **2002**, *124*, 10894-10902.

(37) http://sbio.uct.ac.za/Sbio/documentation/spectrophotometer.pdf

(38) Plieth, W., Wilson, G. S., Gutierrez De La Fe, C. *Pure & Appl. Chem.* **1998**, *70*, 1395-1414.

(39) Jentoft, F. *Modern Methods in Heterogeneous Catalysis* **2004**, 3.

(40) Kalyuzhny, G.; Schneeweiss, M. A.; Shanzer, A.; Vaskevich, A.; Rubinstein, I. *J. Am. Chem. Soc.* **2001**, *123*, 3177-3178.

(41) Cheng, Z.; Cheng, L.; Gao Q., Dong, S.; Yang, X. *J. Mater. Chem.* **2002**, 12, 1724-1729.

(42) Pang, S.-F.; Liang, Y.-Q. *Journal of colloid and Interface Science* **2000**, *231*, 59-65.

(43) Kalyuzhny, G.; Vaskevich, A.; Ashkenasy, G.; Shanzer, A.; Rubinstein, I. *J. Phys. Chem. B* **2000**, *104*, 8238-8244.

(44) Tamada, K.; Akiyama, H.; Wei, T. X. *Langmuir*, **2002**, *18*, 5239-5246.

(45) Sortino, S.; Petralia, S.; Conoci, S.; Bella, S. D. *J. Mater. Chem.* **2004**, *14*, 811-813.

(46) Everaars, M. D.; Marcelis, A. T. M.; Kuijpers, A. J.; Laverdure, E.; Koronora, J. et al. *Langmuir*, **1995**, *11*, 3705-3711.

(47) Shukla, A. D.; Strawser, D.; Lucassen, A. C. B.; Freeman, D.; Cohen, H.; et al. *J. Phys. Chem. B* **2004**, *108*, 17505-5-17511.

(48) Nieuwkerk, A. C.; Marcelis, A. T. M.; Sudholter, E. J. R. *Langmuir*, **1997**, *13*, 3325-3330.

(49) Everaars, M. D.; Marcelis, A. T. M.; Sudholter, E. J. R. *Langmuir*, **1996**, *12*,

3964-3968.

(50) Li, X.; Xu, W.; Jia, H.; Wang, X.; Zhao, B.; et al. *Journal of Colloid and Interface Science* **2004**, *274*, 9-15.

(51) Elking, M. D.; He, G.; Xu, Z. J. *Chem. Phys.* **1996**, *105(15)*, 6565-6573.

(52) Scholz. F. *Electroanalytical methods : guide to experiments and applications* **2002,** 167-189.

(53) Rapta, P.; Neudeck, A.; Petr, A.; Dunsch L. *J. Chem. Soc., Faraday Trans.* **1998**, *94*, 3625-3630.

(54) Hu, X.; Wang, Q.; He, P.; Fang. Y. *Analytical Sciences* **2002**, *18*, 645-650.

(55) Lapkowski, M.; Zak, J.; Kolodziej-Sadlok, M.; Guillerez, S.; Bidan, G. *Synthetic Metals* **2003**, *135-136*, 251-252.

CHAPTER 2

PREPARATION AND CHARACTERIZATION OF OPTICALLY TRANSPARENT PYROLYZED PHOTORESIST FILMS

It has been proved that carbon materials (pyrolyzed photoresist films (PPF)[1], GC[2,3], HOPG[2,4,5], pyrolyzed Teflon[6], carbon fibers[3], carbon blacks[7], carbon nanotubes[8] and diamonds[9]) can be modified by diazonium salts to form a covalently bonded organic monolayer or multilayer on the surface[10]. However, it is very difficult for spectroscopic techniques to monitor chemisorbed organic molecules on conventional carbon materials, in part due to their opaque property. The major challenge for development of spectroelectrochemical methods is to design optically transparent electrodes which are compatible with the desired spectroscopic technique. The objective of current experiments is preparation and characterization of transparent PPF electrodes in the context of applications in UV–vis spectroelectrochemistry. The transparent PPF electrodes are expected to exhibit unusual surface properties and be capable of forming covalently bonded monolayers or multilayers by diazonium ion reduction. This chapter describes the application of several techniques, including UV-vis spectroscopy, atomic force microscopy (AFM), Raman spectroscopy and cyclic voltammetry, to the

characterization of the optical and physical properties of transparent PPF electrodes.

The atomic force microscope was invented in 1986 by Binnig, Quate and Gerber. This technique is being used widely in material, chemical, biological and electronics fields. The materials being investigated include both conducting and insulating surfaces. AFM operates by measuring the interaction (attractive or repulsive) between a tip and the sample surface. Usually, the force between the tip and the sample surface is less than 10^{-9} N. The force is not directly measured by the detection system. The first AFM used a scanning tunneling microscope to sense the bending of the lever, with the change of the tunneling current of an order of magnitude corresponding to a change in spacing of 1 Å between the tip and the sample surface. Currently, most atomic force microscopes employ optical techniques (Figure 2.1)[11]. A position-sensitive photodiode detector is employed to detect the laser beam reflected by the mirrored surface on the backside of the cantilever. A minute deflection of the cantilever tilts the reflected beam and changes the position of the beam on the detector[12]. The interaction force between the tip and the sample surface can be calculated by Hooke's Law applied to the cantilever. According to the interaction between the tip and the sample surface, the operational modes of AFM are classified as contact mode, non-contact mode and tapping mode. In contact mode, the cantilever is pushed against the sample surface by a piezoelectric positioning element. As the scanning proceeds, the tip and sample surface remain in close contact. The vertical deflection of the cantilever, which indicates the local sample height, is

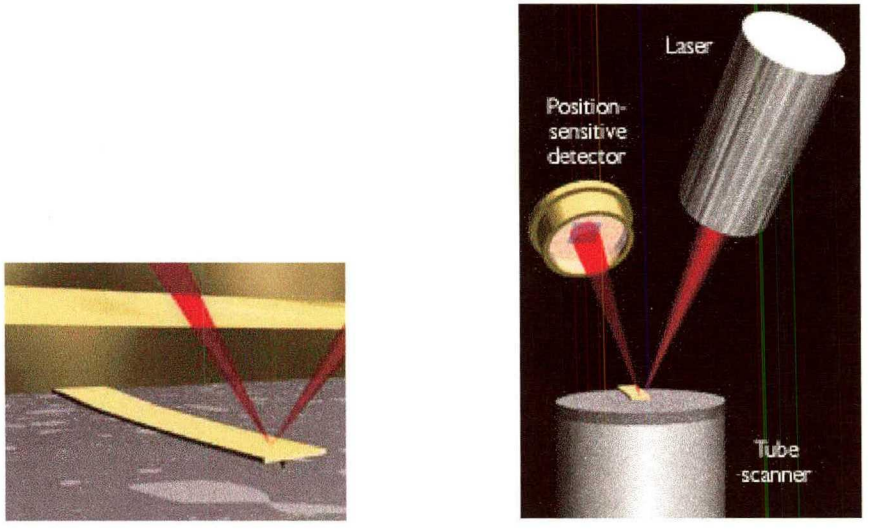

Figure 2.1 Concept of AFM and the optical lever: (left) a cantilever touching a sample; (right) the optical lever. Scale drawing; the tube scanner measures 24 mm in diameter, while the cantilever is 100 μm long[11].

measured. Large lateral forces exist on the sample as the tip is dragged over the surface, which makes the imaging heavily influenced by frictional and adhesive forces. In non-contact mode, the cantilever oscillates above the surface of the sample at such a distance that an attractive force exists between the tip and the surface of the sample. The AFM topographic images are derived from the measurements of the attractive forces. Non-contact imaging generally provides low resolution, and a contaminant layer may interfere with oscillation. In tapping mode, the tip is alternately placed in contact with the surface to provide high resolution and then is lifted off the surface to avoid dragging the tip across the surface. Tapping mode was developed to avoid destructive frictional forces in both air and fluid, and high resolution is achieved at the same time.

The modification of carbon materials has been achieved by irreversible electrochemical reduction of diazonium salts. The thickness of the resulting layer is influenced by electrolysis time, grafting potential and the concentration of diazonium salt[10]. Multilayers are often formed during the electrochemical reduction process[1, 13-15]. A possible mechanism was presented by Combellas (Figure 2.2)[15]. First, a radical is formed after an electron transfer to a diazonium ion (reaction R1); this radical binds to the carbon surface by a covalent carbon-carbon bond (reaction R2); a second electron transfer to another diazonium salt may then form a new radical, this new radical attacks the first grafted aromatic groups to give a cyclohexadienyl radical (reaction R3). Repetition of this process results in a thick polyphenylene layer. The measurements of thickness have been achieved by XPS[13] and AFM[1,14]. In this study, AFM was employed to

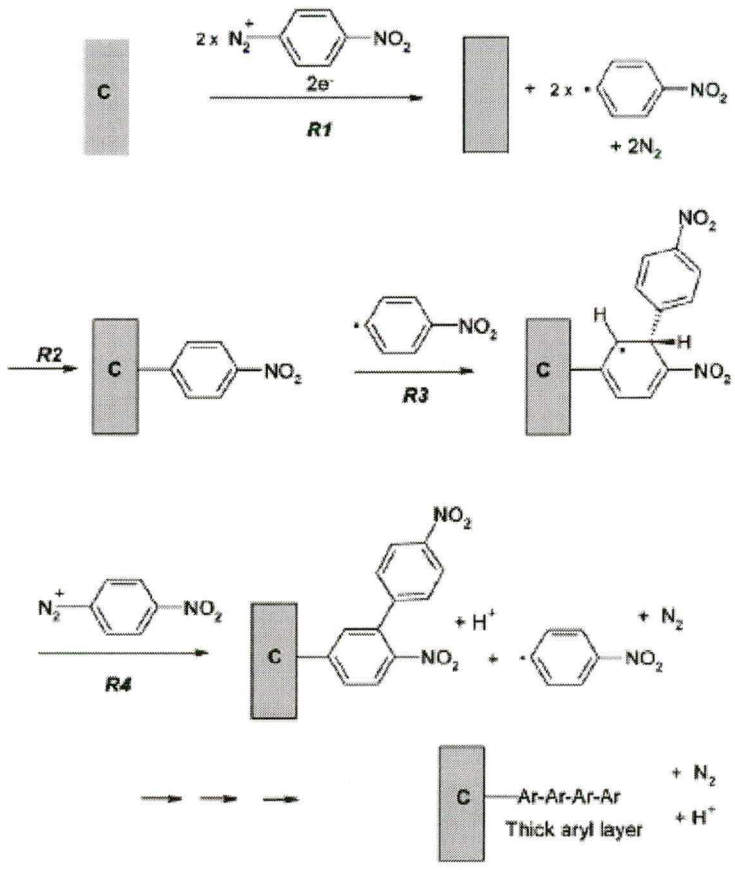

Figure 2.2 Scheme of multilayer formation. Reproduced from reference[10].

measure the thickness of molecules formed on the transparent PPF electrodes. Contact mode AFM was employed to scratch the organic films on the carbon surfaces without damaging the underlying carbon surfaces. Tapping mode AFM was used to determine the film thickness from the depth of the scratch.

2.1 Experimental

Preparation of transparent PPF

Transparent pyrolyzed photoresist films (PPF) were prepared on a quartz substrate (1 cm × 5 cm × 1/16 inch), which was cleaned in a piranha solution (30 % H_2O_2 (Malinckrodt) : 98 % H_2SO_4 (Malinckrodt), 1:3 by volume) for thirty minutes, rinsed rigorously with nanopure water (18 MΩ-cm, Barnsted/Thermolyne, Dubuque, IA), isopropanol (Aldrich Chemical Company, Inc., Milwaukee, WI), acetone (Aldrich) and acetonitrile (Aldrich), then dried with high purity argon. Positive photoresist AZ P4330-RS (AZ Electronic Materials, Clariant Corp., Somerville, NJ) was diluted with 1-methoxy-2-propanol acetate (Aldrich) to a certain concentration (by volume). The diluted photoresist solution was spin-coated onto a piece of clean quartz at 6000 rpm for 30 seconds on a spin coater (WS-400B-6NPP-LITE, Laurell Technologies, Corp., North Wales, PA). The spin-coated sample was soft-baked at 90 °C for 10 minutes, and then transferred into a tube furnace (Lindberg Blue M) fitted with a 1-inch diameter quartz tube. The tube was flushed with forming gas (95% nitrogen and 5% hydrogen) flowing at 100 ml/min throughout the pyrolysis and cooling processes.

Samples were heated at 10 °C/min to 1000°C, and held at 1000 °C for 1 hour, then cooled to the room temperature.

Preparation of transparent PPF electrode

Since the conductivity of transparent PPF is low, it is hard to derivatize a high density of molecules on the surface due to ohmic potential losses during electrochemical reduction. These losses can be decreased by depositing gold on the top of PPF surface by sputter coater (BAL-TEC SCD 050 Sputter Coater). Two designs (Figure 2.3) of Au modification have been attempted. First, on the top of PPF, an area of 1 cm×2 cm was deposited with 10 nm thick gold film (design 1), the gold covered part of this electrode was held above the diazonium salt solution during derivatization. Second, a 10 nm thick gold film was deposited around a rectangle of 0.4 cm×1.5 cm, the rectangle is 2.5 cm from the top, 1cm from the bottom, 0.3 cm from both long edges (design 2). A special electrochemical cell was made for derivatizaion of the central area of the PPF part. The area of PPF exposed to the diazonium solution is 0.3 cm×1.2 cm. The PPF electrodes of design 2 are expected to have more uniform potential distribution over the exposed PPF. 4-nitroazobenzene (NAB) was derivatized on PPF electrodes of design 1 and design 2 under the same condition (Four voltammetric scans between +0.4 V and -0.6 V in 1 mM 4-nitroazobenzene diazonium tetrafluoroborate solution and 0.1 M TBATFB at a scan rate of 0.2 V/s). The UV-vis spectra of these two samples indicate that the optical absorption of NAB on the PPF electrodes of design 2 was significantly higher (Figure 2.4). The

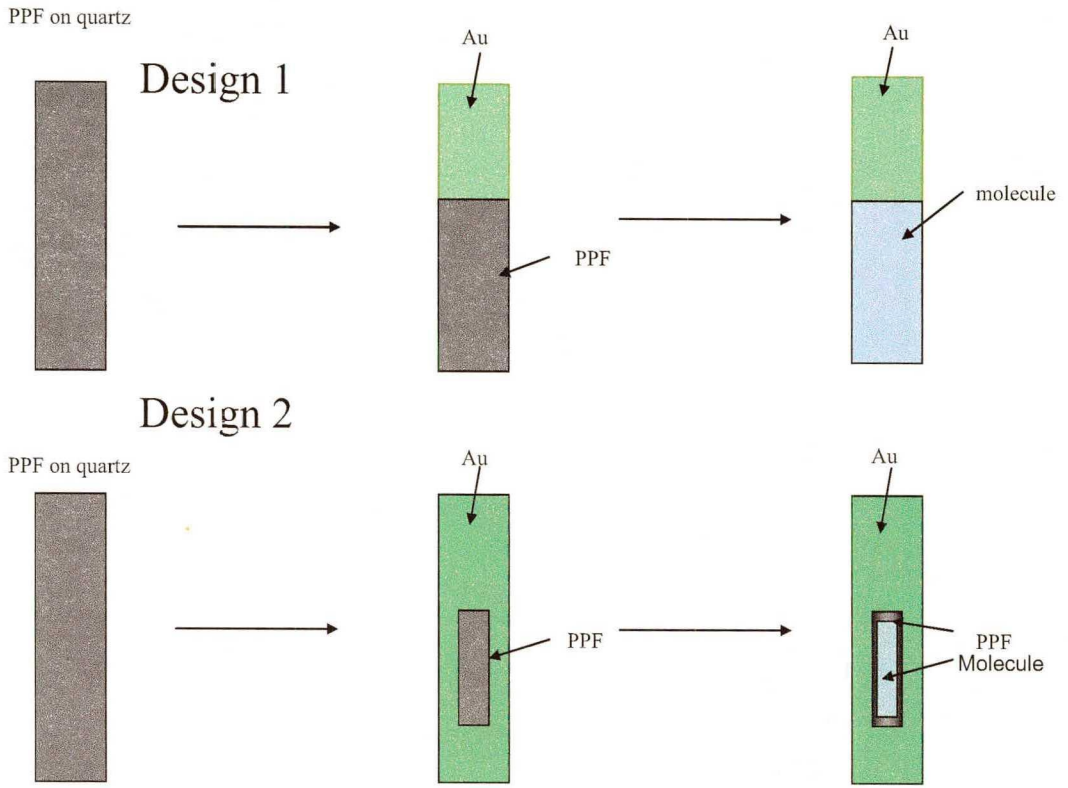

Figure 2.3 Two designs of gold modified transparent PPF electrodes.

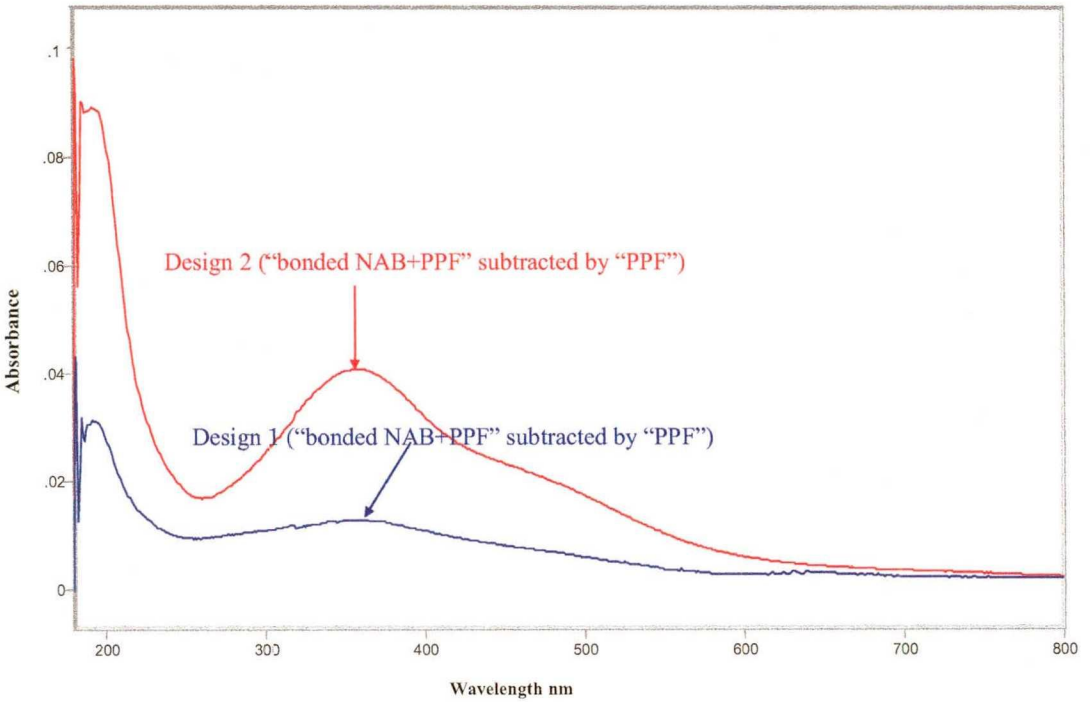

Figure 2.4 UV –vis spectra (overlaid) of chemisorbed NAB film based on design 1 and design 2. The NAB spectra are difference spectra, which were obtained by subtracting the spectrum of bare PPF electrode from the spectrum of NAB modified PPF electrode (spectral subtraction is described in detail in chapter 3).

UV-vis spectra of chemisorbed NAB film were obtained by subtracting the spectrum of bare PPF electrode from the spectrum of NAB modified PPF electrode. The UV-vis spectra of bare PPF electrode and NAB modified PPF electrode of design 2 are shown in Figure 2.5. The gold modified PPF electrodes of design 2 were used for all of the following electrochemical, spectroscopic and spectroelectrochemical experiments.

UV-vis spectroscopy

The UV-vis spectra presented were recorded on a double beam Perkin-Elmer Lambda 900 UV/VIS/NIR spectrometer (PerkinElmer Inc., Boston, MA). Figure 2.6 shows the instrument's optical layout. A deuterium lamp and a tungsten lamp were used as light sources in the ultraviolet and visible regions respectively. The wavelength accuracy in the UV/VIS region is 0.08 nm. The wavelength reproducibility is less than 0.02 nm and the noise level in absorbance mode is less than 0.00007. A photomultiplier is used as detector in the UV/VIS region. The spectral slit width of the spectrometer was 2 nm. The scan speed was 57.69 nm/min with a data interval of 1 nm. Air was used as a reference to obtain absorption spectra. Spectral subtraction, overlay and processing were carried out by Grams AI, version 6.00 (Galactic Industries, Salem, N.H.).

Atomic force microscopy (AFM)

Atomic force microscopy (AFM) measurements were operated on a Nanoscope IIIa Multimode instrument (Digital Instruments, Santa Barbara, CA) in

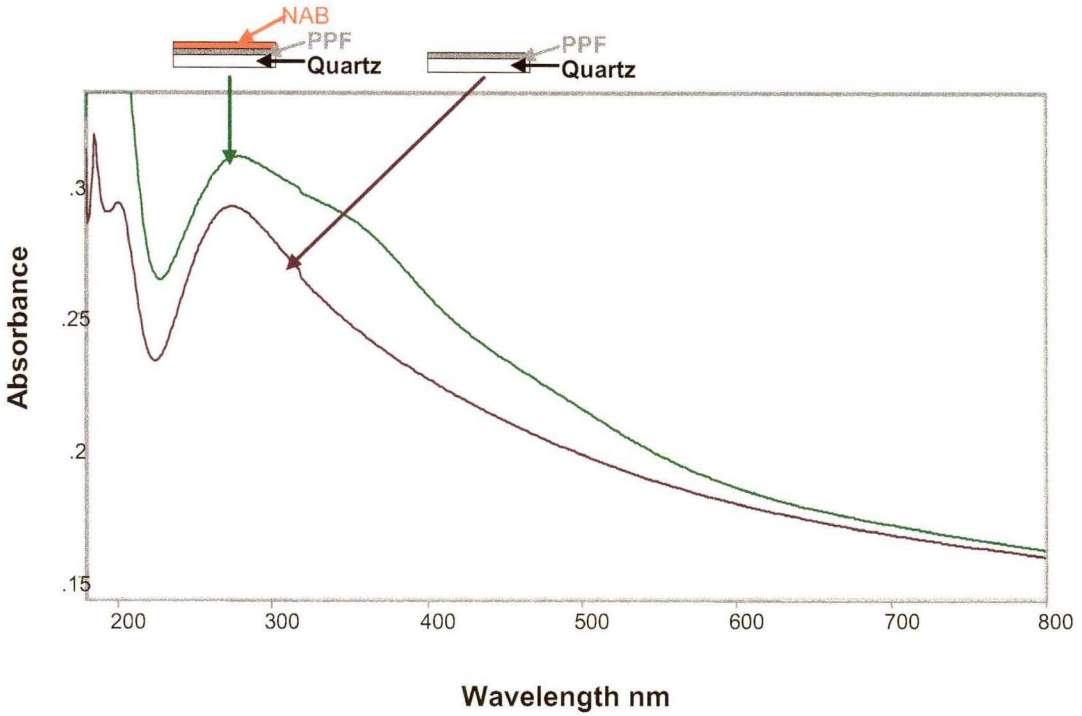

Figure 2.5 UV-vis spectra of bare PPF electrode and NAB modified PPF electrode of design 2.

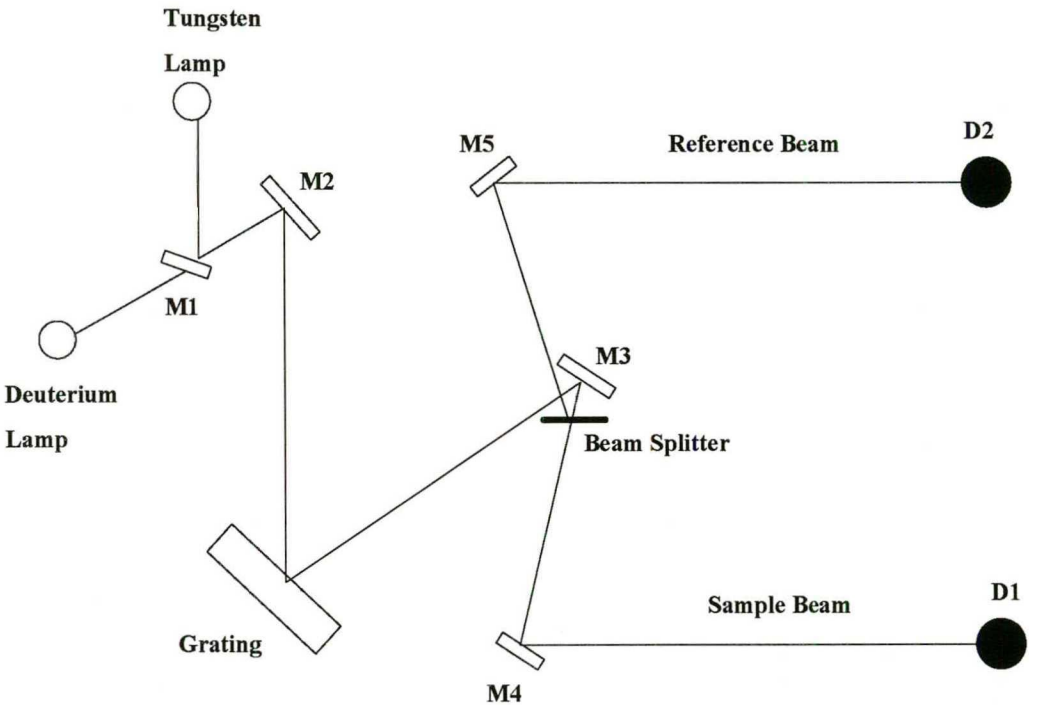

Figure 2.6 Optical layout of the Lambda 900 UV/VIS/NIR spectrophotometer, in which M1-M5 are mirrors, D1 and D2 are detectors.

air. Damage or possible residue adherence to the tip may happen after several "scratches". The resonant frequency of the AFM tip was checked frequently and the tip was replaced when it was worn off. A standard grid provided by Digital Instruments was used to calibrate the *Z*-axis of the AFM. The force of ~1 μN was used for scratching which was sufficient to remove the molecular layer without damaging the substrate[1]. Scratches were made in contact mode and height measurements were made in tapping mode. The images were obtained by tapping mode with a scan rate of 1.0 Hz and were flattened with a first-order polynomial before analysis.

Raman spectroscopy

Raman spectra were acquired with a Dilor XY Raman microprobe (ISA Inc., Edison, NJ). A 514.5 nm Coherent Innova 300 argon ion laser was served as the excitation source. The 2000 × 800 pixels CCD was cooled by liquid nitrogen. The transparent PPF was sampled by a 100 × MPlan Olympus f/0.24 objective, and the focal spot size was approximately 10 μm. Spectra presented in the figures are averages of ten 5-second integrations.

Synthesis of the diazonium tetrafluoroborate derivatives

Approximately 0.01 mol a particular amino precursor (4-amine-4'-nitroazobenzene (Disperse Orange 3, Aldrich), 4-phenylazoaniline (Aldrich), or 4-amino-4'-nitrobiphenyl (Aldrich) was weighed into a 50 ml three-necked round-bottom flask. 10 mL of 50% fluoroboric acid (HBF_4, Fisher Chemicals, Fair Lawn,

NJ) was added to dissolve the precursor. The flask was placed into an ice/sodium chloride bath to cool the mixture to below 0°C. A solution of sodium nitrite ($NaNO_2$, Aldrich) was prepared by dissolving the $NaNO_2$ in Nanopure water (18 MΩ-cm, Barnsted/Thermolyne, Dubuque, IA) at room temperature, in which the $NaNO_2$ was weighed with a mole ratio of 3 $NaNO_2$: 1 amino precursor. The $NaNO_2$ solution was cooled to 0°C. As the mixture was stirred in the flask, the cold $NaNO_2$ was added drop wise. The temperature of the mixture was kept below 4°C during the reaction. After complete addition of $NaNO_2$, the mixture was stirred continuously for 30 minutes in the ice/sodium chloride bath. The precipitate formed was filtered in a Buchner funnel with vacuum filtration. The remaining sediments were removed from the round bottom flask by cold ether (99.9 % assay, Fisher Chemicals). The diazonium salt was recrystallized by dissolving in a minimal amount of cold acetonitrile (Aldrich) and then adding cold anhydrous ether (99.9 % assay, Fisher Chemicals) drop wise to recover the salt. The purified diazonium salts were stored in a desiccator held at 4°C in a freezer. The diazonium tetraflouroborate salts were characterized by mass spectrometry (ESI-TOF) and nuclear magnetic resonance. The diazonium salts were used within 1 month of synthesis. Older diazonium salts need to be recrystallized before use. Diazonium salt solutions were kept in a freezer and should be used within a few hours after preparation.

Derivatization of transparent PPF electrodes with tetrafluoroborate diazonium salts

Electrochemical experiments were performed on a BAS 100-W potentiostat (Bioanalytical Systems, West Lafayette, IN), with an Ag+ (0.01 M)/Ag reference electrode (BAS) and a Pt wire as the auxiliary electrode. Using 1 mm diameter BAS platinum disc electrode as the working electrode, Ag+ (0.01 M)/Ag reference electrode (BAS) was calibrated to the $E_{1/2}$ of ferrocene. An observed $E_{1/2}$ for Fc of 89 ± 5 mV was accepted. Derivatization of a transparent PPF electrode was performed by the electrochemical reduction of the corresponding diazonium salt in acetonitrile (Aldrich) with *n*-tetrabutylammonium tetrafluoroborate (0.1 M; Aldrich) as the supporting electrolyte. Tetrafluoroborate diazonium salts of 4-nitroazobenzene (NAB), azobenzene (AB), and 4-nitrobiphenyl (NBP) were used for derivatization. The diazonium salt solutions were freshly prepared, and had low water content. The concentration of the diazonium salt solution was 1mM, and derivatization scans were from +0.4 to -0.6 V versus Ag+/Ag electrode at 0.2 V/s for four cycles. After derivatization, the modified PPF electrodes were immediately rinsed with acetonitrile and then dried with high purity argon. Figure 2.7 illustrates the mechanism of the covalently grafting an organic molecule onto the PPF electrode.

Calculations of monolayer thickness by Gaussian

Gaussian 98 were used to calculate the theoretical thickness of monolayers with density functional theory (B3LYP/6-31G(d)). Thickness was

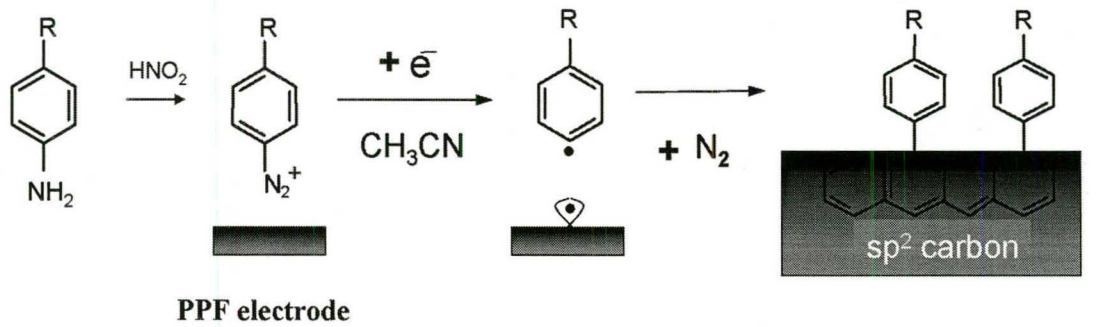

Figure 2.7 Mechanism of electrochemical reduction of an aryl diazonium salt onto a PPF electrode.

defined as the length of the molecule bonded perpendicularly to the PPF surface, including the Van der Waal radius of the terminal atom and a C–C single bond length between the surface and the phenyl ring carbon atom bonded to the surface[1].

2.2 Results

2.2.1 Optical properties of transparent PPF

Transparent PPF samples on quartz were prepared at different concentrations of positive photoresist AZ P4330-RS. The thickness of the resulting PPF varies with the concentration of photoresist, which results in different optical transmissions of PPF. The maximum absorption peaks and their transmission values of PPF samples prepared at various concentrations are listed in table 2.1. Thicker films result from higher concentration of photoresist. The transparency of the PPF increases as the films became thinner.

The transparent PPF resulting from 5% photoresist solution was selected as the carbon substrate for subsequent UV-vis investigations. Keeping all the experimental conditions of preparing procedures as constant as possible, the maximum absorption peak appeared at 270±4 nm, and the transmission at the maximum absorption were in the range of 57%±4% (Figure 2.8). The transmission of 5% transparent PPF in the 200-800 nm regions range from 0.5 to 0.8, which is acceptable for an optically transparent substrate in the UV-vis region.

Concentration of photoresist (volume)	maximum absorption peak (nm)	Transmission at maximum absorption
50%	257	4×10^{-2} %
33%	260	2%
25%	265	26%
10%	270	37%
5%	272	57%
1%	274	94%

Table 2.1 Variations of transmission at the maximum absorption with the concentrations of photoresist.

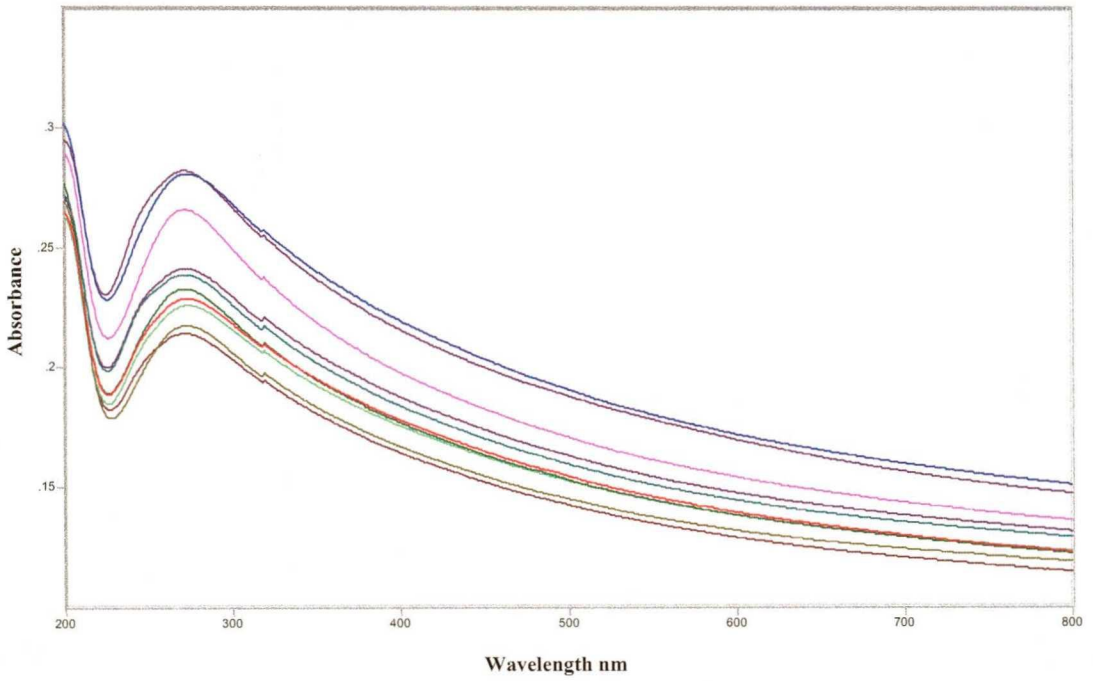

Figure 2.8 UV-vis spectra (overlaid) of transparent PPF of ten samples. The maximum absorption peaks are at 270 ± 4 nm with transmissions of 57% ± 4%.

2.2.2 Film morphology

The AFM image and line profile of a transparent PPF are showed in figure 2.9 A and B respectively. Figure 2.9 A shows the tapping mode 3D AFM image of a 5 μm × 5 μm area on a transparent PPF. The line profile along a 5 μm line in figure 2.9 B shows the variation of the z-axis height. The root-mean-square (RMS) roughness of the transparent PPF is approximately 0.5 nm and the peak-to-valley distance along this line is 0.995 nm. This roughness is typical of several locations not only on a given sample but also on several samples.

2.2.3 Film structure

Raman spectra of transparent PPF were acquired to evaluate the carbon structure and uniformity of the PPF. Raman peaks at ~1360 and ~1600 cm^{-1} are characteristic sp^2 carbon bands (disorder band, D) and graphitic band (E_{2g}) respectively[16-18]. Their peak area ratio (D/E_{2g} ratio) has been correlated with the degree of disorder of the sp^2 carbon material[16]. Higher D/E_{2g} ratio corresponds to smaller graphite crystallite size (La), which is an indication of greater disorder. A series of 10 microscopic Raman spectra (Figure 2.10) was obtained along a 900 μm line with a focal spot ~ 5 μm. The average D/E_{2g} peak ratio is 1.634 and the standard deviation is 0.124 (Table 2.2). The relatively constant D/E_{2g} ratios along the 900 μm line indicate the microstructures of the pyrolyzed film are uniform on a scale of the laser size (5 μm). The relatively constant intensities of D and E_{2g} bands imply that PPF is almost evenly formed on the quartz surface. Since the laser focus was maintained along the 900 μm line, constant intensities and peak

A

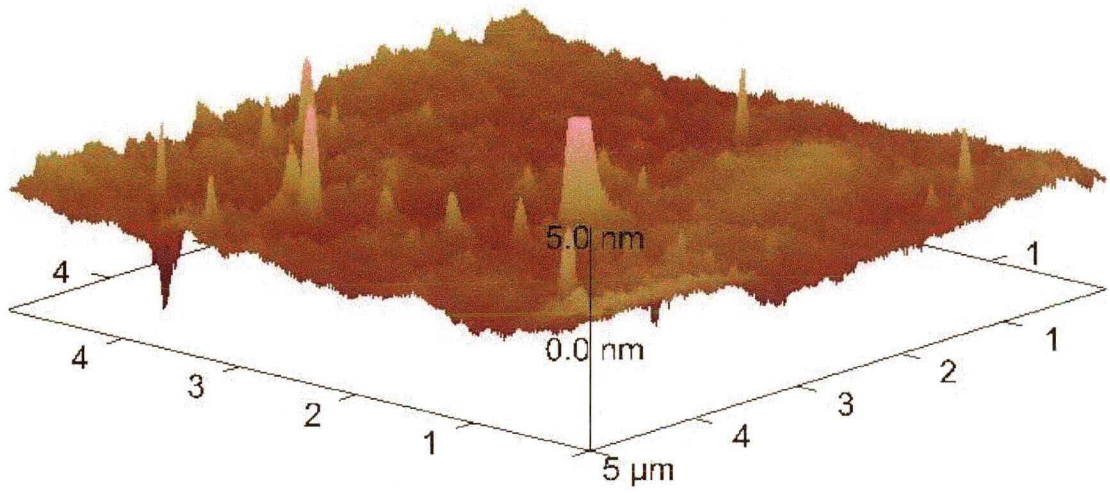

B

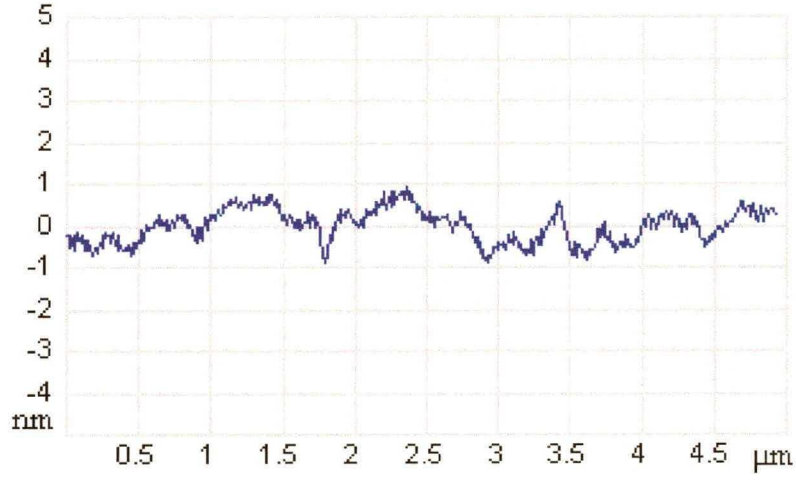

Figure 2.9 AFM image of a transparent PPF obtained by tapping mode.
A) 3D AFM image
B) Line Profile along a 5 µm line showing z-axis variations

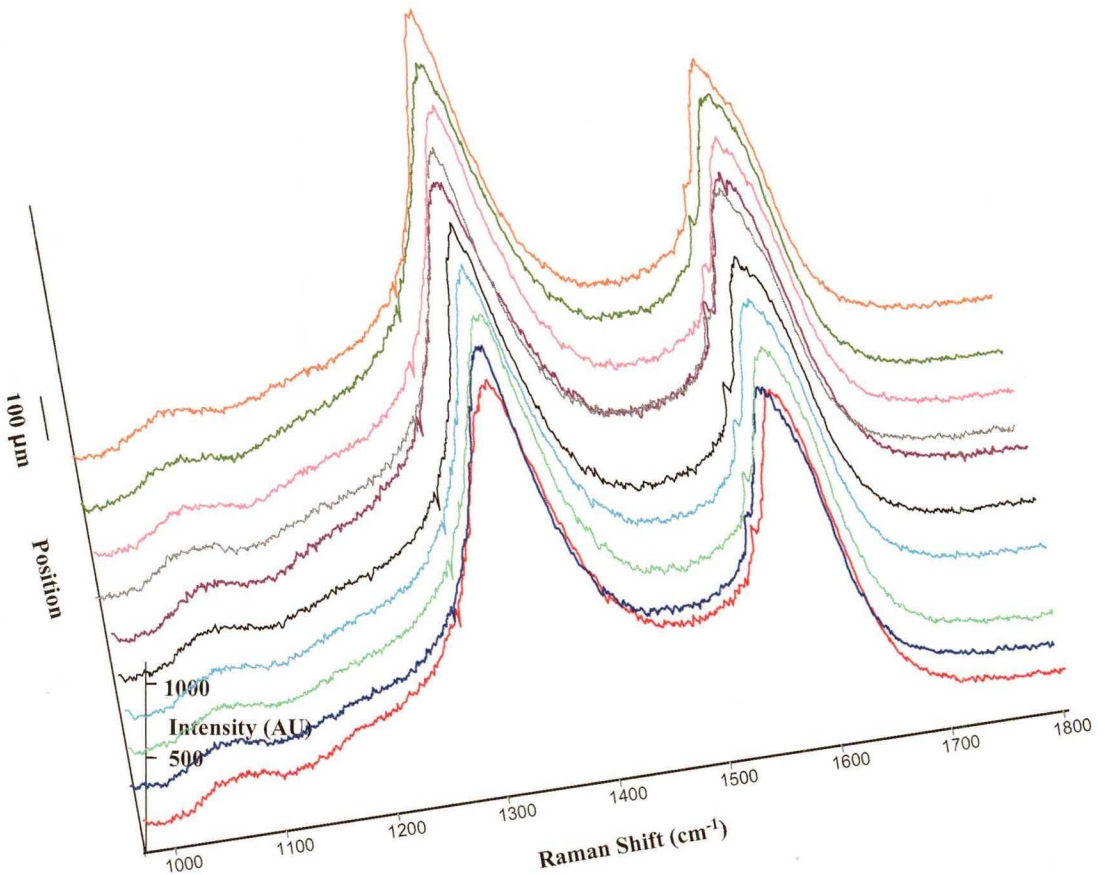

Figure 2.10 Raman profile of transparent PPF. Ten Raman spectra were taken along a 900 µm line.

Position	Intensity of D band	Intensity of E_{2g} band	Peak area ratio of D/ E_{2g}
1	68043	46539	1.46
2	100368	56490	1.78
3	78841	51188	1.54
4	81519	49002	1.66
5	76198	52181	1.46
6	83983	50553	1.66
7	83129	53609	1.55
8	93109	53712	1.73
9	91537	53645	1.71
10	105762	58996	1.79

Table 2.2 Band intensities of D and E_{2g} and their peak area ratios along a 900 μm line.

ratios imply the microstructure of transparent PPF is uniform.

2.2.4 Electrochemistry of diazonium tetrafluoroborate salts at transparent PPF electrodes

Modifications of the PPF surfaces by the electrochemical reduction of diazonium salts have been reported[1,14,19]. Diazonium salts of 4-nitroazobenzene (NAB), azobenzene (AB) and 4-nitrobiphenyl (NBP) have been used to produce NAB, AB and NBP modified PPF. The derivatization conditions of NAB, AB and NBP diazonium salts on PPF surfaces are equivalent. The applied potential was scanned from +0.4 V to -0.6 V with a scan rate of 0.2 V/s for 4 cycles. Figure 2.11 shows cyclic voltammograms of reduction of 1 mM 4-nitroazobenzene (Figure 2.11a), nitroazobenzene (Figure 2.11b) and 4-nitrobiphenyl (Figure 2.11c) diazonium tetrafluoroborates in 0.1M TBATFB/acetonitrile solution at transparent PPF electrodes. The voltammograms indicate the chemically irreversible reduction process of these three diazonium salts, which was attributed to the formation of the 4-nitroazobenzene, azobenzene and 4-nitrobiphenyl radicals from the diazonium precursors. Since the transparent PPF has aromatic carbon character, the carbon-carbon covalent bonds formed between the PPF electrodes and the organic radicals, NAB, AB and NBP are conjugated with the large π system of graphitic carbon. The cyclic voltammograms of these three diazonium salts are similar. The reduction wave was greatly attenuated on the second scan and disappeared completely on the fourth scan (Figure 2.11). Four cycles were applied to ensure the completion of modification. This observation

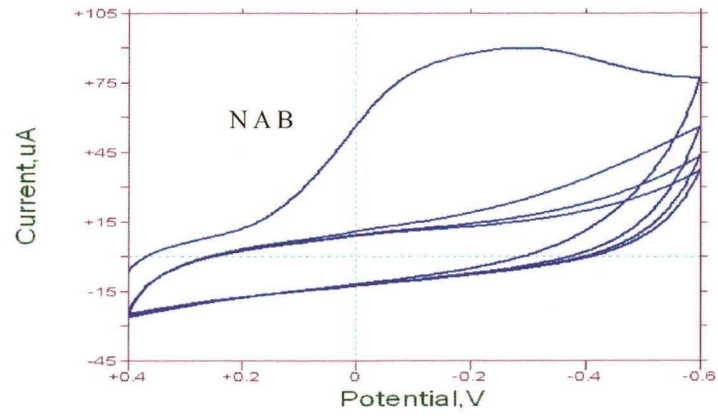

(a)

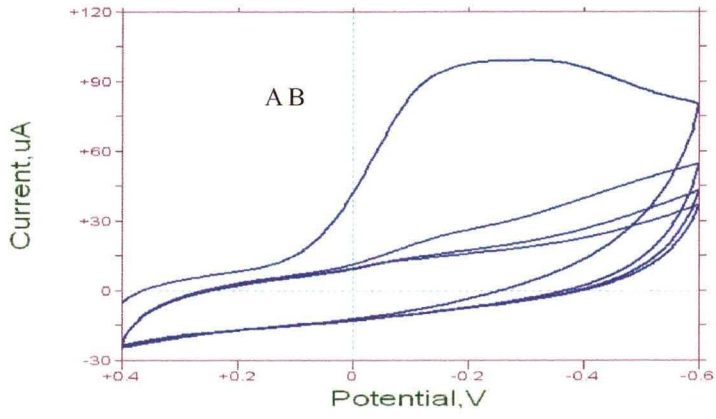

(b)

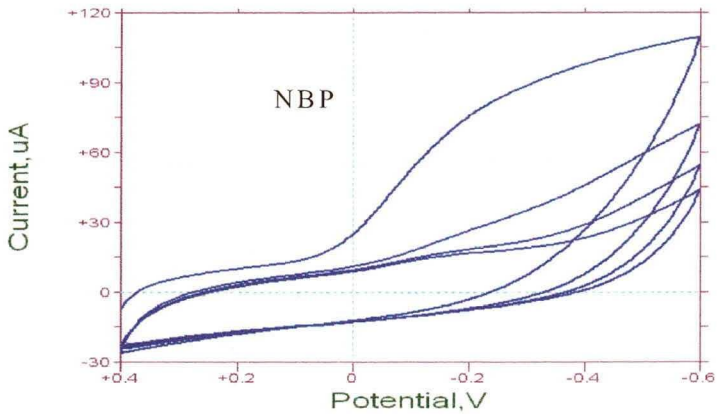

(c)

Figure 2.11 Cyclic voltammetry of 1 mM NAB (a), AB (b) and NBP (c) diazonium salts in 0.1 M TBATFB/ACN, 0.2 V/s scan rate.

indicates an inhibition of the electron transfer by the organic groups which are initially attached to the PPF surface. From the cyclic voltammograms of reduction of NAB, AB and NBP diazonium salts, the surface concentrations of NAB and AB are higher than that of NBP. The modified samples were thoroughly rinsed with acetonitrile to remove any physisorbed materials, and then probed by AFM and UV-vis spectrometry.

It has been reported that multilayers may be formed during electrochemical reduction of diazonium salts[1,14]. Atomic Force Microscopy (AFM) was applied to obtain the images (Figure 2.12, 2.13 and 2.14) of the modified PPF surfaces after derivatization. These images clearly show the formation of molecular layers of variable height.

The applied force was set to disrupt the molecular layer but not to damage the substrate. A set-point voltage force of 0.25 V was empirically determined to apply to all contact mode "scratching" experiments because it was sufficient to remove covalently bonded monolayer or multilayer from PPF without damaging the PPF surface. For all the samples, an area of 500 nm $\times$ 500 nm was carved out in the molecular layers in contact mode. The images shown in Figure 2.12, 2.13 and 2.14 were obtained by tapping mode after "scratching".

To obtain the accurate thickness of a film, the trench depths over a large fraction of the scratched area were averaged by a statistical procedure. A rectangle was arbitrarily defined on the image, which crossed both scratched and unscratched regions. From this rectangle, 10 pairs of lines were selected to collect data. Each pair of lines was restricted to consist of one inside the scratch

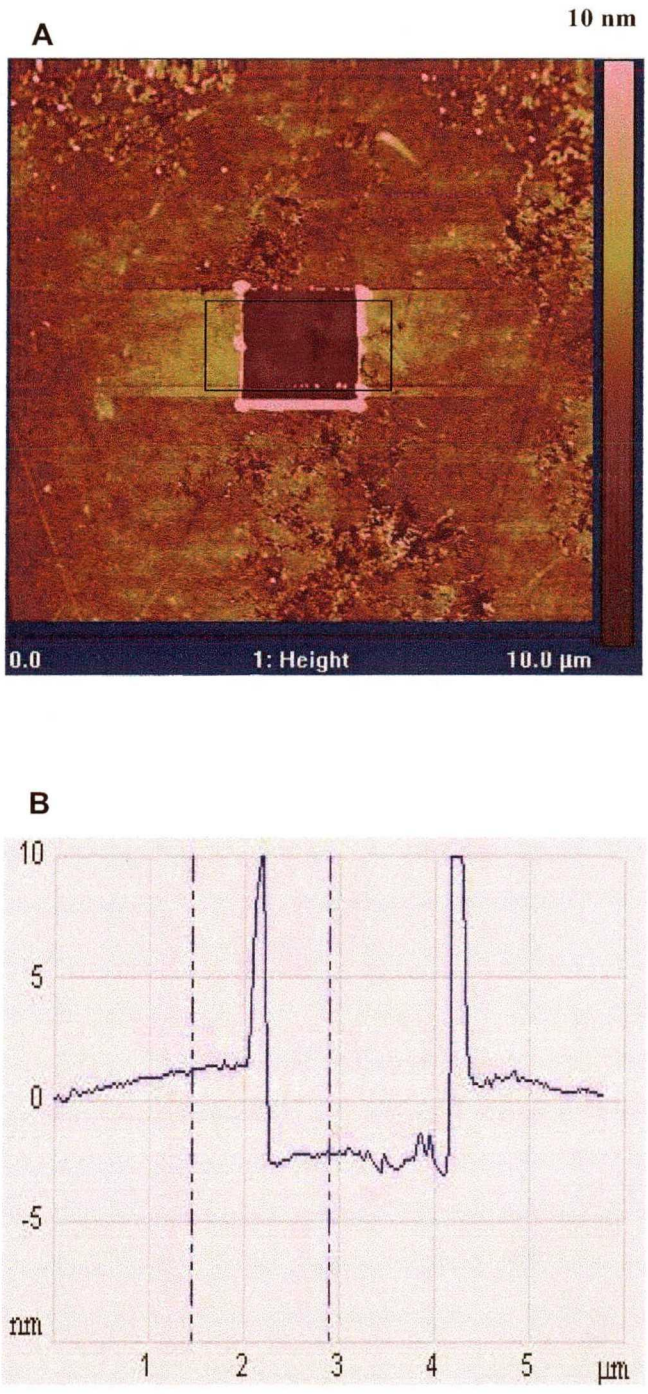

Figure 2.12 Tapping mode AFM image of a 4-nitroazobenzene (NAB) modified transparent PPF electrode with a 500 nm × 500 nm trench in the molecular layer (A); line profile across the trench in the upper image (B).

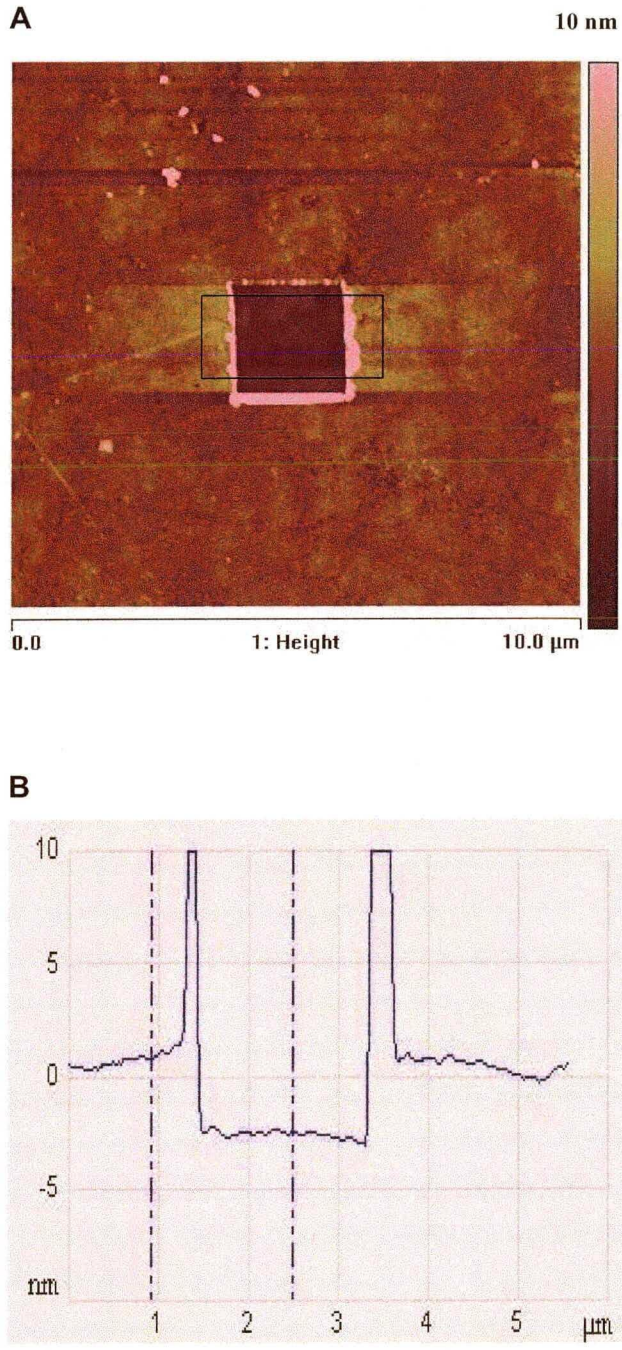

Figure 2.13 Tapping mode AFM image of a nitroazobenzene (AB) modified transparent PPF electrode with a 500 nm × 500 nm trench in the molecular layer (A); line profile across the trench in the upper image (B).

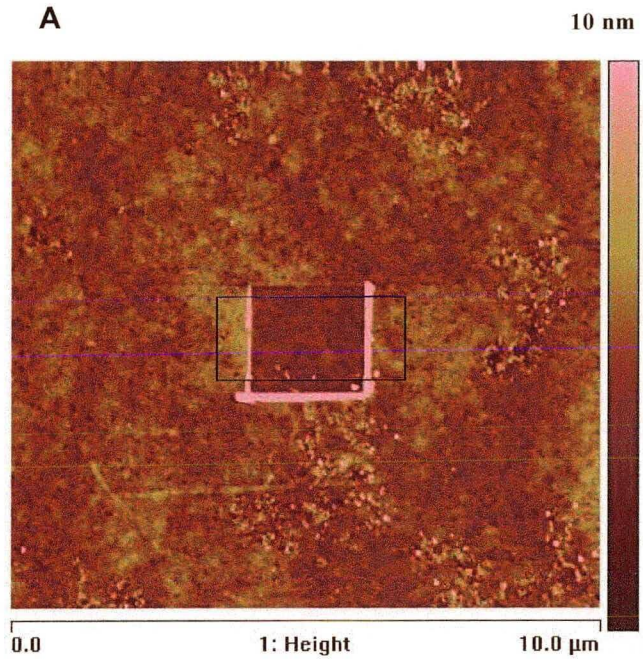

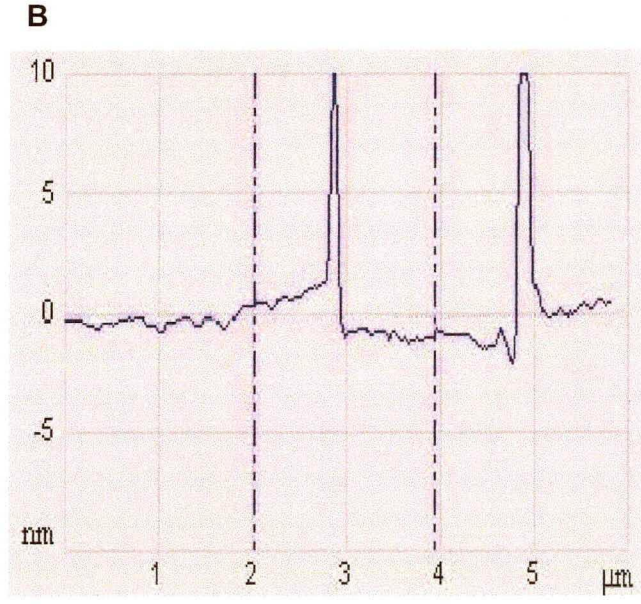

Figure 2.14 Tapping mode AFM image of a 4-nitrobiphenyl (NBP) modified transparent PPF electrode with a 500 nm × 500 nm trench in the molecular layer (A); line profile across the trench in the upper image (B).

Molecule	Calculated length (nm)	Thickness measured by AFM (nm)
NAB	1.419	3.961±0.686
AB	1.370	3.224±0.586
NBP	1.484	1.347±0.293

Table 2.3 The molecular lengths of NAB, AB and NBP calculated by Gaussian (density functional theory (B3LYP/6-31G(d))) and the measured thickness by AFM after 4 cycles of cyclic voltammetry of 1 mM corresponding diazonium salt from +0.4 V to -0.6 V with a scan rate of 0.2 V/s on transparent PPF electrodes.

and one outside. The average height along each line was calculated by the AFM software (Nanoscope). The height difference of the two lines was calculated as the depth of the trench. The trench depths, i.e. film thickness, were obtained from the mean and standard deviation of the height difference of these "lines". Table 2.3 lists film thickness of NAB, AB and NBP on transparent PPF derivatized with four voltammetric scans from +0.4 V to -0.6 V versus Ag^+/Ag in 1mM diazonium ion solutions at 0.2V/s. Compare the measured thickness by AFM with the calculated molecular length, NAB and AB formed multilayers, and NBP formed monolayer on the transparent PPF electrodes.

2.3 Discussion

Pyrolyzed photoresist films (PPF) were selected to prepare optically transparent carbon electrodes for UV-vis spectroelectrochemical study for the following reasons: First, the molecule-electrode interface is critical to electrochemical effects because it may limit or completely modify the electron

transfer process. Self assembled monolayers have been used to investigate the electron transfer through organic monolayers. However, the sulfur-gold bond between molecule and electrode is not a conjugated bond, and an energy barrier at the interface may partially or fully alter the electronic characteristics of the molecule. PPF has an aromatic carbon structure, which can form carbon-carbon bonds at the interface by electrochemical reduction of diazonium salts. Second, using of photoresist in the preparation can control the size and shape of resulting carbon film. The optical property of the PPF varies with the thickness of the film, which can be controlled by the concentration of the photoresist, the number of coatings applied to the substrate and the rate of spin coating.

Table 2.1 demonstrates that the transmission of PPF is related to the concentration of photoresist during preparation. Higher concentration of photoresist results in thicker PPF, which corresponds to less transmission. Overlaid UV-vis spectra of ten transparent PPF samples (Figure 2.8) show some variation in transmission. Even when the preparation conditions of PPF were controlled as constant as possible, there were no two identical PPF electrodes. The maximum absorption wavelength of transparent PPF was 270 ± 4 nm, and transmission at the maximum absorptions was in the range of 57% ± 4%. The Raman spectra of transparent PPF (Figure 2.10) show the characteristic sp^2 carbon bands at ~ 1360 cm^{-1} (D band) and ~ 1600 cm^{-1} (E_{2g} band). The relatively constant D/E_{2g} ratios and peak intensities along the 900 μm line indicate the microstructure of the pyrolyzed film is uniform on a scale of the laser spot size (~5 μm). The tapping mode image of transparent PPF (Figure 2.9) indicates an

almost atomically flat surface with a root-mean-square (rms) roughness of 0.5 nm. All these evidences confirm the conclusion that pyrolysis of diluted photoresist can form transparent and atomically flat carbon films, which can be used as substrates for UV-vis investigation.

It has been reported that electrochemical reduction of diazonium salts on PPF may result in monolayers or multilayers[1,14]. Transparent PPF is thinner than normal PPF, and it is formed on nonconductive quartz. As an electrode, it is less conductive than a normal PPF electrode which is formed on glassy carbon or silicon. It is expected that the molecular layer formed on a transparent PPF electrode is thinner than that formed on a normal PPF electrode under the same derivatization conditions. For a cyclic voltammetric reduction of 1 mM NAB diazonium salt (4 cycles from +0.4 V to -0.6 V with a scan rate of 0.2 V/s) the thickness of NAB formed on a transparent PPF electrode is 3.961±0.686 nm, while the thickness of NAB formed on a normal PPF electrode is 4.508 ± 0.682 nm[1]. Comparison of the thickness of NBP on a transparent PPF electrode (1.347±0.293 nm) with that on a normal PPF electrode (2.526 ± 0.531 nm)[1] under the same derivatization condition confirms the assumption of thinner films on transparent PPF. Table 2.3 indicates that under the same derivatization conditions, NAB and AB formed multilayers on transparent PPF electrodes, while NBP formed monolayer on a transparent PPF electrode. Comparing the AFM measured thickness of NAB and AB with the calculated molecular thickness, it is likely that NAB and AB formed two to three layers, depending on molecular orientation. The cyclic voltammograms of reduction of diazonium salt show that

the reduction wave was significantly decreased on the second scan and vanished on the fourth scan. These phenomena indicate the inhibition of electron transfer by the organic groups initially bonded to the PPF surface. In order to form a second layer, an electron must transfer through 1-1.5 nm of monolayer of NAB, AB or NBP, and an electrogenerated diazonium radical must react with a phenyl ring of the first momolayer. Molecular band gaps play an important role in electron transfer through organic molecules. The HOMO-LUMO gaps of NAB, AB and NBP are 3.549, 3.951 and 4.254 eV respectively. Larger HOMO-LUMO gaps are responsible for higher energy barrier to electron transfer, which may result in thinner film formation.

2.4 Conclusions

Transparent PPF electrodes were prepared by pyrolysis of photoresist at different concentrations, which permits the fabrication of transparent PPF with different optical transmissions. UV-vis, Raman spectroscopy and AFM have confirmed that homogeneous and transparent PPF can be achieved with this procedure. UV-vis spectra show that the transparent PPF is optically transparent in the region of 200-800 nm with the transmission of 0.5-0.8. The AFM image and Raman spectra indicate that the transparent PPF has a uniform and nearly atomically flat surface with a carbon sp^2 structure.

The transparent PPF electrodes can be modified by electrochemical reduction of diazonium salts to yield covalently bonded monolayer or multiplayer. Electrochemical reduction of the diazonium salts of 4-nitroazobenzene (NAB),

azobenzene (AB) and 4-nitrobiphenyl (NBP) were conducted by cyclic voltammetry. Film thicknesses of NAB, AB and NBP on transparent PPF electrodes were measured by AFM "scratching". With equivalent modification conditions, NAB and AB formed multilayer, while NBP formed monolayer on the transparent PPF electrodes.

References

(1) Anariba, F.; DuVall, S. H.; McCreery, R. L. *Anal. Chem.*, **2003**, *75*, 3837–3844.

(2) Allongue, P.; Delamar, M.; Desbat, B.; Fagebaume, O.; Hitmi, R.; Pinson, J.; Save´ant, J.-M. *J. Am. Chem. Soc.*, **1997**, *119*, 201–207.

(3) Delamar, M.; De´sarmot, G.; Fagebaume, O.; Hitmi, R.; Pinson, J.; Save´ant, J.-M. *Carbon*, **1997**, *35*, 801–807.

(4) Kariuki, J. K.; McDermott, M. T. *Langmuir*, **2001**, *17*, 5947–5951.

(5) Liu, Y.-C.; McCreery, R. L. *J. Am. Chem. Soc.*, **1995**, *112*, 11254–11259.

(6) Combellas, C.; Kanoufi, F.; Mazouzi, D.; Thie´bault, A.; Bertrand, P.; Me´dard, N. *Polymer*, **2003**, *44*, 19–24.

(7) Cooke, J. M.; Galloway, C. P.; Bissell, M. A.; Adams, C. E.; Yu, M. C.; Belmont, J. A.; Amici, R. M. *US Pat, 6 110 9994 A*, **2003** (to Cabot Corp.) and references therein.

(8) Dyke, C. A.; Tour, J. M. *Nano Lett.*, **2003**, *3*, 1215–1218.

(9) Wang, J.; Firestone, M. A.; Auciello, O.; Carlisle, J. A. *Langmuir*, **2004**, *20*, 11450–11456.

(10) Pinson, J.; Podvorica, F. *Chem. Soc. Rev.* **2005**, *34,* 429-439.

(11) http://stm2.nrl.navy.mil/how-afm/how-afm.html

(12) http://www.chembio.uoguelph.ca/educmat/chm729/afm/introdn.htm

(13) Saby, C.; Ortiz, B.; Champagne, G. Y.; Belanger, D. *Langmuir*, **1997**, *13*, 6805-6813.

(14) Brooksby, P. A.; Downard, A. *Langmuir* **2004**, A-H.

(15) Combellas, C.; Kanoufi, F.; Pinson, J.; Podvorica, F. I. *Langmuir*, **2005**, *21*, 280-286.

(16) Ranganathan, S.; McCreery, R. L.; Majji, S. M.; Madou, M. *J. Electrochem. Soc.* **2000**, *147*, 277 - 282.

(17) Wang, Y.; Alsmeyer, D.; McCreery, R. L. *Chem. Mater.* **1990**, *2*, 557-563.

(18) Dresselhaus M. S.; Dresselhaus G.; Sugihara K.; Spain I. L.; Goldberg M. A. *Graphite Fibers and Filaments, 98,* Springer-Verlag, New York, 1988.

(19) Ranganathan, S.; McCreery, R. L. *Anal. Chem.* **2001**, *73*, 893-900.

CHAPTER 3

MONITORING STRUCTURAL CHANGES OF ORGANIC MOLECULES BY IN SITU UV-VIS SPECTROELECTROCHEMISTRY

UV-vis spectroscopy has been used to monitor chemisorbed organic molecules on surfaces, but most measurements have been done with ultrathin metal films. Transmission mode UV-vis spectroscopy has been used to monitor the reversible trans ↔ cis photoisomerization of azobenzene-based self assembled monolayers on an ultrathin platinum film[1]. Kalyuzhny obtained the transmission UV/vis spectra of metalloporphyrin and metallophthalocyanine monolayers self-assembled on ultrathin gold films[2]. He also employed differential plasmon spectroscopy (DPS) in the transmission mode for the quantitative determination of molecular binding to a gold surface[3]. Covalent assemblies of siloxane-based stilbene derivatives on hydrophilic substrates (glass) formed high density monolayers, which have been used to investigate the intermolecular chromophore-chromophore interactions in the solid state by UV-vis spectroscopy[4]. To our knowledge, the current investigation is the first time that organic molecules on transparent carbon films have been observed by UV-vis spectroscopy.

By coupling a spectroscopic technique to an electrochemical experiment,

spectroelectrochemistry provides information on short-lived unstable intermediates which are unattainable with normal chemical synthesis. Optically transparent electrodes (OTE) have been used in UV-vis spectroelectrochemistry for several decades, and include thin metal film electrodes, indium-doped tin oxide (ITO) electrodes and metal mesh electrodes. The first UV-Visible transmission OTEs were invented by Kuwana[5-10] to study the reaction rates of electrochemical reactions occurring at or near an electrode surface. He applied tin oxide and thin film platinum electrodes in UV-vis spectroelectrochemistry to monitor the redox reactions of inorganic and organic molecules in an electrochemical cell. Subsequently, UV/VIS/NIR spectroelectrochemistry has been widely used to identify intermediates and products of electrochemical reactions[11-54]. UV/vis spectroelectrochemistry also offers new routes to characterization of kinetics and mechanism of redox reactions[55-66]. Oligothiophene thin films undergo reversible morphology changes in different redox states, which was supported by UV-vis spectroelectrochemical observations of Oligothiophene thin films on transparent Au electrodes[67]. The electrochemical reduction mechanism of ethidium bromide was investigated by fluorescence and UV-vis spectroelectrochemistry[68]. Using optically transparent indium tin oxide (ITO)-coated glass and gold mesh as electrodes, the quantitative time dependences of oxidation states in polypyrrole layers was monitored by UV-vis spectroelectrochemistry during redox cycling[66]. In situ UV-vis spectroscopy has been used to determine the reduction sites in a porphyrin-viologen donor-acceptor diad[55]. Recently, diamond OTEs have been invented to provide another

electrode substrate for spectroelectrochemical investigation in both the UV-vis and IR regions[69].

The transparent PPF electrodes are both optically transparent and conductive. The surface of transparent PPF electrodes can be modified by diazonium salt reduction to form covalently bonded monolayer or multilayer. The objective of the current experiments is applying transparent PPF electrodes in UV-vis spectroelectrochemistry to investigate the structural changes of organic molecules under applied potentials. Structural changes of molecules as a function of applied potential provide indisputable evidence that molecules rearrange in response to applied bias. In addition, the correlation between structural changes and applied potentials provides insights into the conduction mechanism. In this chapter, the first example of chemisorbed organic monolayer and multilayer on optically transparent carbon electrodes has been shown. In situ spectral monitoring of reactive intermediates resulted from electron transfer process has been investigated.

3.1 Experimental

Spectra calculation

The effect of the quartz and PPF substrates on UV-vis spectra were calculated by Filmstar Version 2.30 (FTG Software Associates, Princeton, NJ). The optical constants of quartz substrate were calculated from the transmission spectra of quartz (Figure 2.1), which was taken by a double beam Perkin-Elmer

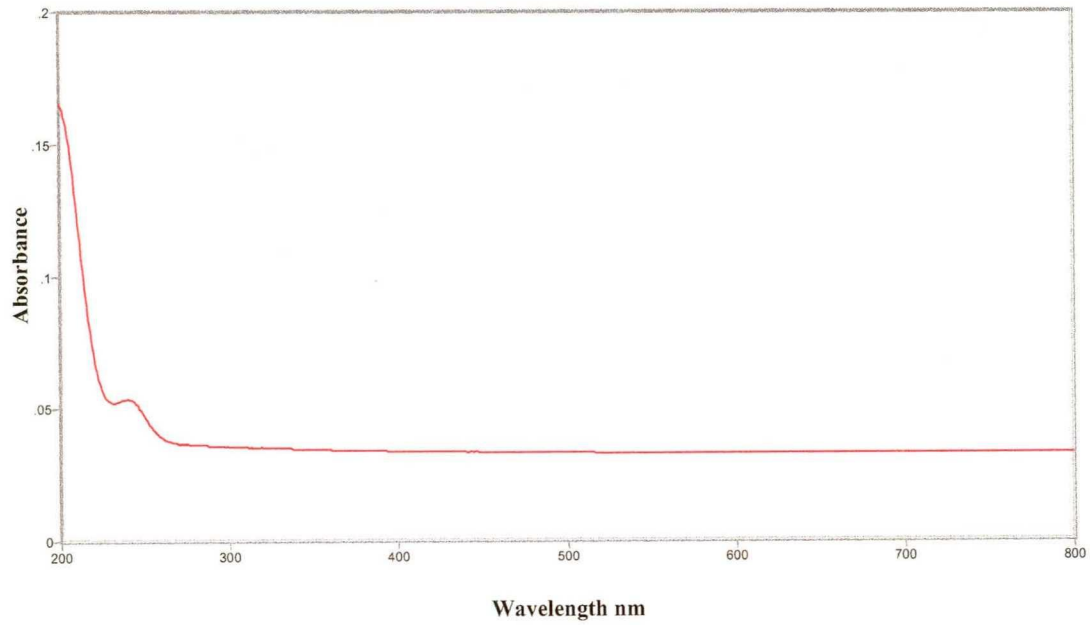

Figure 3.1 UV-vis spectrum of quartz.

Lambda 900 UV/VIS/NIR spectrometer. The FilmStar program INDEX was used to calculate the refractive index and extinction coefficient of the quartz substrate. Algorithm 5 was employed, in which extinction coefficient was set to be zero. The optical constants of the quartz substrate with a wavelength interval of 50 nm are listed in Table 3.1. Since PPF and glassy carbon have similar structures, the optical constants of glassy carbon were used for PPF. The optical constants of glassy carbon were reported by Arakawa[70]. Table 3.2 lists the optical constants of glassy carbon in the range of 190-830 nm. The refractive indices of 4-nitroazobenzene are 1.68 for a 1.9 nm thick NAB and 1.88 for a 4.5 nm thick NAB at 632.8 nm wavelength, which were measured by a discrete wavelength ellipsometer (PhE-101, Micro Photonics Inc.). The measured thickness of NAB on transparent PPF electrode under certain derivatization condition (4 cycles of cyclic voltammetry of 1 mM NAB diazonium salt from +0.4 V to -0.6 V with a scan rate of 0.2 V/s) is 3.961±0.686 nm (Chapter 2). The variations of refractive indices of organic films in the range of 200-800 nm are generally not large. Therefore, refractive index of NAB was set to be a constant value of 1.88 for a 4 nm thick NAB in the range of 200-800nm. The exponential decay relationship of light intensity I with extinction coefficient k is shown:

$I = I_0 e^{-\alpha z}$ (1)

$\alpha = \frac{4\pi k}{\lambda}$ (2)

In which, I is light intensity, I_0 is initial light intensity, α is absorption coefficient, z is propagation depth, λ is wavelength, and k is extinction coefficient. Chemists

λ (nm)	n	k
200	2.52875	0
250	1.59365	0
300	1.48193	0
350	1.47115	0
400	1.46357	0
450	1.45869	0
500	1.45477	0
550	1.4519	0
600	1.44989	0
650	1.44769	0
700	1.44572	0
750	1.44441	0
800	1.44297	0

Table 3.1 Optical constants of quartz.

λ (nm)	n	k
192	1.18	2.80E-01
207	1.13	4.15E-01
226	1.17	6.10E-01
249	1.33	7.54E-01
262	1.42	7.59E-01
276	1.51	7.64E-01
311	1.64	7.23E-01
355	1.68	6.81E-01
414	1.73	6.78E-01
497	1.78	6.96E-01
622	1.87	7.39E-01
829	1.94	8.16E-01

Table 3.2 Optical constants of glassy carbon (PPF)[70].

more commonly use Beer's Law, $A = \varepsilon b c$ (3), in which A is absorbance, ε is molar extinction coefficient, b is the length of the path through which the light travels in the sample, c is the concentration of the material that absorbs the light. The formula of extinction coefficient is deduced from equations (1), (2) and (3).

$$k = \frac{2.303\varepsilon c\lambda}{4\pi} \quad (4)$$

The extinction coefficients of NAB as a function of wavelength were calculated from molar extinction coefficient ε, which were calculated from the absorption spectrum of 0.1 mM NAB solution in cyclohexane. c in formula (4) is the NAB film concentration. $C_{film} = (1000 * \Gamma) / (d * 0.00000001)$, in which Γ is the surface coverage calculated by integration of the cyclic voltammogram of reduction of 1 mM NAB diazonium salt in 0.1 M TBATFB/ACN. The thickness of the NAB film is 37 Å when the surface coverage has a value of 4×10^{-10} moles/cm^2. The NAB film concentration was calculated to be 1.0811 mole/L. Table 3.3 lists the refractive indices and extinction coefficients of NAB with the wavelength interval of 50 nm. In order to calculate k for NAB from the solution spectrum, it is assumed that the absorption spectrum is the same in both solution and in a thin film. Finally, FilmStar was used to predict the absorption of Quartz/PPF/NAB samples from the refractive indices and extinction coefficients of quartz, PPF and NAB, in the range of 200-800nm. UV-vis spectral calculations were performed by FilmStar DESIGN, Side 2 compensation (FWD include side 2) was considered during the calculation.

λ (nm)	n	k
200	1.88	1.04E-01
250	1.88	2.05E-02
300	1.88	8.79E-02
350	1.88	1.30E-01
400	1.88	2.60E-03
450	1.88	5.68E-03
500	1.88	3.86E-03
550	1.88	7.21E-04
600	1.88	5.38E-05
650	1.88	3.22E-05
700	1.88	1.42E-05
750	1.88	9.60E-06
800	1.88	9.48E-06

Table 3.3 Optical constants of 4-nitroazobenzene (NAB).

UV-vis spectroscopy

The UV-vis spectra were taken by a double beam Perkin-Elmer Lambda 900 UV/VIS/NIR spectrometer (PerkinElmer Inc., Boston, MA). The chemisorbed NAB, AB and NBP were prepared by electrochemical reduction of corresponding diazonium tetrafluoroborate salts on transparent PPF electrodes as described in chapter 2. The modified transparent PPF electrodes were rinsed with acetonitrile and dried by high purity argon. 0.1 mM NAB, AB and NBP solutions were prepared in cyclohexane (Aldrich). A 1 cm thick quartz cell was used as the sample container for all UV-vis measurements involving a solution. Thin films of solid NAB, AB and NBP were prepared by dissolving the solid NAB, AB and NBP in anhydrous ether (99.9 % assay, Fisher Chemicals), then adding the NAB, AB and NBP solutions drop wise onto a clean quartz, then air-drying the sample between drops until a thin film formed. Air was always used as a reference to obtain absorption spectra. Spectral subtractions and overlays were carried out by Grams AI software, version 6.00 (Galactic Industries, Salem, N.H.). Since each PPF electrode is optically unique, each PPF electrode was measured by UV-vis before modification. The UV-vis spectra of chemisorbed NAB, AB and NBP were obtained by subtracting the spectrum of each individual PPF electrode from the spectrum of the same PPF electrode after surface modification.

UV-vis spectroelectrochemistry

In situ spectroelectrochemical experiments were performed on a double beam Perkin-Elmer Lambda 900 UV/VIS/NIR spectrometer (PerkinElmer Inc.,

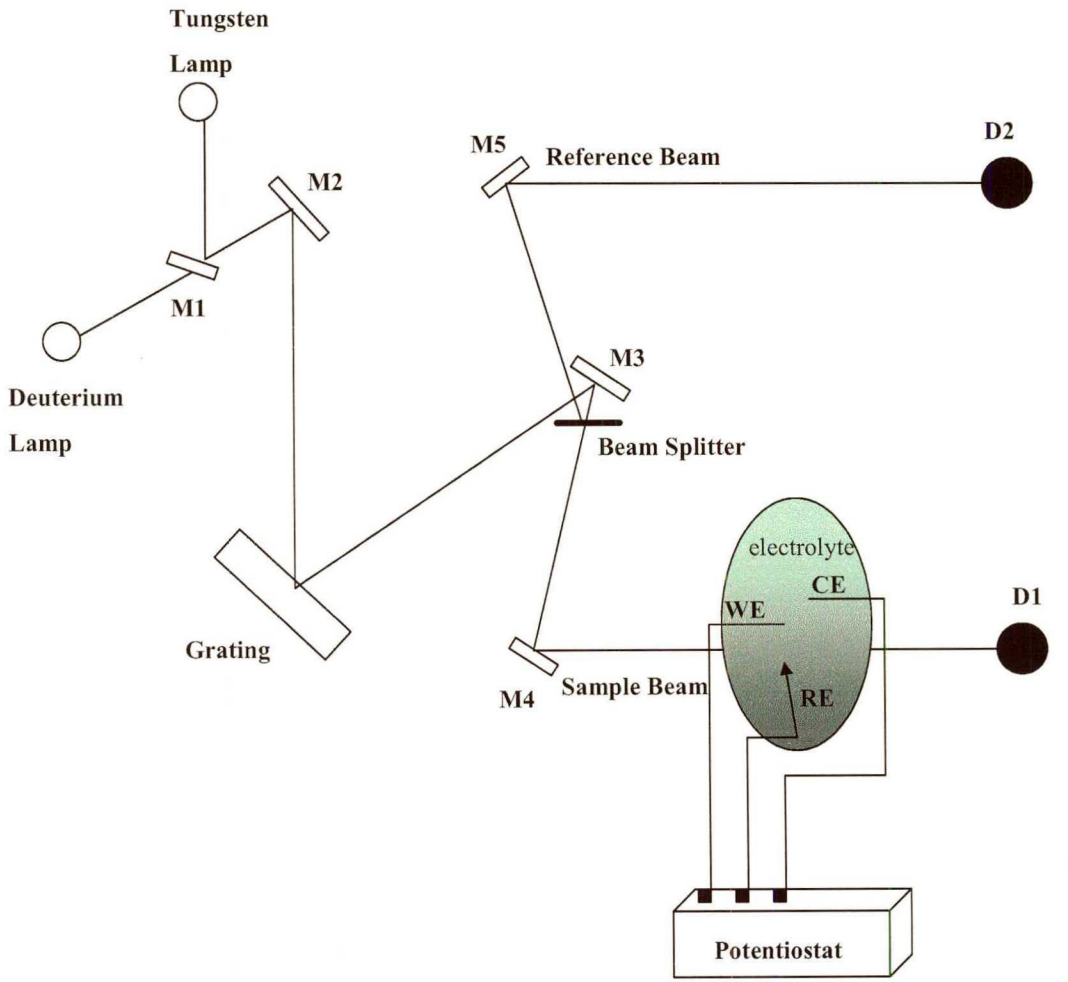

Figure 3.2 Schematic diagram of a UV-vis spectroelectrochemical system, in which WE is working electrode, RE is reference electrode, CE is counter electrode.

Boston, MA) and a BASi Epsilon-EC potentiostat (Bioanalytical Systems, Inc., West Lafayette, IN). Figure 3.2 shows a schematic diagram of a computer controlled UV-vis spectrometer and a computer controlled potentiostat system coupled to a quartz-made electrochemical cell. A piece of transparent PPF electrode (design 2 described in chapter 2) was inserted into the electrochemical cell with a 0.5 cm path length. It was adjusted to be perpendicular to the light path and the center part of the PPF is in the light path. An Ag+ (0.01 M)/Ag reference electrode (BAS) and a Pt wire auxiliary electrode were also inserted into the electrochemical cell, and the positions of these two electrodes were adjusted to avoid interference with the light beam. When monitoring free molecules, 0.1 mM NAB (Aldrich), AB (Aldrich) and NBP (Aldrich) with *n*-tetrabutylammonium tetrafluoroborate (0.1 M; Aldrich) in acetonitrile as the supporting electrolyte were added into the electrochemical cell respectively, and the bare transparent PPF was used as the working electrodes. When monitoring chemisorbed molecules, NAB, AB and NBP were derivatized on transparent PPF electrodes by electrochemical reduction of corresponding diazonium tetrafluoroborate salts as described in chapter 2. The modified transparent PPF electrodes were used as working electrodes. 0.1 M *n*-tetrabutylammonium tetrafluoroborate (Aldrich) in acetonitrile (Aldrich) was used as electrolyte solution. Controlled potential electrolysis (CPE) was applied by a BASi Epsilon-EC potentiostat. Solutions were degassed thoroughly by high purity argon before electrochemical experiments, and the electrochemical cell was protected by dry N_2 continuously during the experiment. Spectra subtraction and overlay were

carried out by Grams AI, version 6.00 (Galactic Industries, Salem, NH). The UV-vis spectrum of each PPF electrode in electrolyte solution was measured at the beginning of each experiment. The UV-vis spectra of NAB, AB or NBP as free molecules in solution were obtained by subtracting the spectra of PPF electrode in electrolyte solution from the spectra of PPF electrode in NAB, AB or NBP solutions. The UV-vis spectra of NAB, AB or NBP as chemisorbed molecules on PPF electrodes were obtained by subtracting the spectra of PPF electrode in electrolyte solution from the spectra of NAB, AB or NBP modified PPF electrode in electrolyte solution. The subtraction removes the contributions from windows, electrode (quartz and PPF) and electrolyte solution. The UV-vis spectra were taken 6 minutes after the potential was applied, which allowed the electrochemical system to equilibrate. The potential was held while the spectrum was acquired. Air was used as reference for all the spectral measurements.

3.2 Results

3.2.1 Calculated UV-vis spectra

The UV-vis spectrum of transparent PPF on quartz calculated with FilmStar using the optical constants listed in section 3.1 is shown in Figure 3.3. The thickness of the PPF was determined to be 9.1 nm, which generated a calculated spectrum with transmissions closest to the experimental spectra. There are two absorption peaks at 248 nm and 275 nm, which may correspond to the absorption of quartz and PPF respectively. Figure 3.4 shows the UV-vis

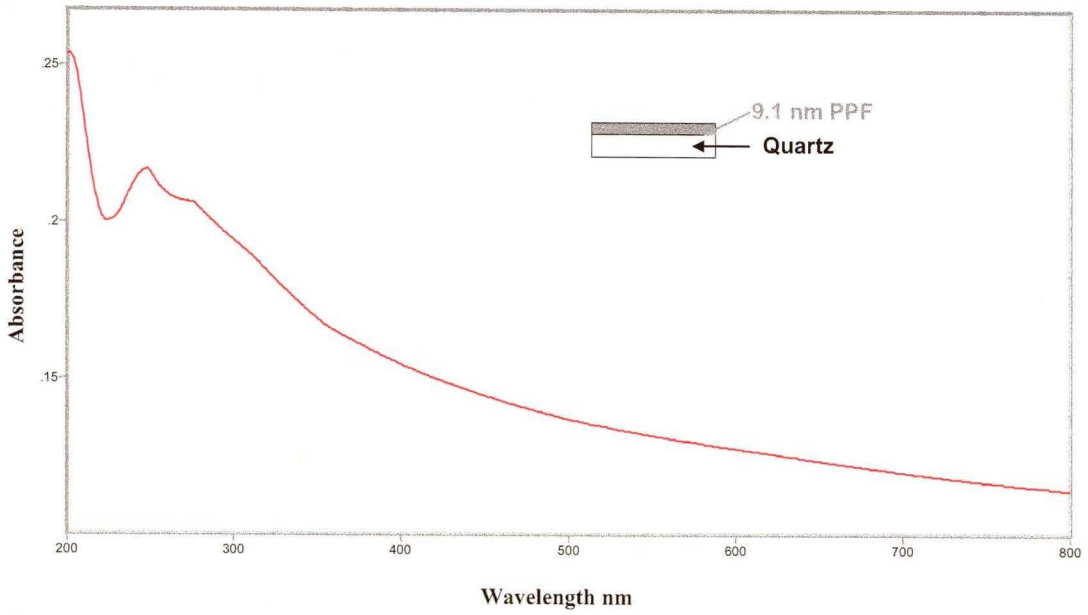

Figure 3.3 UV-vis spectrum of transparent PPF on quartz, the thickness of PPF is 9.1 nm.

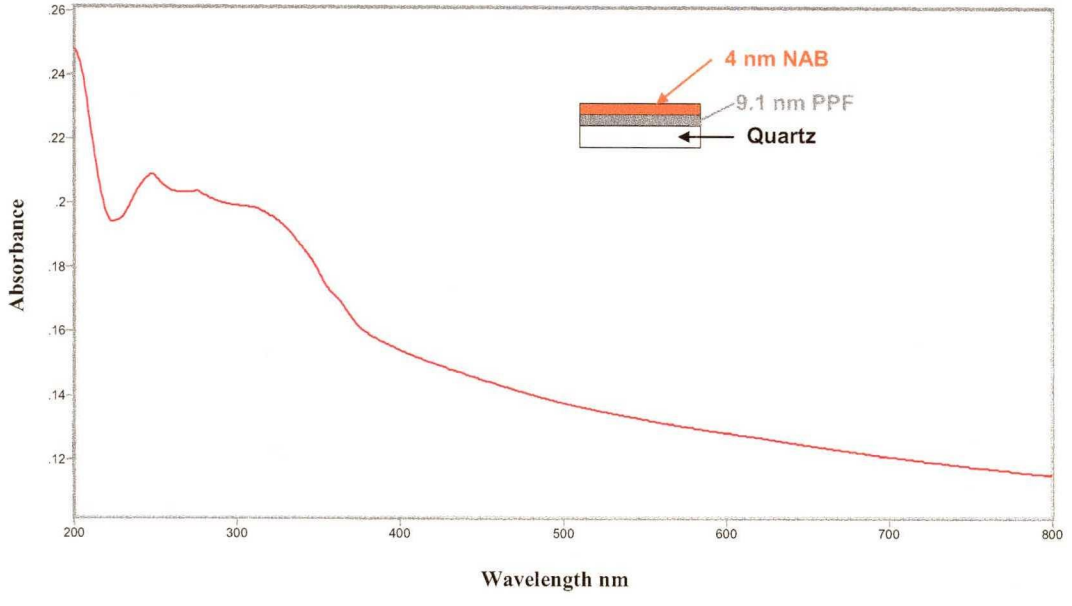

Figure 3.4 UV-vis spectrum of 4 nm NAB with transparent PPF on quartz.

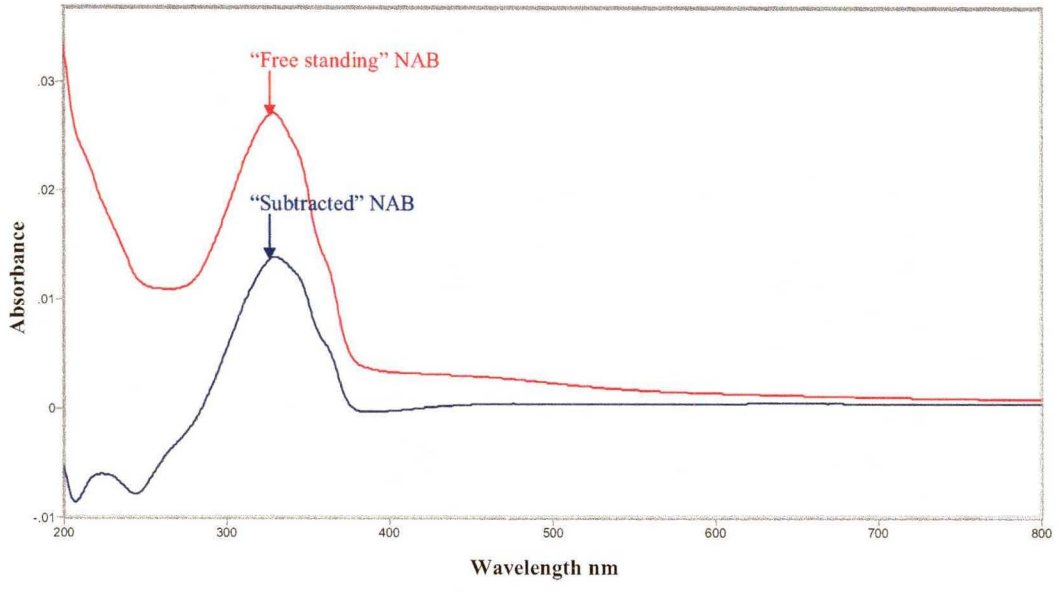

Figure 3.5 The overlaid spectra of "subtracted" NAB and "free standing" NAB.

spectrum of a 4 nm thick NAB film on transparent PPF on quartz. Subtraction of the spectrum of transparent PPF in Figure 3.3 from the spectrum of 4 nm thick NAB on PPF in Figure 3.4, the "subtracted" spectrum of NAB in Figure 3.5 is obtained. "Free standing" NAB denotes the spectrum of a 4 nm thick NAB film calculated with FilmStar. Figure 3.5 indicates that the absorbance of the "subtracted" NAB is lower than that of "free standing" NAB, but the peak positions of the maximum absorption are similar.

3.2.2 UV-vis spectroscopy of organic molecules

Diazonium salts of 4-nitroazobenzene (NAB), azobenzene (AB) and 4-nitrobiphenyl (NBP) were used to produce PPF modified with thin layers of NAB, AB and NBP. UV-vis spectra of chemisorbed NAB, AB and NBP are shown in Figure 3.6. These spectra were obtained by subtracting the spectrum of each individual PPF electrode from the spectrum of the same PPF electrode after surface modification. The UV-vis spectra of NAB, AB and NBP modified PPF electrodes and their original unmodified PPF electrodes are shown in Figure 3.7, 3.8 and 3.9. The wavelengths of maximum absorbance of chemisorbed NAB, AB and NBP were 356, 340 and 325 nm respectively (Figure 3.6), corresponding to the π-π^* transitions. Compared to AB, NAB has a longer conjugated system due to the nitro group, and a smaller HOMO-LUMO gap (Table 3.4), which correspond to the longer wavelength of the maximum absorption. Compared to NAB and AB, NBP has larger HOMO-LUMO gap, and is less conjugated because the phenyl rings in the molecule are twisted with respect to each other

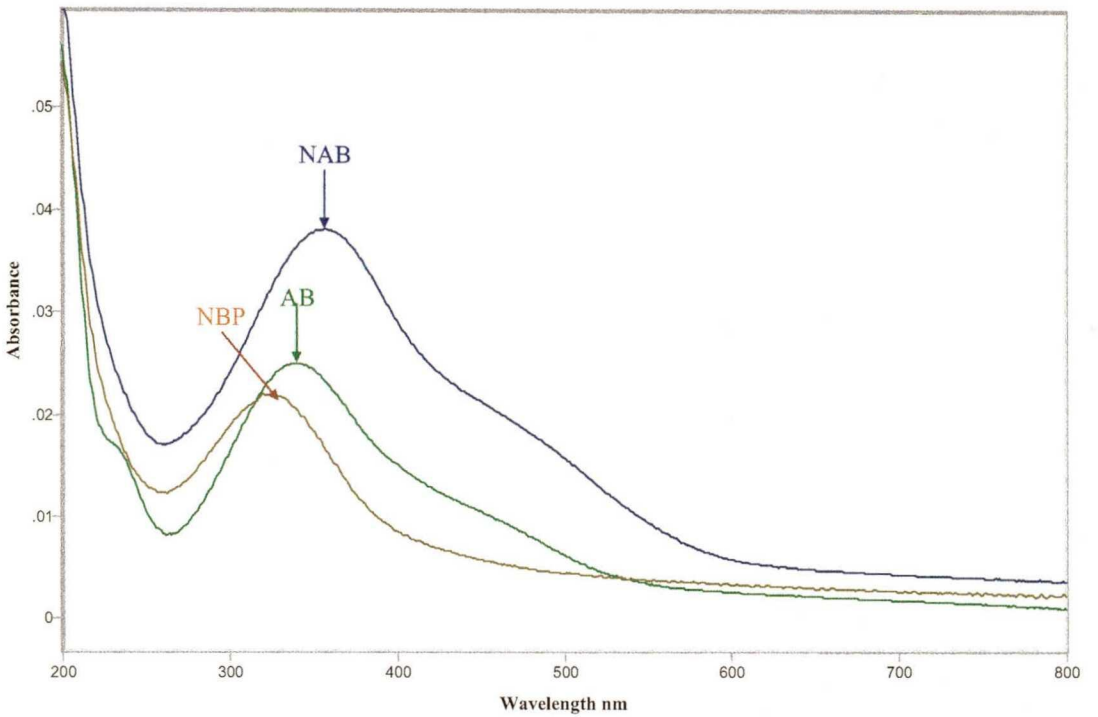

Figure 3.6 UV-vis spectra (overlaid) of chemisorbed NAB, AB and NBP, which were obtained by subtracting the spectra of bare transparent PPF from the spectra of organic molecules modified transparent PPF.

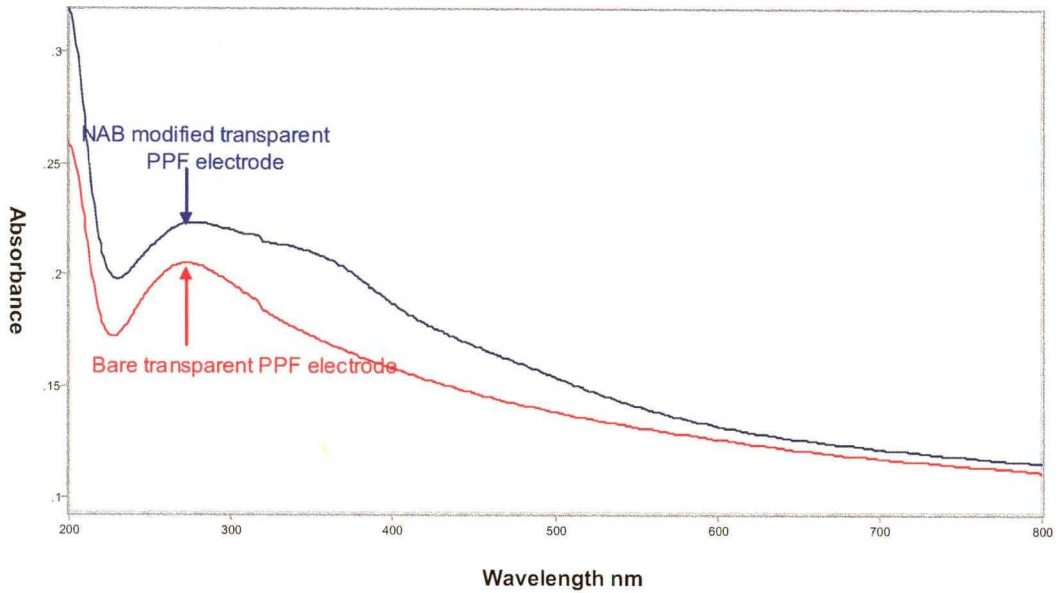

Figure 3.7 UV-vis spectra of a NAB modified transparent PPF electrode and its original unmodified transparent PPF electrode.

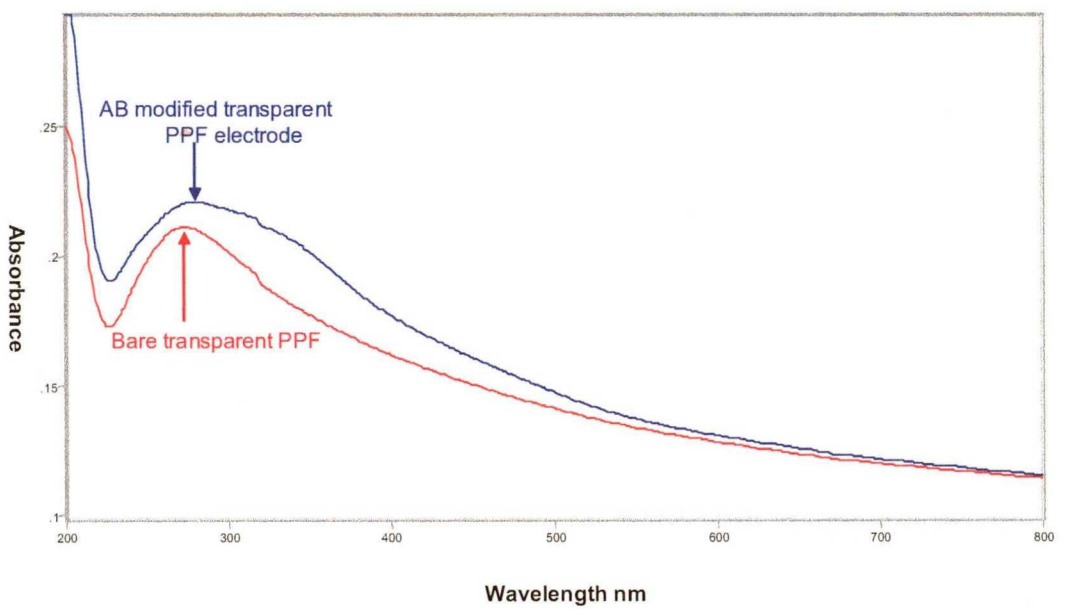

Figure 3.8 UV-vis spectra of an AB modified transparent PPF electrode and its original unmodified transparent PPF electrode.

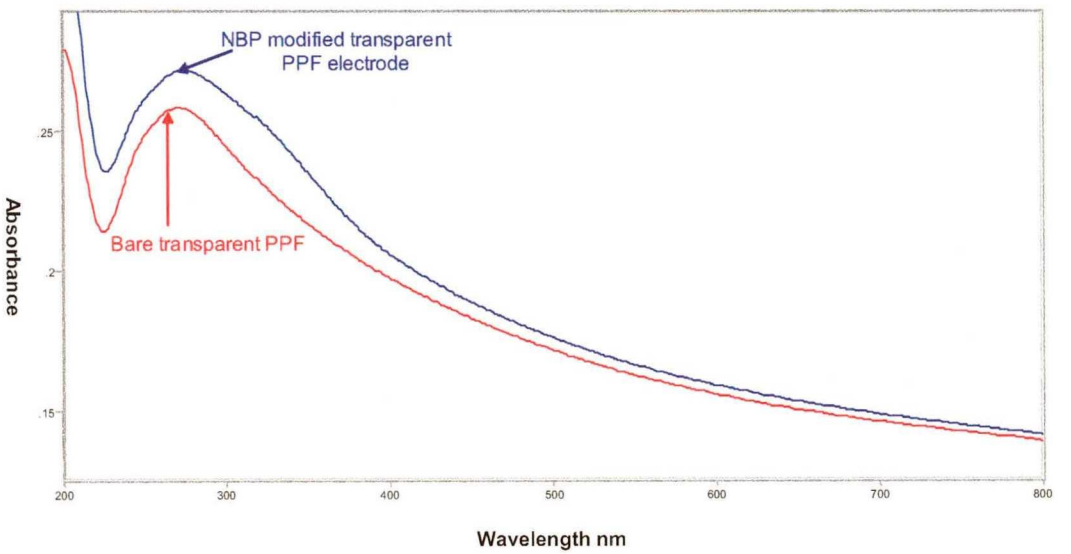

Figure 3.9 UV-vis spectra of a NBP modified transparent PPF electrode and its original unmodified transparent PPF electrode.

Molecule	HOMO-LUMO Gap (eV)
NAB	3.549
AB	3.951
NBP	4.254

Table 3.4 The HOMO-LUMO gaps of NAB, AB and NBP calculated by Gaussian.

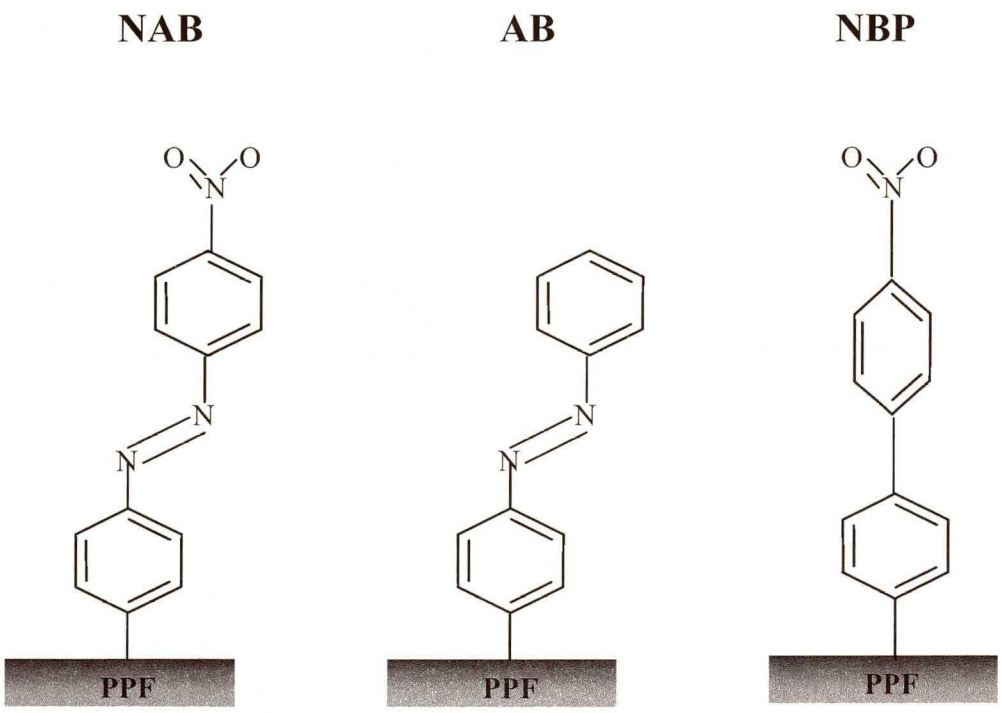

Figure 3.10 Chemical structures of NAB, AB and NBP.

(Figure 3.10). Therefore, NBP has the shortest wavelength of maximum absorption, as predicted from HOMO-LUMO gap.

The UV-vis absorption spectra of 0.1 mM NAB, AB and NBP in cyclohexane are shown in Figure 3.11. The maximum absorptions of NAB, AB and NBP appeared at 330, 316 and 296nm respectively, which correspond to the π-π^* transitions in the molecules. The absorption peaks of NAB and AB at about 450 nm may due to the n-π^* transitions in the molecules. Peak absorbencies of NAB, AB and NBP at the same concentration indicate molar extinction coefficients ε in the order NAB > AB > NBP. Large ε values occur for more probable transitions. Since the n-π^* transition is "symmetry forbidden", it is less intense than the π-π^* transition.

Figure 3.12 shows the UV-vis absorption spectra of thin films of solid NAB, AB and NBP on quartz. The maximum absorptions of NAB, AB and NBP appeared at 336, 320 and 312 nm respectively, which correspond to the π-π^* transitions in the molecules.

The UV-vis spectra of NAB in the chemisorbed, solution and solid forms are shown in Figure 3.13, with similar comparisons for AB and NBP shown in Figure 3.14 and Figure 3.15 respectively. The peak absorption wavelengths of NAB, AB and NBP in different states are listed in Table 3.5. Compared to molecules in solution, molecules in solid state show small red shifts of the maximum absorption, which is presumably due to the increased MO interaction and planarity of molecules in solid state leading to a reduced HOMO-LUMO gap. The maximum absorption peaks of chemisorbed NAB, AB and NBP show red

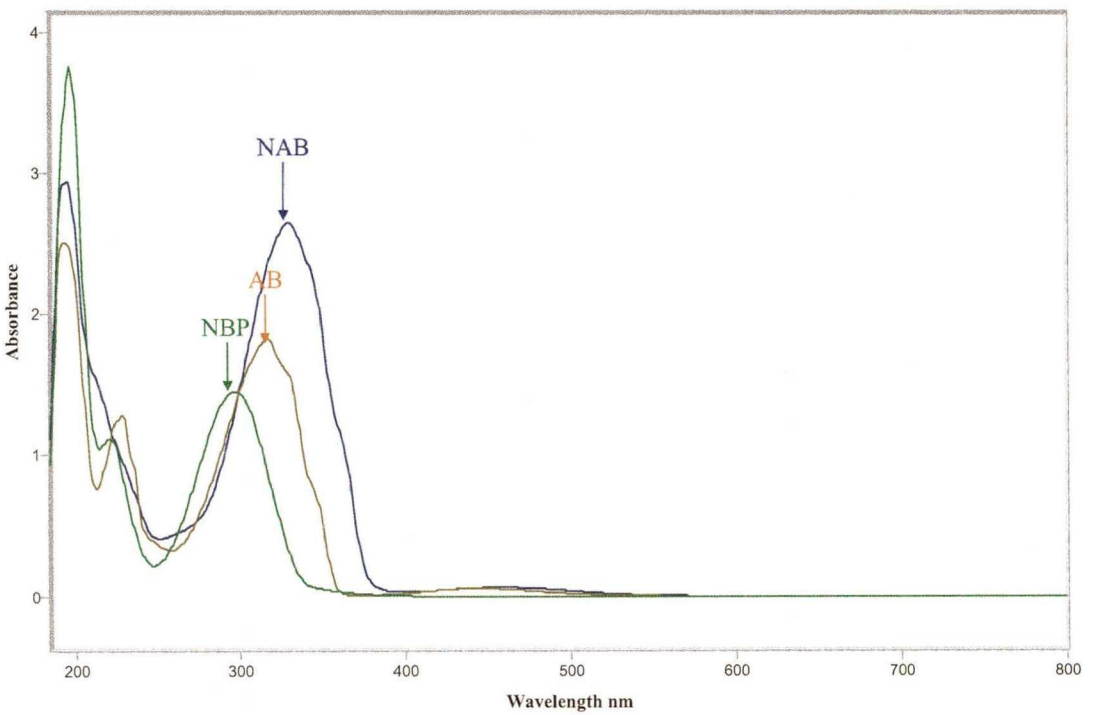

Figure 3.11 UV-vis spectra (overlaid) of 0.1 mM NAB, AB and NBP in cyclohexane.

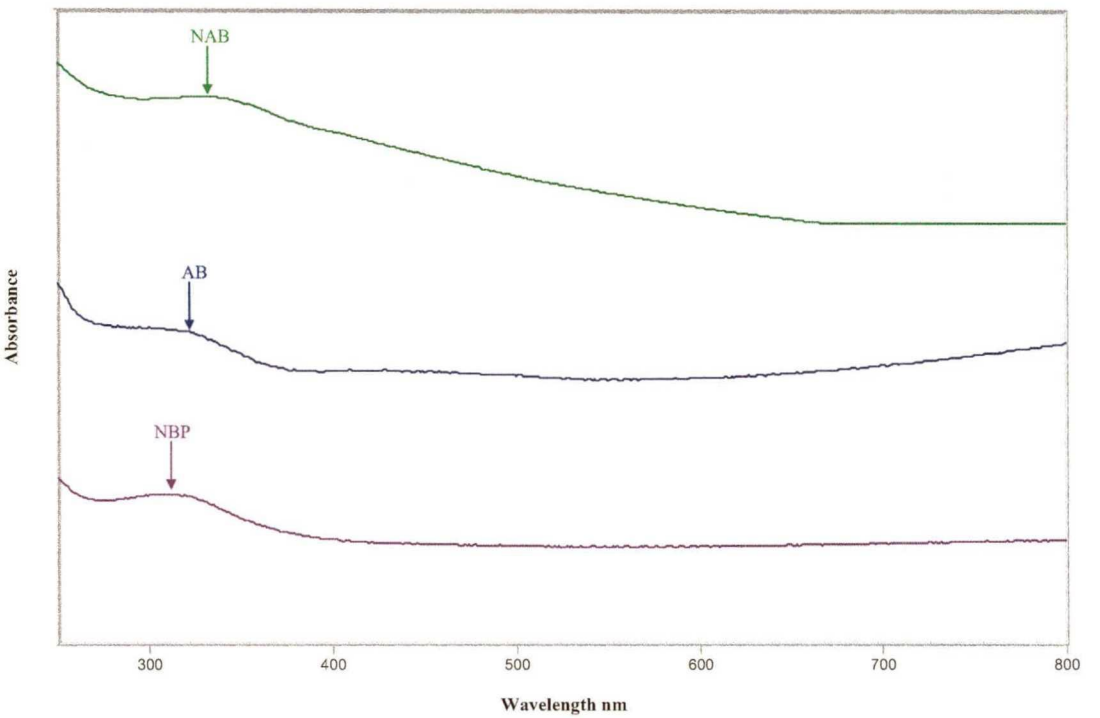

Figure 3.12 UV-vis spectra of solid NAB, AB and NBP films.

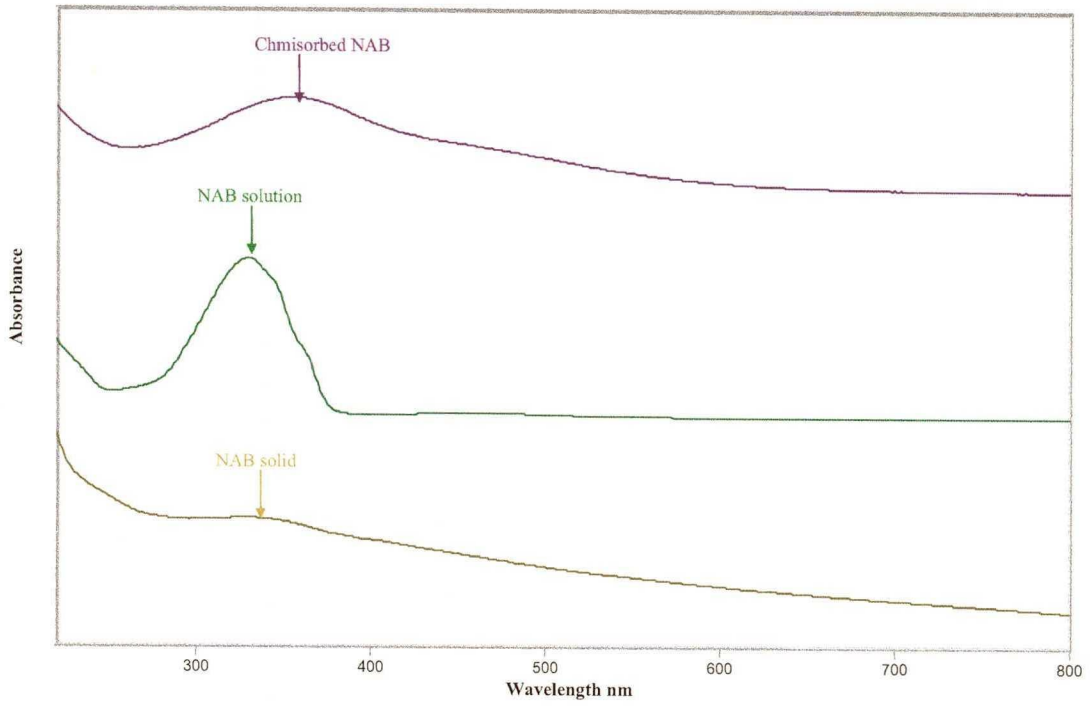

Figure 3.13 UV-vis spectra of chemisorbed NAB, NAB solution and solid NAB film.

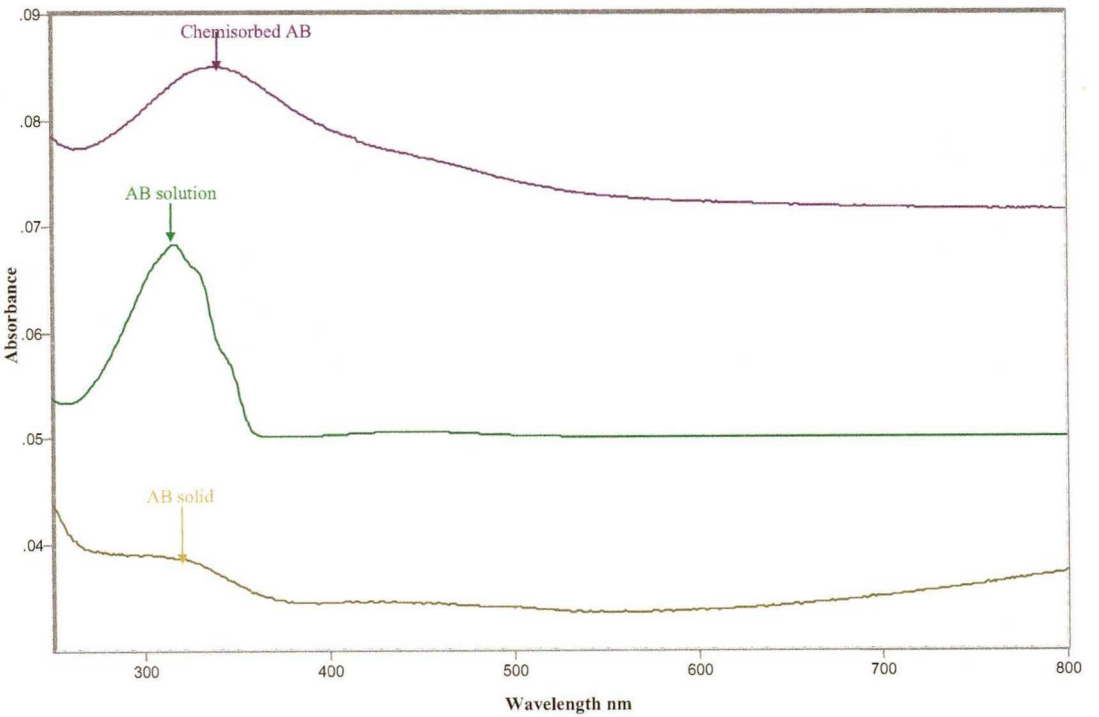

Figure 3.14 UV-vis spectra of chemisorbed AB, AB solution and solid AB film.

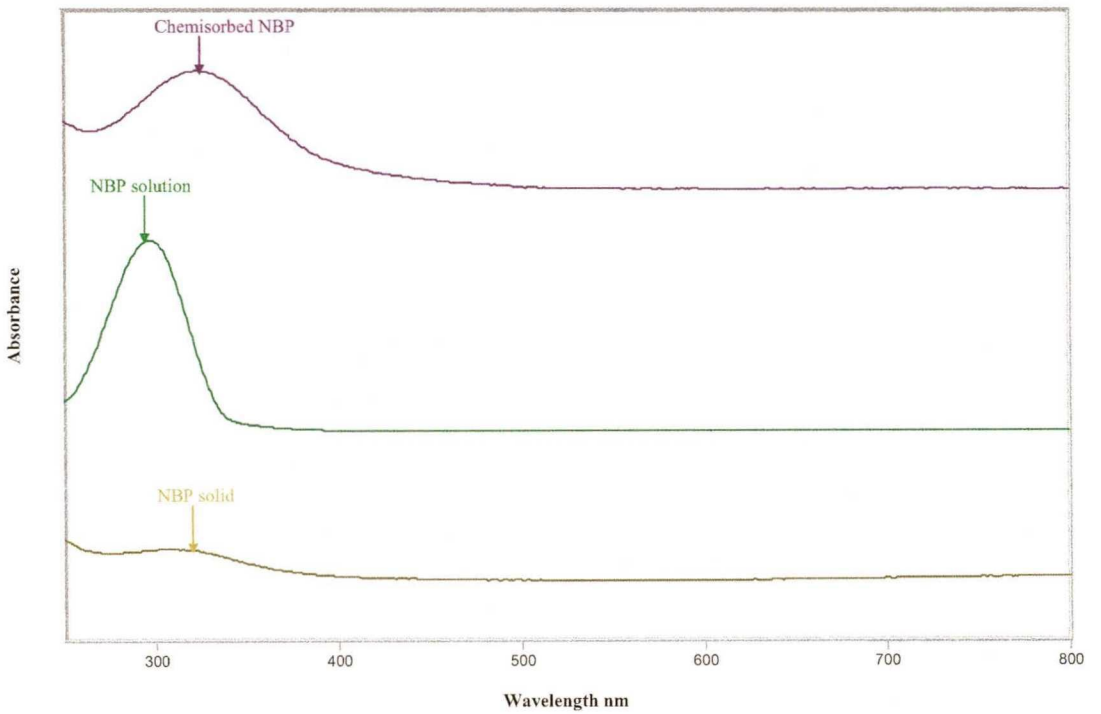

Figure 3.15 UV-vis spectra of chemisorbed NBP, NBP solution and solid NBP film.

Molecule	Chemisorbed	Solution (in C_6H_{12})	Solid
NAB	356 nm	330 nm	336 nm
AB	340 nm	316 nm	320 nm
NBP	325 nm	296 nm	312 nm

Table 3.5 UV-vis transition bands of NAB, AB and NBP in different states.

shifts relative to their corresponding bands in solution and solid states. This observation indicates that the red shifts are not only due to the stacking of molecules as they are in solid state, but also a strong interaction between the aryl groups and the carbon of PPF.

3.2.2 Structure changes of reduced organic molecules

The UV-vis spectroelectrochemical monitoring of 0.1 mM free NAB in 0.1M TBATFB/ACN solution was attempted using the transparent PPF electrode. Figure 3.16 shows the UV-vis spectra of free NAB under different applied potentials. For the first spectrum, 0 V was applied, and the maximum absorption peak appeared at 330 nm. For the second spectrum, -1.2 V was applied, and a new absorption peak appeared at 500 nm, while the intensity of the absorption peak at 330 nm decreased. For the third spectrum, 0 V was applied again, the intensity of the absorption peak at 500 nm decreased, and the intensity of the absorption peak at 330 nm increased. Compared to the first spectrum, the absorbance at 330 nm for the third spectrum is weaker than that of the first spectrum. For the fourth spectrum, -1.2 V was applied, and an absorption peak appeared at 490 nm, the intensity of absorption peak at 330nm decreased

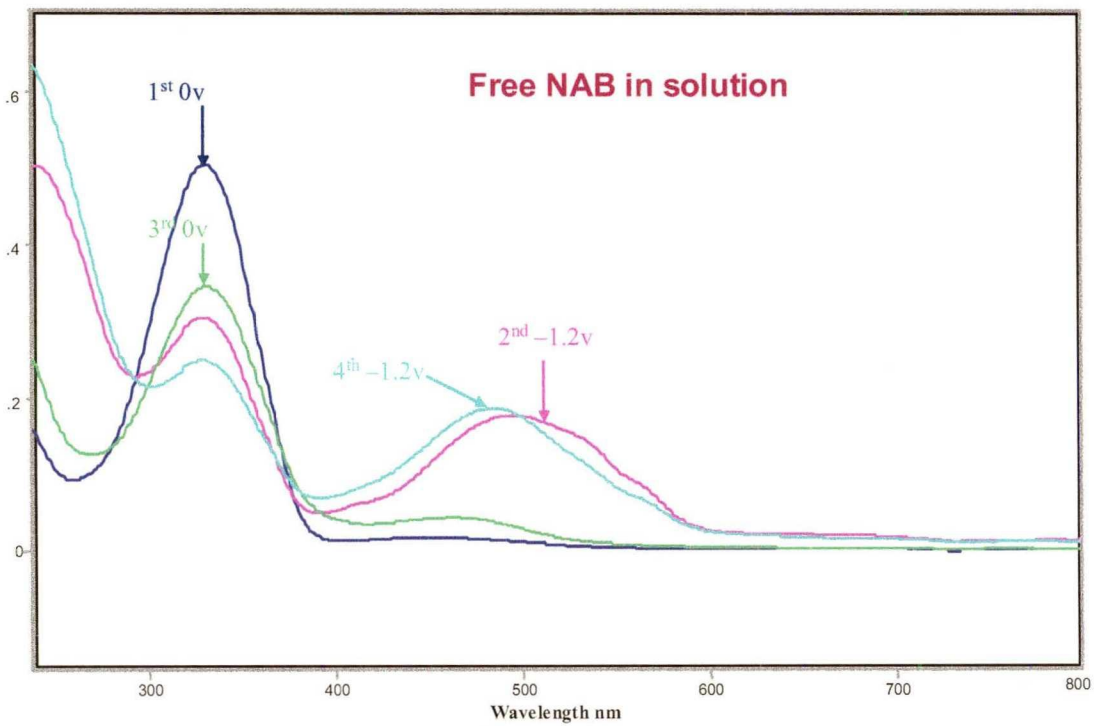

Figure 3.16 UV-vis spectra (overlaid) of free NAB under different applied potentials, which were obtained by subtracting the spectra of a bare transparent PPF electrode in 0.1 M TBATFB/ACN solution from the spectra of a transparent PPF electrode in 0.1 mM free NAB of 0.1 M TBATFB/ACN solution.

again. The absorption peaks at 330 nm and 500 nm correspond to electronic transitions of NAB and its reduction product respectively. These two peaks could be increased and decreased for at least two redox cycles.

Figure 3.17 shows the UV-vis spectra of the spectroelectrochemical experiment of chemisorbed NAB on a transparent PPF electrode in 0.1 M TBATFB/ACN solution. For the first spectrum, 0 V was applied, the maximum absorption peak appeared at 356 nm. For the second spectrum, -1.2 V was applied, a new absorption peak appeared at 502 nm, and the absorption peak at 356 nm vanished. For the third spectrum, 0 V was applied, the absorption peak at 502 nm disappeared, the absorption peak at 330 nm reappeared. Compared to the spectra of the first spectrum, the intensity of absorption peak at 330 nm in the third spectrum is weaker than that of the first spectrum. For the fourth spectrum, -1.2 V was applied, the peak at 502 nm reappeared, and the absorbance at 330 nm decreases significantly. The absorption peak at 356 nm and 502 nm correspond to electronic transitions of chemisorbed NAB and its reduction product respectively.

The UV-vis spectroelectrochemical experiment of chemisorbed NAB on a transparent PPF electrode in 0.1 M TBATFB/ACN solution was repeated over a wider potential range. Figure 3.18 shows the UV-vis spectra of chemisorbed NAB under different applied potentials. For the first spectrum, 0 V was applied, the maximum absorption peak appeared at 356 nm. For the second spectrum, -1.2 V was applied, a new absorption peak appeared at 502 nm, the intensity of absorption peak at 356 nm decreased significantly. For the third spectrum, 0 V

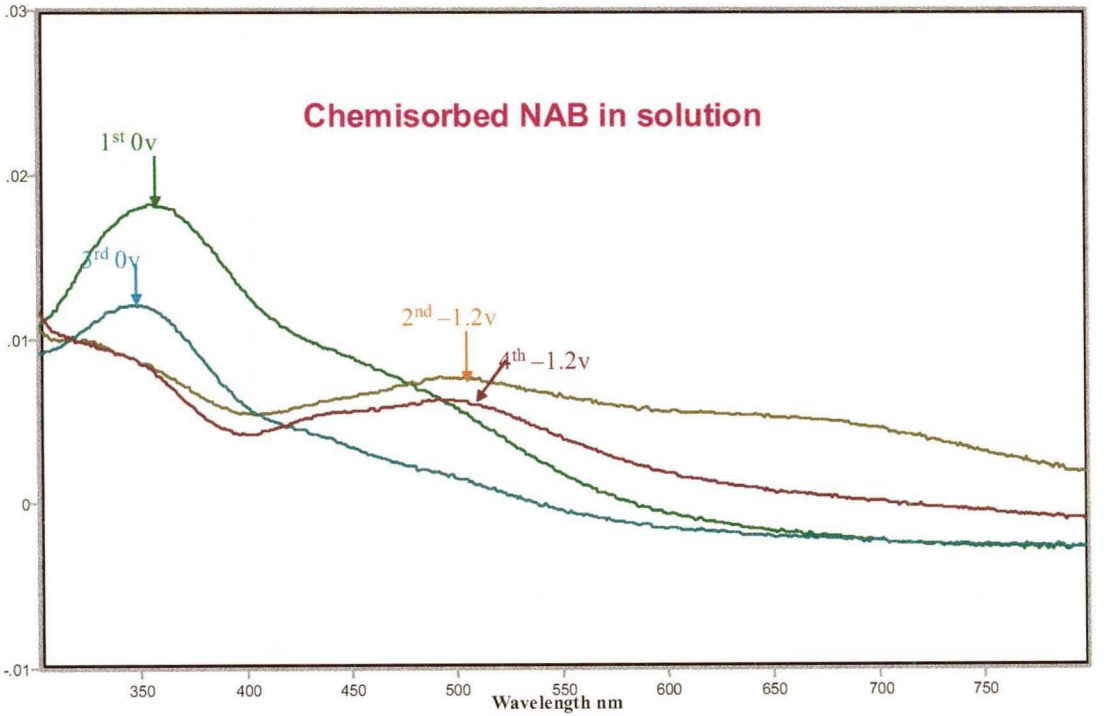

Figure 3.17 UV-vis spectra (overlaid) of chemisorbed NAB under different applied potentials, which were obtained by subtracting the spectra of a bare transparent PPF electrode in 0.1 M TBATFB/ACN solution from the spectra of a NAB modified transparent PPF electrode in 0.1M TBATFB/ACN solution.

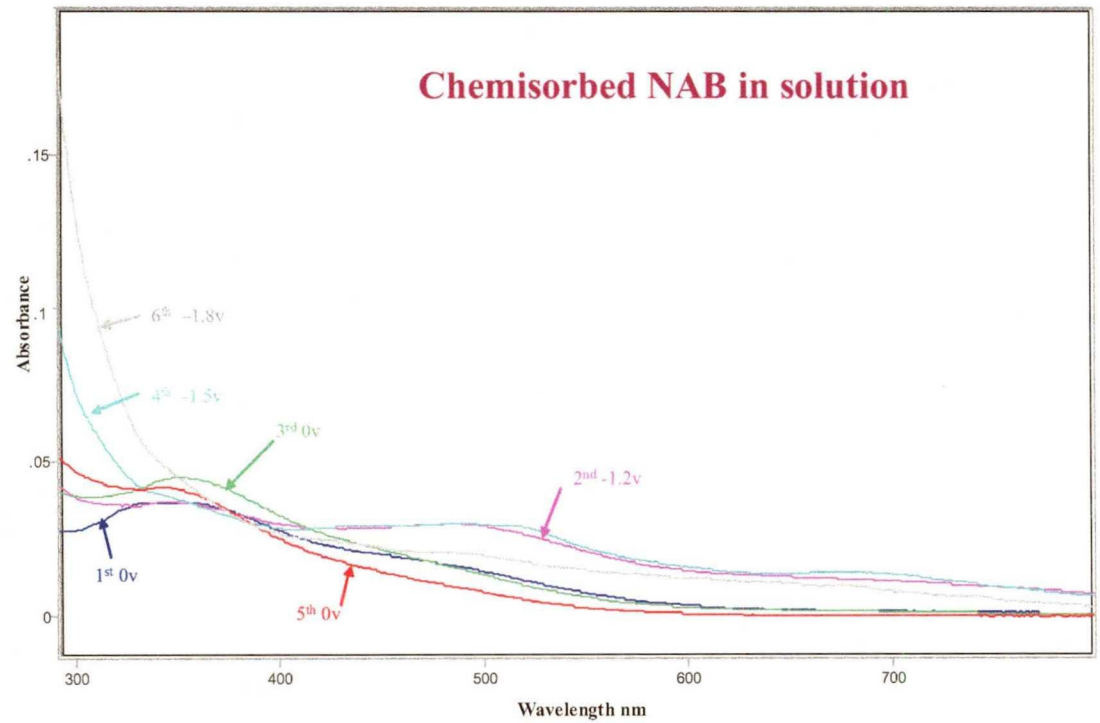

Figure 3.18 UV-vis spectra (overlaid) of chemisorbed NAB under wide potential range, which were obtained by subtracting the spectra a bare transparent PPF electrode in 0.1 M TBATFB/ACN solution from the spectra of a NAB modified transparent PPF electrode in 0.1 M TBATFB/ACN solution.

was applied, the absorption peak at 502 nm vanished, the absorption peak at 356 nm reappeared, as was noted previously. For the fourth scan, -1.5 V was applied, the maximum absorption peak appeared at 522 nm, the absorption peak at 356 nm vanished. For the fifth scan, 0 V was applied, the absorption peak at 522 nm vanished, the absorption peak at 356 nm reappeared. For the sixth scan, -1.8 V was applied, a weak absorption peak appeared at 490 nm, and the absorption peak at 356 nm vanished.

The spectra obtained from the UV-vis spectroelectrochemical experiment of 0.1 mM free AB in 0.1 M TBATFB/ACN solution are shown in Figure 3.19. The absorbance at 316 nm decreased and a new peak at 422 nm appeared when negative potentials were applied. These changes are partially reversible when the potential is returned to 0 V. The decrease at 316 nm and increase at 422 were comparable at both -1.8 V and -2.0 V.

Figure 3.20 depicts the UV-vis spectroelectrochemical responses of chemisorbed AB on a transparent PPF electrode in 0.1 M TBATFB/ACN. A shoulder appeared at 470 nm when negative potentials were applied (-1.0 V). The absorbance at 335 nm changed slightly with applied potentials.

Figure 3.21 shows the UV-vis spectral changes of free NBP at different applied potentials. When negative potentials applied (-1.4 V), a weak peak appeared at 526 nm and the peak at 326 nm blue shifted slightly accompanying an increase in absorbance.

The in situ UV-vis spectroelectrochemical behaviors of chemisorbed NBP on a transparent PPF electrode in 0.1 M TBATFB/ACN solution are shown in

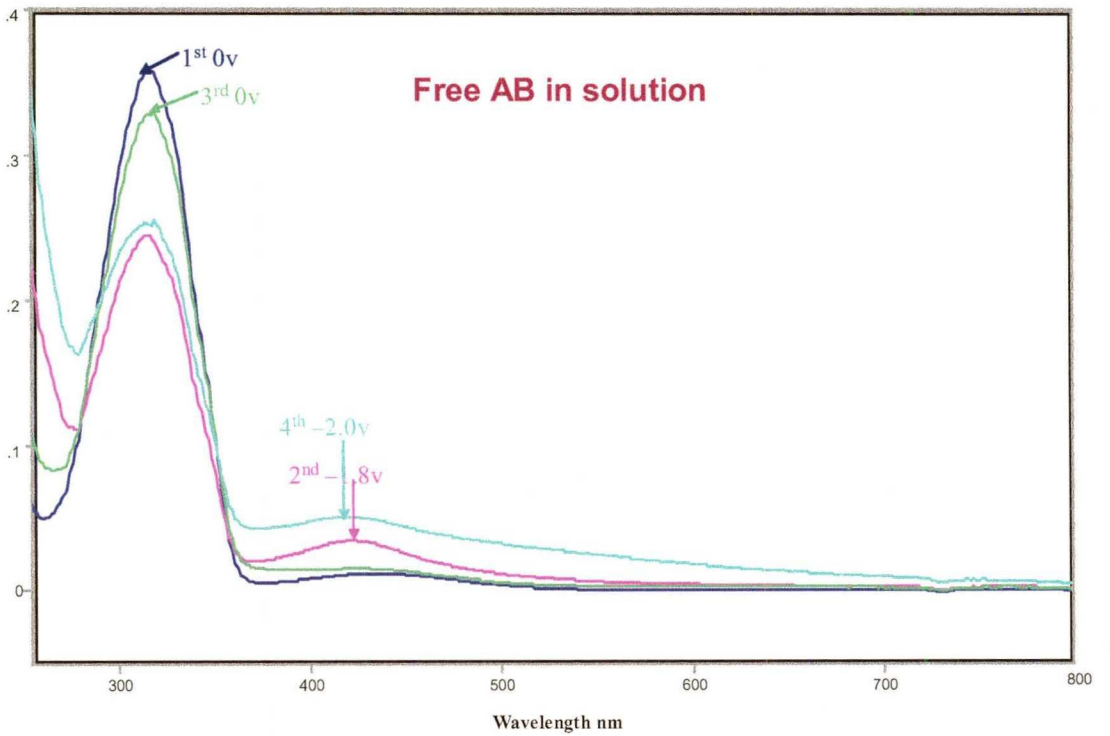

Figure 3.19 UV-vis spectra (overlaid) of free AB under different applied potentials, which were obtained by subtracting the spectra of a bare transparent PPF electrode in 0.1 M TBATFB/ACN solution from the spectra of a transparent PPF electrode in 0.1 mM free AB of 0.1 M TBATFB/ACN solution.

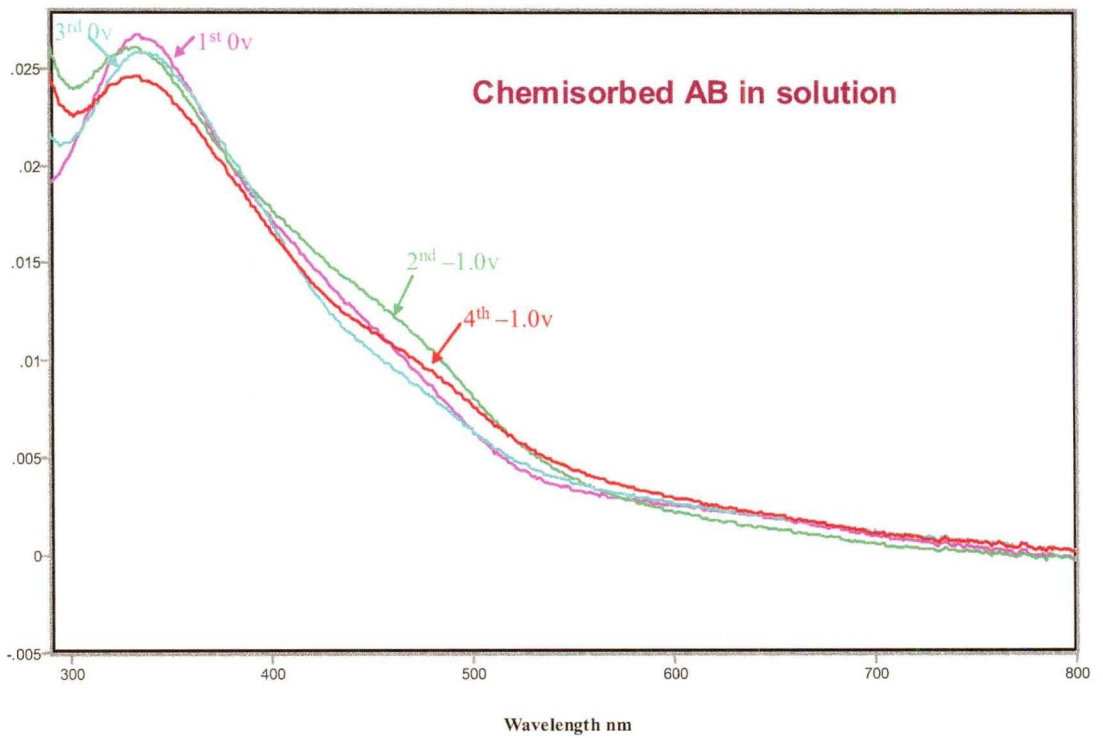

Figure 3.20 UV-vis spectra (overlaid) of chemisorbed AB under different applied potentials, which were obtained by subtracting the spectra of a bare transparent PPF electrode in 0.1M TBATFB/ACN solution from the spectra of an AB modified transparent PPF electrode in 0.1 M TBATFB/ACN solution.

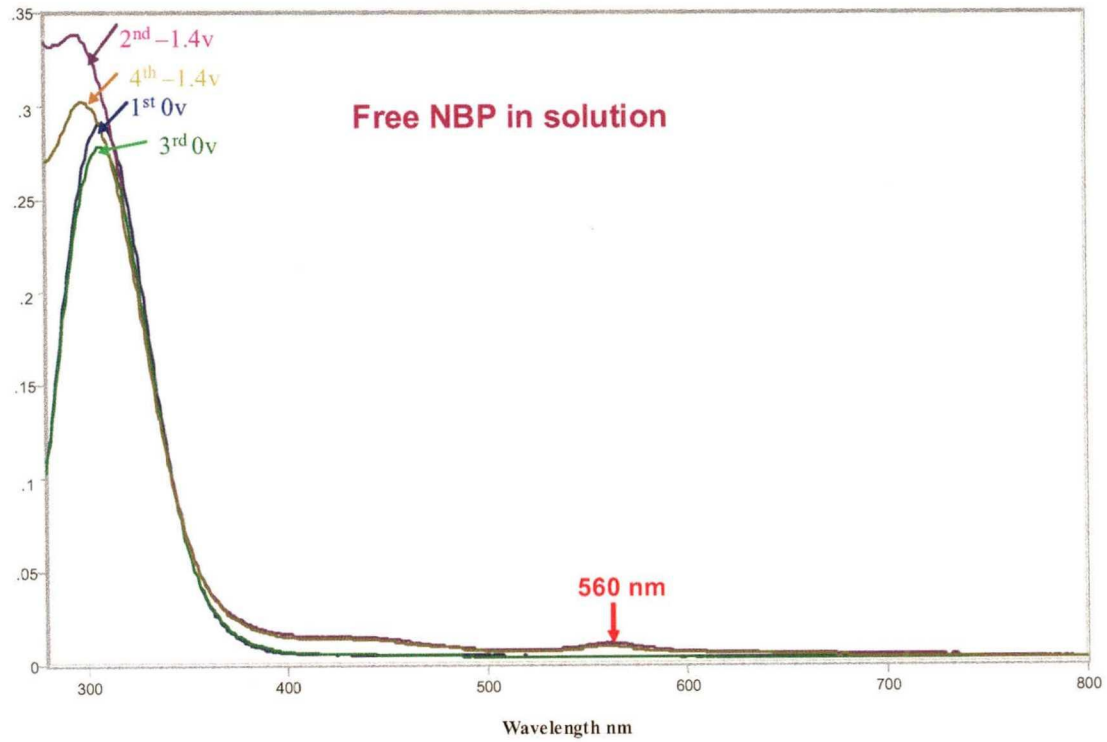

Figure 3.21 UV-vis spectra (overlaid) of free NBP, which were obtained by subtracting the spectra of a transparent PPF electrode in 0.1 M TBATFB/ACN solution from the spectra of a transparent PPF electrode in 0.1 mM NBP of 0.1 M TBATFB/ACN solution.

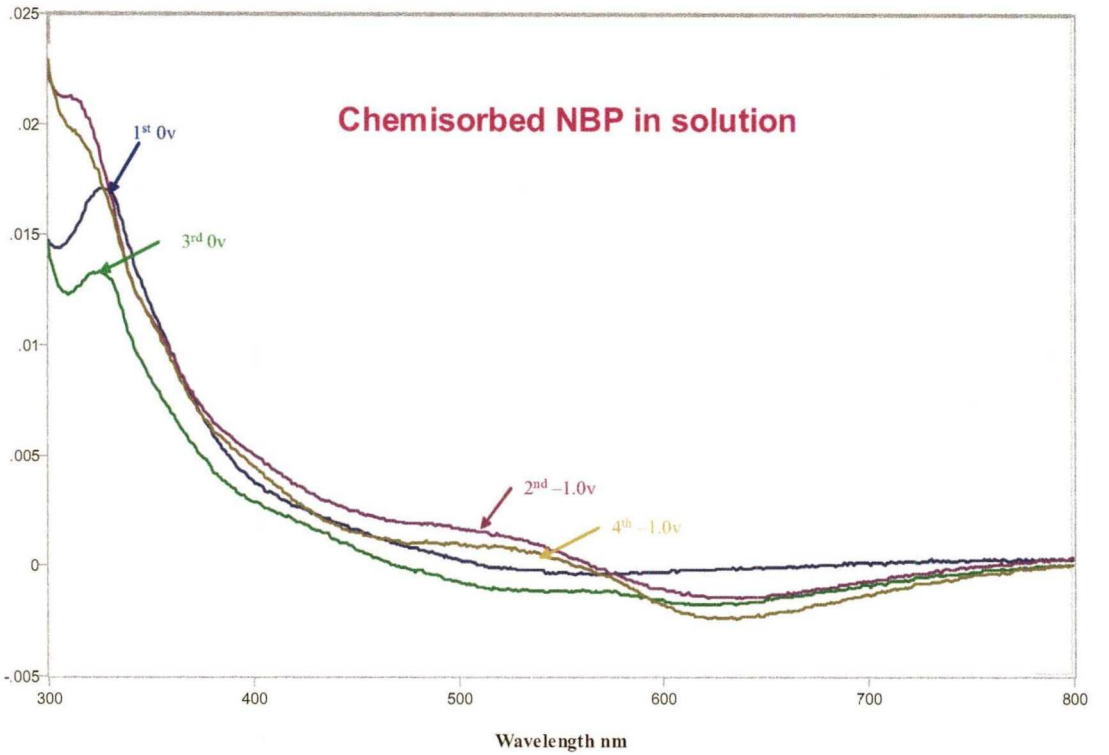

Figure 3.22 UV-vis spectra (overlaid) of chemisorbed NBP under different applied potentials, which were obtained by subtracting the spectra of a bare transparent PPF electrode in 0.1M TBATFB/ACN solution from the spectra of a NBP modified transparent PPF electrode in 0.1 M TBATFB/ACN solution.

Figure 3.22. The absorption peak at 326 nm vanished and a new peak at 526 nm appeared when negative potentials were applied (-1.0 V).

The in situ UV-vis spectroelectrochemical behaviors of NAB, AB and NBP as both free molecules in solution and covalently bonded organic molecules on PPF electrodes are summarized in Table 3.6.

3.3 Discussion

Figure 2.8 in chapter 2 indicates that the experimental UV-vis spectra of transparent PPF vary from sample to sample, which is presumably due to variations in the thickness and uniformity of the PPF. The calculated and experimental UV-vis spectra of transparent PPF are shown in Figure 3.23. The thickness of the PPF was determined to be 9.1 nm, which generated a calculated spectrum with transmissions closest to the experimental spectra. Basically, they are similar especially in the range of 270-800 nm. Figure 3.24 shows the calculated and experimental UV-vis spectra of 4 nm thick NAB film on a transparent PPF electrode. The experimental spectra are the UV-vis spectra of chemisorbed NAB on a transparent PPF electrode. The calculated spectra are the UV-vis spectra predicted by FilmStar for a 4 nm NAB film on PPF film on quartz as the substrate. The calculated and experimental spectra are similar in shape but differ in magnitude. Figure 3.5 shows that the intensity of absorbance of the "subtracted" NAB is lower than that of "free standing" NAB, but the peak positions of the maximum absorption are the same, which indicates peak positions of the "subtracted" spectra of a molecular film can represent that of the

Molecule	$A^1(\lambda/V)$		$A^2(\lambda/V)$	$A^3(\lambda/V)$		$A^4(\lambda/V)$
NAB[a]	0.50(330nm/0V)	0.30(330nm/-1.2V)	0.17(500nm/-1.2V)	0.34(330nm/0V)	0.24(330nm/-1.2V)	0.18(490nm/-1.2V
NAB[b]	0.018(356nm/0V)		0.0076(502nm/-1.20V)	0.012(356nm/0V)		0.0061(502nm/-1.2V)
AB[a]	0.36(316nm/0V)	0.24(316nm/-1.8V)	0.030(422nm/-1.8V)	0.33(316nm/0V)	0.25(316nm/-1.2V)	0.050(422nm/-2.0V)
AB[b]	0.027(335nm/0V)	0.026(335nm/-1.0V)	0.011(470nm/-1.0V)	0.026(335nm/0V)	0.025(335nm/-1.0V)	0.010(470nm/-1.0V)
NBP[a]	0.29(308nm/0V)	0.34(296nm/-1.4V)	0.011(560nm/-1.4V)	0.28(308nm/0V)	0.30(299nm/-1.4V)	0.010(560nm/-1.0V)
NBP[b]	0.017(326nm/0V)		0.0013(526nm/-1.0V)	0.013(326nm/0V)		8E-5(526nm/-1.0V)

Table 3.6 In situ UV-vis spectroelectrochemical behaviors of NAB, AB and NBP. a stands for free molecules in solution. b stands for chemisorbed molecules on PPF electrodes. V is applied potential, λ is the wavelength of absorption peak when potential V is applied, A is the absorbance of the peak at wavelength λ. 1, 2, 3 and 4 are the order of obtaining spectra.

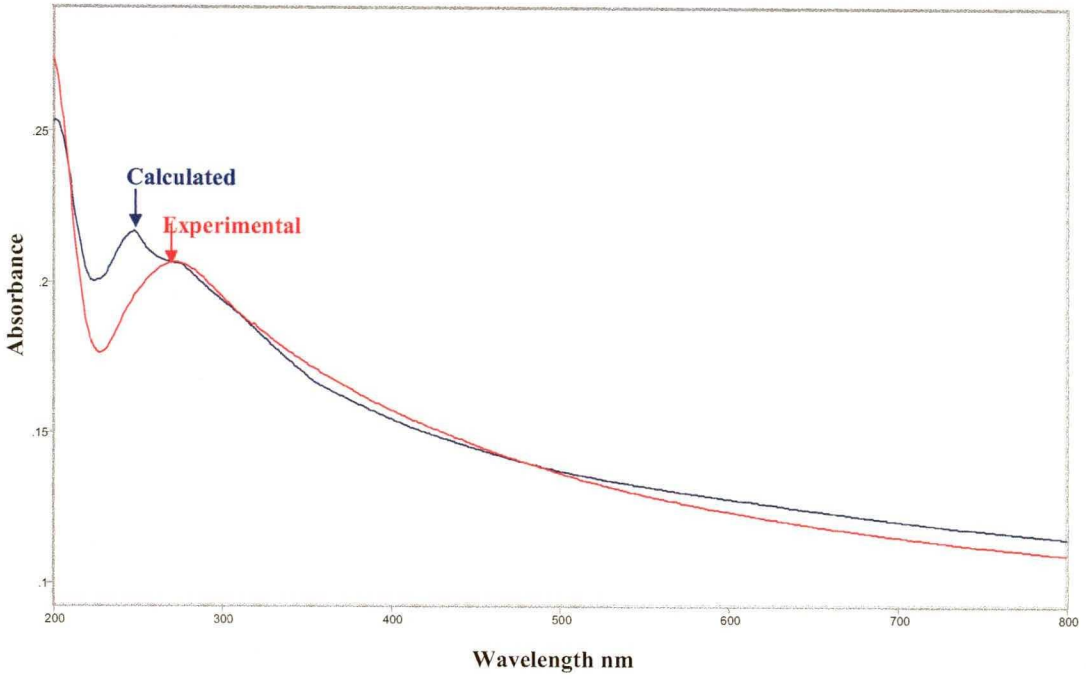

Figure 3.23 The calculated and experimental UV-vis spectra (overlaid) of transparent PPF.

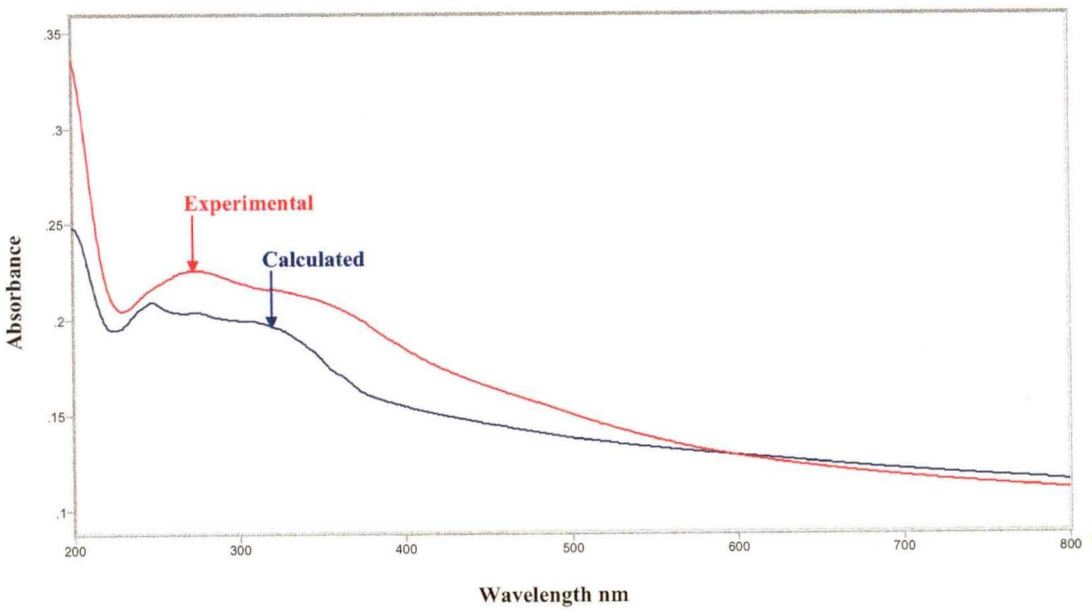

Figure 3.24 The calculated and experimental UV-vis spectra (overlaid) of 4nm thick NAB on a transparent PPF which include quartz as substrate.

same molecular film in "free standing" state.

The wavelengths of the maximum absorption are in the order NAB > AB > NBP for free molecules in solution, as solids, or chemisorbed (Table 3.5), and this is the order expected from their HOMO-LUMO gaps. The UV-vis absorption peaks of chemisorbed NAB, AB and NBP show red shifts relative to their corresponding bands as molecules in the solution or solid state. Chemisorbed NAB, AB and NBP form carbon-carbon bonds on the PPF surface. The strong interaction between the aryl group and the carbon of PPF extends the conjugated system. In solution, the phenyl rings are relatively freely rotating, which results in relatively short conjugation lengths. Compared to molecules in solution, molecules in solid state are closer to each other, such that intermolecular interactions and molecular planarity increase, possibly resulting in the small red shifts of the maximum absorption of molecules in solid state (Table 3.5).

For the UV-vis spectroelectrochemical experiments of free NAB, AB and NBP in solution, the second and fourth spectra have two absorption peaks (Figure 3.16, 3.19 and 3.21), with the absorbance at longer wavelength appearing upon electrochemical reduction. These absorption peaks are assigned to the mixture of the molecule and the reduced form of the molecule. The UV-vis spectroelectrochemical experiments of the third spectra were intended to oxidize the reduced molecules back to their original state. From the spectra of NAB and AB in solution, the maximum absorption of the third scan is weaker than that of the first scan, which indicates the redox process is not completely reversible. A possible reason is the interference of the residual O_2, which may react with the

electrogenerated products.

The calculated transitions of NAB, AB, NBP and their reduced species are listed in Table 3.7. The most likely component corresponding to the 500 nm absorption of reduced "free NAB" is the NAB anion radical, whose energy of radical-HOMO transition is 504.3 nm (Figure 3.25). This deduction is consistent with Moti's observation of the absorption peak of NAB radical anion in *i*-PrOH at 470 nm[71]. The NAB anion radical has also been detected by in situ Raman spectroelectrochemistry of free NAB being reduced by glassy carbon electrode[72]. The absorption peak of reduced AB at 422 nm is in good agreement with the LUMO-radical transition of azobenzene anion (420.6 nm, Figure 3.25), which is also consistent with Neta's observation of AB anion in THF solution at 430 nm[73]. The absorption peak observed for reduced free NBP (560 nm) is close to the calculated LUMO-radical transition of NBP anion (598.5 nm, Figure 3.25).

NAB, AB and NBP are capable of being reduced to their anion radical forms by negative potentials, and the structures of the anion forms are depicted in Figure 3.26. The reduction potentials of free NAB, AB and NBP solutions are -1.2 V, -1.8 V and -1.4 V respectively. The reduction potentials of AB and NBP are more negative than that of NAB, which indicates that AB and NBP are more difficult to reduce than NAB. Flamigni pointed out that the $-NO_2$ group increases the likelihood of a one-electron reduction[74]. It was found that electrons transfer into the nitro compounds via the nitro group and the reduction potential is determined by molecule's ability to delocalize the additional electron over the rest of the molecule. The reduction potentials of NAB and NBP are more positive than

Molecule	HOMO-LUMO Gap (nm)	Radical-HOMO Gap (nm)	LUMO-radical Gap (nm)
4-nitroazobenzene	349.5		
4-nitroazobenzene anion radial, restricted	298.4	504.3	730.9
4 nitro 4' azobenzene methide anion	588.3		
azobenzene	314.0		
azobenzene anion, restricted	241.2	565.7	420.6
azobenzene monomethide anion	488.1		
4-nitrobiphenyl (planar)	303.0		
4-nitrobiphenyl (37 dihedral)	291.7		
4-nitrobiphenyl anion restricted. 21 o dihedral)	236.8	391.8	598.5
4-nitrobiphenyl 4' methide anion (1.1 o dihedral)	633.1		

Table 3.7 Calculated band transitions of NAB, AB, NBP and their reduced species from Gaussian 98, B3LYP with 6-31 G (d) basis set.

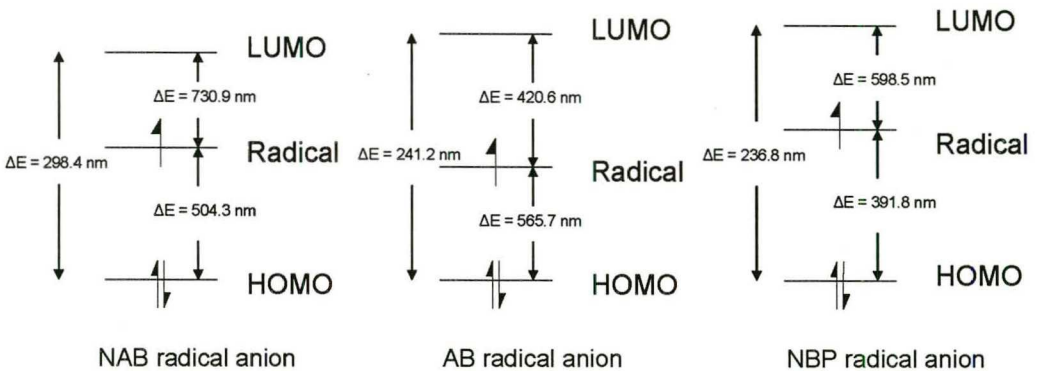

Figure 3.25 Electronic transitions of radical anions of NAB, AB and NBP.

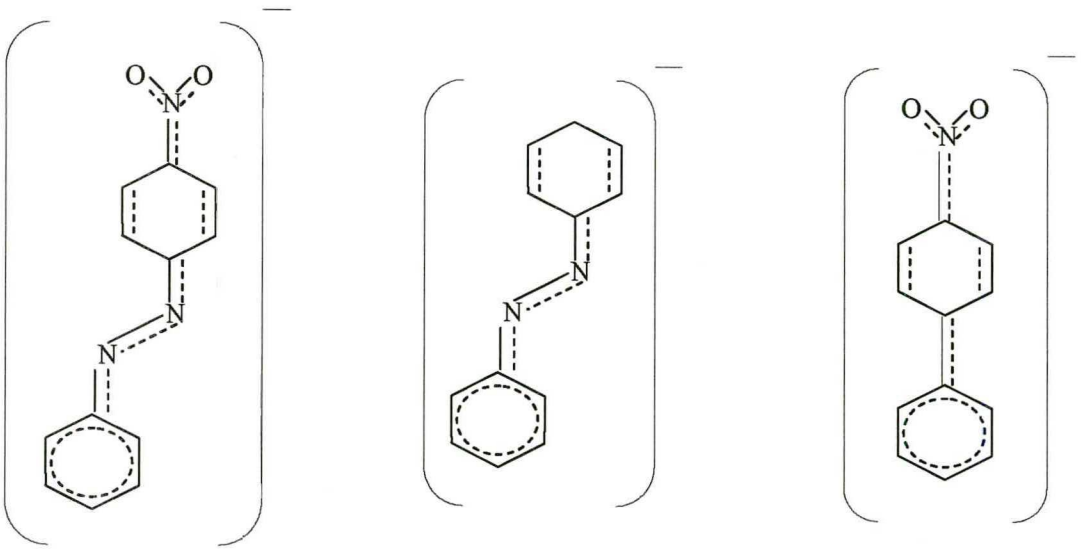

Figure 3.26 Structures of radical anions of NAB, AB and NBP.

that of AB due to their nitro substitutions. Comparing the molecular structures of NAB and NBP, electrons are more delocalized in NAB through the azo group and two phenyl rings. The two phenyl rings of NBP are twisted relative to each other, which results in less delocalization of electrons in the molecule.

NAB and NBP modified GC electrodes have been observed to exhibit "conductance switching" in electrolyte solution[72,75]. Raman spectra of reduced chemisorbed NAB are consistent with the formation of a methide structure containing a C=C double bond between the NAB and the graphitic surface[72]. NBP modified GC electrodes exhibit much faster electron transfer kinetics through the molecular layer after negative potential excursion which has been attributed to a structural change upon reduction[75]. The product of electron injection could be an anion radical or a methide, both of which have smaller HOMO-LUMO gaps than the parent NBP molecule. A smaller gap may yield faster electron transfer through the molecule, due to a decreased tunneling barrier. The switching behaviors of carbon based molecular electronic junctions of NAB and NBP have also been reported[76,77]. Therefore, it is likely for chemisorbed aromatic molecules to form their radical anion or methide anion under negative potentials. The methide anions of NAB, AB and NBP are depicted in Figure 3.27.

Compared to the reduction of free NAB, the reduction of chemisorbed NAB is more complete (Figure 3.28). The original peak of chemisorbed NAB almost vanished during the reduction. An absorption peak at 502 nm of reduced "chemisorbed NAB" was observed, which is close to the radical- HOMO transition

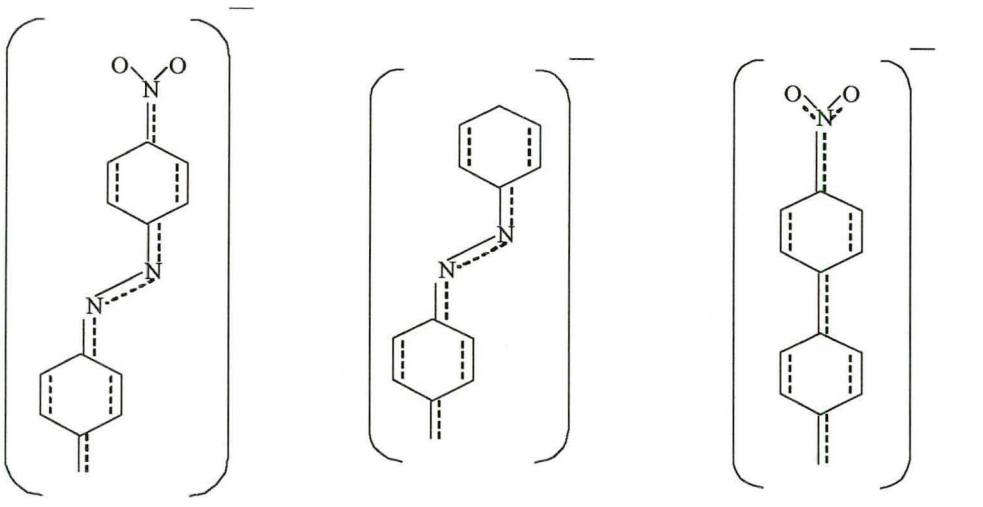

Figure 3.27 Structures of methide anions of NAB, AB and NBP.

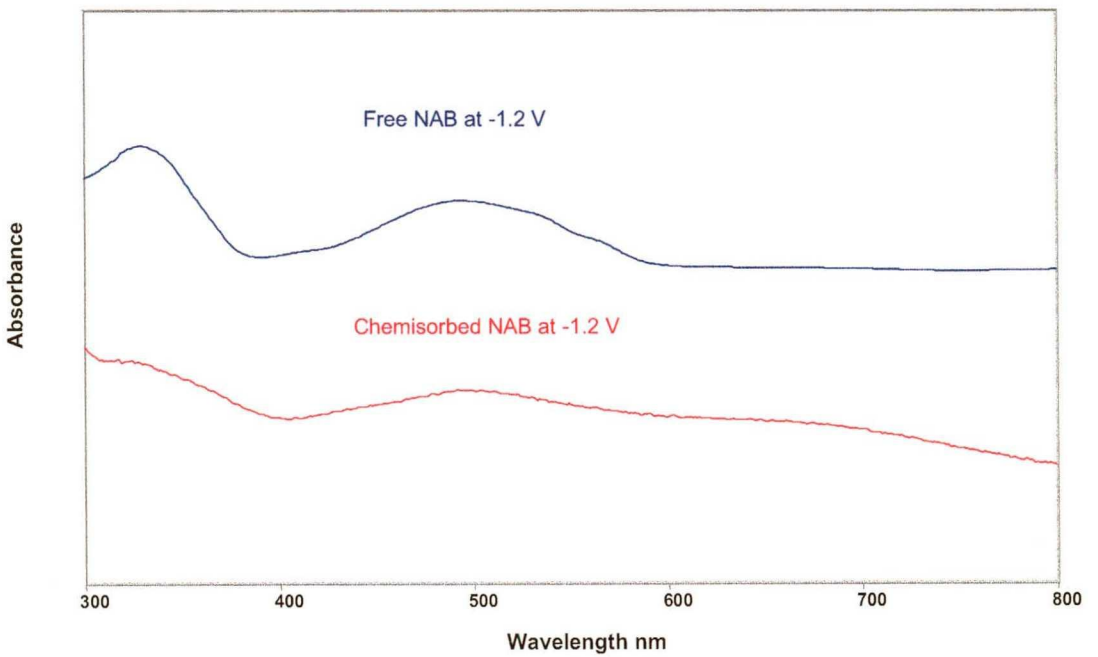

Figure 3.28 UV-vis spectra of free NAB and chemisorbed NAB at -1.2 V.

of NAB radical anion (504.3 nm), and deviates somewhat from the HOMO-LUMO transition of NAB 4'-methide anion (588.3 nm). During spectroelectrochemical monitoring of chemisorbed NBP (Figure 3.22), a new absorption peak appeared at 526 nm at -1.0 V accompanying the disappearance of the original absorption peak of NBP at 326 nm. The absorption of reduced NBP (526 nm) deviates from both the electronic transitions of NBP radical anion (598.5 and 398.1 nm) and the HOMO-LUMO transition of NBP methide anion (633.1 nm). The second and fourth scans of UV-vis spectroelectrochemical experiment of chemisorbed AB (Figure 3.20) showed two absorption peaks whose relative intensities change upon reduction, which indicates that chemisorbed AB molecules were partially reduced. The absorption peak of reduced AB (470 nm) is close to the HOMO-LUMO transition of the AB monomethide anion (488.1 nm) and deviates from the electronic transitions of AB radical anion (565.7 nm and 420.6 nm).

The absorptions of reduced NAB, AB and NBP as "free molecules" in solution are consistent with the electronic transitions of NAB, AB and NBP anions calculated by density functional theory. However, the absorptions of reduced NAB and NBP as chemisorbed molecules on PPF surfaces have some deviations from the electronic transitions of the methide anions of NAB and NBP. Compared to the reduction of chemisorbed AB, the chemisorbed NAB and NBP are completely reduced under negative potentials, which indicates the nitro group plays an important role in the reduction. The fact that the chemisorbed molecules exhibit significant red shifts implies that strong electronic coupling exists between the aromatic molecules and the PPF electrode surface through a conjugated

carbon-carbon bond. The chemisorbed molecules and the PPF electrode may be considered as one electronic system. As the potential of PPF electrode becomes negative, electrons transfer to the chemisorbed molecules and distribute over the molecules and carbon of the PPF electrode. The nitro group in a molecule enhances the molecule's ability of delocalizing electrons in the conjugated system. There are several factors which may influence the observed UV-vis spectra. First, the applied potential generates an electric field at the PPF /solution interface, which may affect the electronic transition of UV-vis absorption. Second, the reduced chemisorbed molecules may not be fully reduced due to their multilayer structure as indicated by the incomplete reduction of chemisorbed AB. The UV-vis spectra have contributions from the electronic transitions of both oxidized and reduced AB.

Since NAB has a longer conjugated system, high molar absorptivity and significant spectral change under negative potentials, it was selected to study the electron transfer mechanism of chemisorbed molecules on PPF. From the UV-vis spectroelectrochemical experiment (Figure 3.18), a new absorption peak appeared at 502 nm when the potential reached -1.2 V and -1.5 V. This peak decreased significantly when the potential reached -1.8 V (Figure 3.29). The wide potential windows of reduction of chemisorbed NAB imply that electron transfer between PPF and NAB is gradual rather than a discrete Nernstian electron transfer. When negative potential is applied, electrons transfer to NAB and the neutral NAB rearranges to distribute the extra electrons over the whole conjugated system. This deduction is consistent with Itoh's in situ Raman

spectroelectrochemical experiment of a chemisorbed NAB monolayer on glassy carbon[72].

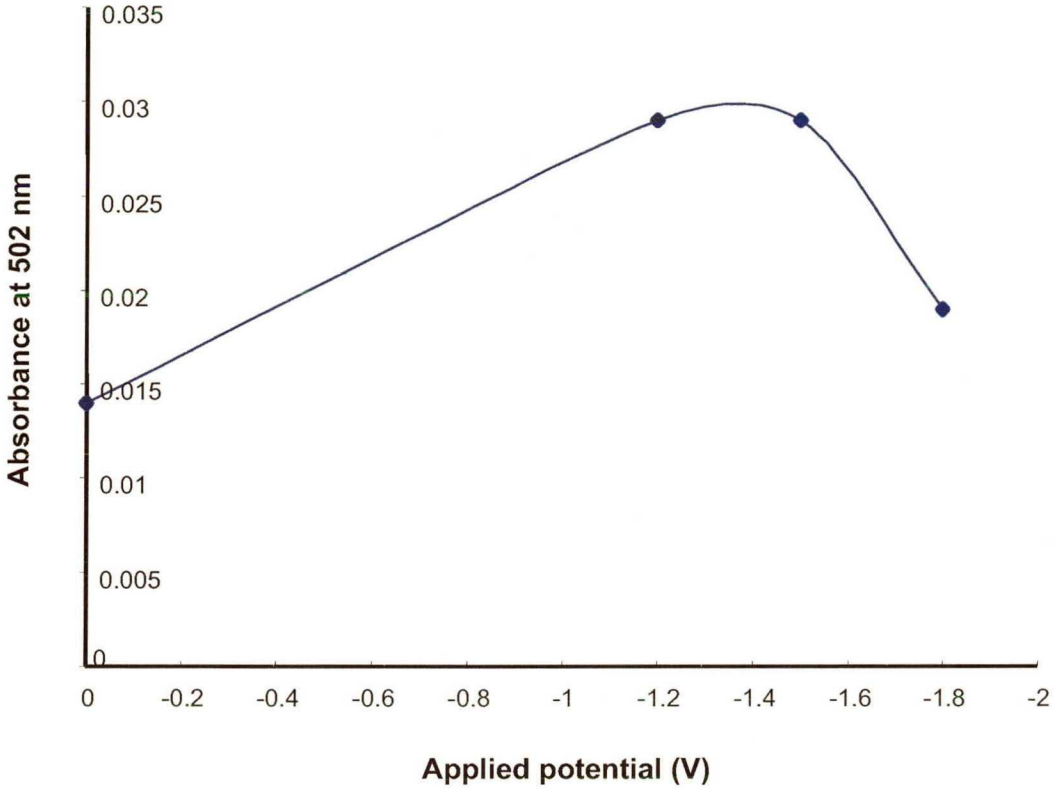

Figure 3.29 Absorbance of chemisorbed NAB at 502 nm at different applied potentials.

3.3 Conclusions

In summary, the first example of UV-Vis absorption of chemisorbed organic molecules on an optically transparent carbon has been demonstrated. The covalent carbon-carbon bond between organic molecules and PPF electrode has been confirmed by UV-vis spectroscopy. The red shift of chemisorbed organic molecules relative to the solution and solid state is considered as the

indication of the extension of the conjugated system.

In situ UV-vis spectroelectrochemical experiments successfully monitored the structure changes of both free molecules in solution and covalently bonded organic molecules on PPF electrodes under applied electrochemical potentials. This technique addresses issues of structural changes with reduction potentials, promising new insights into the mechanism of electron transfer through organic molecules.

The reduction of free NAB, AB and NBP in solutions generates their corresponding radical anions. The UV-vis absorptions of reduced NAB, AB and NBP are in agreement with the electronic transitions of their corresponding radical anions calculated by Gaussian. The reduction potentials are determined by a molecule's ability to delocalize the additional electrons over the molecule. UV-vis absorption peaks of reduced forms of chemisorbed NAB, AB and NBP red shift relative to their native unreduced forms. The wide potential window of reduction of chemisorbed NAB implies that the electron transfer through chemisorbed molecules is gradual, and is likely driven by the electric field at the electrode/solution interface.

References

(1) Sortino, S.; Petralia, S.; Conoci, S.; Bella, S. D. *J. Mater. Chem.* **2004**, *14*, 811-813.

(2) Kalyuzhny, G.; Vaskevich, A.; Ashkenasy G.; Shanzer, A.; Rubinstein, I. *J. Phys.. Chem.* **2000**, *104*, 8238-8244.

(3) Kalyuzhny, G.; Schneeweiss, M. A.; Shanzer, A.; Vaskevich, A.; Rubinstein, I. *J. Am. Chem. Soc.* **2001**, *123*, 3177-3178.

(4) Shukla, A. D.; Strawser, D.; Lucassen, A. C. B.; et al. *J. Phys. Chem. B* **2004**, *108*, 17505-17511.

(5) Blount, H. N.; Winograd, N.; Kuwana, T. *J. Phys. Chem.* **1970**, *74*, 3231-3236.

(6) Hawkridge, F. M.; Kuwana, T. *Anal. Chem.* **1973**, *45*, 1021-1027.

(7) Winograd, N.; Blount, H. N.; Kuwana, T. *J Phys Chem* **1969**, *73*, 3456-3462.

(8) Winograd, N.; Kuwana, T. *J. Electroanal. Chem* **1969**, *23*, 333-342.

(9) Winograd, N.; Kuwana, T. *J Am Chem Soc* **1970**, *92*, 224-226.

(10) Winograd, N.; Kuwana, T. *Anal. Chem.* **1971**, *43*, 252-259.

(11) Barthram A. M.; Ward, M. D. *New J. Chem.* **2000**, *24*, 501-504.

(12) Frapart, Y.-M.; Boussac, A.; Albach, R.; et al. *J. Am. Chem. Soc.* **1996**, *118*, 2669-2678.

(13) Page, S. E.; Gordon, K. C.; Burrell, A. K. *Inorg. Chem.* **1998**, *37*, 4452-4459.

(14) Graf, D. D.; Mann, K. R. *Inorg. Chem.* **1997**, *36*, 141-149.

(15) Berger, S.; Klein, A.; Kaim, W.; Fiedler, J. *Inorg. Chem.* **1998**, *37*, 5664-5671.

(16) Meyer, F.; Winter, R. F.; Kaifer, E. *Inorg. Chem.* **2001**, *40*, 4597-4603.

(17) Hornung, F. M.; Heilmann, O.; Kaim, W.; Zalis, S. Fiedler, J. *Inorg. Chem.* **2000**, *39*, 4052-4058.

(18) Chen, S.-P.; Williams, A.; Ejeh, D.; Hambright, P.; Hosten, C. *Langmuir*, **1999**, *15*, 3998-4004.

(19) Zotti, G.; Schiavon, G.; Zecchin, S.; Morin, J.-F.; Leclerc, M. *Macromolecules*, **2002**, *35*, 2122-2128.

(20) McGale, E. M.; Robinson, B. H.; Simpsom, J. *Organometallics*, **2003**, *22*, 931-939.

(21) Klein, R. A.; Elsevier, C. J.; Hartl, F. *Organomellics*, **1997**, *16*, 1284-1291.

(22) Winter, R. F.; Wolmershauser, G. *J. Organometallic Chem.* **1998**, *570*, 201-218.

(23) Winter, R. F. *Chem. Commun.,* **1998**, *20*, 2009-2210.

(24) Malinauskas, A.; Holze, R. *Synthetic Metals*, **1998**, *97*, 31-36.

(25) Zimmermann, A.; Kunzelmann, U.; Dunsch, L. *Synthetic Metals*, **1998**, 17-25.

(26) Berger, R. M.; Holcombe, J. R.. *Inorganica Chimica Acta*, **1995**, *232*, 217-221.

(27) Tarabek, J.; Rapta, P.; Kalbac, M.; Dunsch, L. *Anal. Chem.* **2004**, *76*, 5918-5923.

(28) Rapta, P.; Kress, L.; Hapiot, P.; Dunsch, L. *Phys. Chem. Chem. Phys.* **2002**, *4*, 4181-4185.

(29) Kaim, W.; Sixt, T.; Weber, M.; Fiedler, J. *J. Organometallic Chem.* **2001**, *637-639*, 167-171.

(30) Farrell, I. R.; Hartl, F.; Zalis, S.; et al. *Inorganica Chimica Acta*, **2001**, *318*, 143-151.

(31) Nikolaou, S.; Toma, H. E. *Polyhedron*, **2001**, *20*, 253-259.

(32) Wen, T.-C.; Sivakumar, C.; Gopalan, A. *Electrochimica Acta*, **2001**, *46*, 1071-1085.

(33) Rapta P.; Faber, R.; Dunsch, L.; Neudeck, A.; Nuyken, O. *Spectrochimica Acta Part A*, **2000**, *56*, 357-362.

(34) Kvarnstrom, C.; Neugebauer, H.; Blomquist, S.; et al. *Electrochimica Acta*, **1999**, *44*, 2739-2750.

(35) Malinauskas, A.; Holze, R. *Electrochimica Acta*, **1999**, *44*, 2613-2623.

(36) Freydank, A.; Janietz, S.; Schulz, B. *J. Electroanalytical Chem.* **1998**, *456*, 61-69.

(37) Chung, C.-Y.; Wen, T.-C.; Gopalan, A. *Spectrochimica Acta Part A*, **2004**, *60*, 585-593.

(38) Hartmann, H.; Sarkar, B.; Kaim, W.; Fiedler, J. *J. Organometallic Chem.* **2003**, *687*, 100-107.

(39) Meunier-Prest, R.; Lamblin, G.; Mailfert, A.; Raveau, S. *J. Electroanalytical Chem.* **2003**, *541*, 175-183.

(40) Lezna, R. O.; Romagnoli, R.; de Tacconi, N.R.; Rajeshwar, K. *J. Electroanalytical Chem.* **2003**, *544*, 101-106.

(41) Hartmann, S.; Winter, R. F.; Brunner, B. M.; et al. *Eur. J. Inorg. Chem.* **2003**, 876-891.

(42) Su, C.-Y.; Liao, S.; Wanner, M.; et al. *Dalton Trans.* **2003**, 189-202.

(43) Abd-Elwahed, A.; Holze, R. *Synthetic Metals*, **2002**, *131*, 61-70.

(44) Dauginet-De Pra, L.; Demoustier-Champagne, S. *Thin Solid Films*, **2005**, *479*, 321-328.

(45) Papiteiro, C.; Sobral, A. *Electrochimica Acta* **2005**, *50*, 2445-2451.

(46) Mason, C. R.; Skabara, P. J.; Cupertino, D.; et al. *J. Mater. Chem.* **2005**, 15, 1446-1453.

(47) Dauginet-De Pra, L.; Demoustier-Champagne, S. *Polymer* **2005**, 46, 1583-1594.

(48) Brisach-Wittmeyer, A.; Lobstein, S.; Gross, M.; Giraudeau, A. *J. Electroanalytical Chem.* **2005**, *576*, 129-137.

(49) Tarabek, J.; Rapta, P.; Jahne, E.; et al. *Electrichimica Acta* **2005**, *50*, 1643-1651.

(50) Frantz, S.; Fiedler, J.; Hartenbach, I.; Schleid, T.; Kaim, W. *J. Organometallic Chem.* **2004**, *689*, 3031-3039.

(51) Damlin, P.; Kvarnstrom, C.; Ivaska, A. *J. Electroanalytical Chem.* **2004**, *570*, 113-122.

(52) Battistuzzi, G.; Bellei, M.; Bortolotti, C. A. *Archives of Biochemistry and Biophysics* **2004**, *423*, 317-331.

(53) Niemz, A.; Imbriglio, J.; Rotello, V. M. *J. Am. Chem. Soc.* **1997**, *119*, 887-892.

(54) Petr, A.; Dunsch, L.; Neudeck, A. *J. Electroanalytical Chem.* **1996**, *412*, 153-158.

(55) Barton, M. T.; Rowley, N. M.; Ashton, P. R.; et al. *New J. Chem.* **2000**, *24*, 555-560.

(56) Wang, Z.; Li, X.; Wu, Y.; Tang, Y.; Ma, S. *J. Electroanalytical Chem.* **1999**, *464*, 181-186.

(57) Zhu, Y.; Cheng, G.; Dong, S. *Electroanalysis* **1998**, *10(14)*, 955-958.

(58) Malinauskas, A.; Holze, R. *J. Electroanalytical Chem.* **1999**, *461*, 184-193.

(59) Sun H.-R.; Yang Y.-X.; Liu, G. F.; Cao, X.-Z. *J. Porphyrins Phthalocyanines* **1999**, *3*, 712-719.

(60) Al-Obaidi, A. H. R.; Gorgon, K. C.; McGarvey, J. J.; Bell, S. E. J.; Grimshaw, J. *J. Phys. Chem.* **1993**, *97*, 10942-10947.

(61) Keyes, T. E.; Forster, R. J.; Jayaweera, P. M.; et al. *Inorg. Chem.* **1998**, *37*, 5925-5932.

(62) Qu, Z.; Kadish, K. M.; Crossley, M. J.; et al. *Inorg. Chem.* **2004**, *43*, 2078-2086.

(63) Bernhard, S.; Takada, K.; Jenkins, D.; Abruna, H. D. *Inorg. Chem.* **2002**, *41*, 765-772.

(64) Liu, X.; Zhang, Z.; Cheng, G.; Dong, S. *Electrolysis* **2003**, *15(2)*, 103-107.

(65) Cifuentes, M. P.; Humphrey, M. G.; Heath, G. A. *Inorganica Chimica Acta* **1997**, *259*, 273-280.

(66) Rapta, P.; Neudeck, A.; Petr, A.; Dunsch, L. *J.Chem. Soc., Faraday Trans.* **1998**, *94*, 3625-3630.

(67) Lapkowski, M.; Zak, J.; Kolodziej-sadlok, M.; Guillerez, S.; Bidan, G. *Synthetic Metals* **2003**, *135-136*, 251-252.

(68) Hu, X.; Wang, Q.; He, P.; Fang, Y. *Analytical Sciences* **2002**, *18*, 645-650.

(69) Scotter, J.; Haymond, S.; Zak, J. K.; et al. *The Electrochemical Society Interface* **2003**, *Spring*, 33-38.

(70) Williams, M. W.; Arakawa, E. T. *J. Appl. Phys.* **1972**, *43(8)*, 3460-3463.

(71) Monti, S.; Flamigni, L. *J. Phys. Chem.* **1986**, *90*, 1179-1184.

(72) Itoh, T.; McCreery, R. *J. Am. Chem. Soc.* **2002**, *124*, 10894-10902.

(73) Neta, P.; Levanon, H. *J. Phys. Chem.* **1977**, *81(24)*, 2288-2292.

(74) Meisel, D.; Neta, P. *J. Am. Chem. Soc.* **1975**, *97(18)*, 5198-5203.

(75) Solak, A. O.; Eichorst, L. R.; Clark, W. J.; McCreery, R. L. *Anal. Chem.* **2003**, 296-305.

(76) McCreery, R.; Dieringer, J.; Solak, A. O.; Snyder, B.; Nowak, A. M.; et. Al. *J. Am. Chem. Soc.* **2003**, *125*, 10748-10758.

(77) Solak, A. O.; Ranganathan, S.; Itoh, T.; McCreery, R. L. *Electrochemical and Solid-State Letters* **2002**, *5(8)*, E43-E46.

BIBLIOGRAPHY

References from chapter 1:

(1) McCreery, R. L.; Cline, K. K.; McDermott, C. A.; McDermott, M. T. *Colloids Surf.* **1994**, *93*, 211-219.

(2) Kinoshita, K. *Carbon: Electrochemical and Physicochemical Properties.* Wiley: New York, **1988**.

(3) McCreery, R. L. *Interfacial Electrochemistry*, Wieckowski, A., Ed.; Dekker: New York, **1999**; Chapter 35.

(4) McCreery, R. L. *Electroanalytical Chemistry*, Bard, A. J., Ed.; Dekker: New York, **1991**; Vol. 17, 221-374.

(5) McCreery, R. L. *Laboratory Techniques in Electroanalytical Chemistry,* 2nd ed..; Kissinger, P. T., Heineman, W. R., Eds.; Dekker: New York, **1996**; Chapter 10.

(6) Antoniadou, S.; Jannakoudakis, A. D.; Jannakoudakis, P. D.; Theodoridou, E. *J. Appl. Electrochem.* **1992**, 22, 1060-1064.

(7) Tanaka, H.; Aramata, A. *J. Electroanal. Chem.* **1997**, *437*, 29-35.

(8) Nowall, W. B.; Wipf, D. O.; Kuhr, W. G. *Anal. Chem.* **1998**, 70, 2601-2606.

(9) Hayes, M. A.; Kuhr, W. G. *Anal. Chem.* **1999**, *71*, 1720-1727.

(10) Chen, P.; McCreery, R. L. *Anal. Chem.* **1996**, *68,* 3958-3965.

(11) Yang, H.-H.; McCreery, R. L. *Anal. Chem.* **1999**, *71*, 4081-4087.

(12) Nowak, A. M.; McCreery, R. L. *J. Am. Chem. Soc.* **2004**, *126*, 16621-16631.

(13) Ranganathan, S.; McCreery, R. L.; Majji, S. M.; Madou, M. *J. Electrochem. Soc.* **2000**, *147*, 277 – 282.

(14) Wang, Y.; Alsmeyer, D.; McCreery, R. L. *Chem. Mater.* **1990**, *2*, 557-563.

(15) Dresselhaus M. S.; Dresselhaus G.; Sugihara K.; Spain I. L.; Goldberg M. A. *Graphite Fibers and Filaments, 98,* Springer-Verlag, New York, 1988.

(16) Ranganathan, S.; McCreery, R. L. *Anal. Chem.* **2001**, *73*, 893-900.

(17) McDermott, C. A.; Kneten, K. R.; McCreery, R. L. *J. Electrochem. Soc.* **1993**, *140*, 2593-2599.

(18) Chen, P.; Fryling, M. A.; McCreery, R. L. *Anal. Chem.* **1995**, *67*, 3115-3122.

(19) Duvall, S. H.; McCreery, R. L. *J. Am. Chem. Soc.* **2000**, *122*, 6759-6764.

(20) Xu, J.; Granger, M. C.; Chen, Q.; Strojek, J. W.; Lister, T. E.; Swain, G. M. *Anal. Chem.* **1997**, *69*, 591A-597A.

(21) Duvall, S. H.; McCreery, R. L. *Anal. Chem.* **1999**, *71*, 4594-4602.

(22) Xu, J.; Huang, W.; McCreery, R. L. *J. Electrochem. Chem.* **1996**, *410*, 235-242.

(23) Yang, H.-H.; McCreery, R. L. *J. Electrochem. Soc.* **2000**, *147*, 3420-3428.

(24) Delamar, M.; Hitmi, R.; Pinson J.; Saveant, J. M. *J. Am. Chem. Soc.* **1992**, *114*, 5883-5884.

(25) Liu. Y.-C., McCreery, R. L. *Anal. Chem.* **1997**, *69*, 2091-2097.

(26) Allongue, P.; Delamar, M.; Desbat, B.; Fagebaume, O.; Hitmi, R.; Pinson J.; Saveant, J. M. *J. Am. Chem. Soc.* **1997**, *119*, 201-207.

(27) Dequaire, M.; Degrand, C.; Limoges, B. *J. Am. Chem. Soc.* **1992**, *121*, 6946-6947.

(28) Delamar, M.; Desarmot, G.; Fagebaume, O.; Hitmi, R.; Pinson, J.; Saveant,

J.-M. *Carbon* **1997**, *35*, 801-807.

(29) Liu, Y.-C.; McCreery, R. L. *J. Am. Chem. Soc.* **1995**, *117*, 11254-11259.

(30) Brooksby, P. A.; Downard, A. *Langmuir* **2004**, A-H.

(31) Anariba, F.; DuVall, S. H.; McCreery, R. L. *Anal. Chem.* **2003**, *75*, 3837-3844.

(32) Kariuki, J. K.; McDermott, M. T. *Langmuir* **2001**, *17*, 5947-5951.

(33) Ranganathan, S.; Steidel, I.; Anariba, F.; McCreery, R. L. *Nano Lett.* **2001**, *1*, 491-494.

(34) Solak, A. O.; Ranganathan, S.; Itoh, T.; McCreery, R. L. *Electrochem. Solid State Lett.* **2002**, *5*, E43-E46.

(35) Solak, A. O.; Eichorst, L. R.; Clark, W. J.; McCreery, R. L. *Anal. Chem.* **2003**, *75*, 296-305.

(36) Itoh, T.; McCreery, R. L. *J. Am. Chem. Soc.* **2002**, *124*, 10894-10902.

(37) http://sbio.uct.ac.za/Sbio/documentation/spectrophotometer.pdf

(38) Plieth, W., Wilson, G. S., Gutierrez De La Fe, C. *Pure & Appl. Chem.* **1998**, *70*, 1395-1414.

(39) Jentoft, F. *Modern Methods in Heterogeneous Catalysis* **2004**, 3.

(40) Kalyuzhny, G.; Schneeweiss, M. A.; Shanzer, A.; Vaskevich, A.; Rubinstein, I. *J. Am. Chem. Soc.* **2001**, *123*, 3177-3178.

(41) Cheng, Z.; Cheng, L.; Gao Q., Dong, S.; Yang, X. *J. Mater. Chem.* **2002**, 12, 1724-1729.

(42) Pang, S.-F.; Liang, Y.-Q. *Journal of colloid and Interface Science* **2000**, *231*, 59-65.

(43) Kalyuzhny, G.; Vaskevich, A.; Ashkenasy, G.; Shanzer, A.; Rubinstein, I. *J. Phys. Chem. B* **2000**, *104*, 8238-8244.

(44) Tamada, K.; Akiyama, H.; Wei, T. X. *Langmuir*, **2002**, *18*, 5239-5246.

(45) Sortino, S.; Petralia, S.; Conoci, S.; Bella, S. D. *J. Mater. Chem.* **2004**, *14*, 811-813.

(46) Everaars, M. D.; Marcelis, A. T. M.; Kuijpers, A. J.; Laverdure, E.; Koronora, J. et al. *Langmuir*, **1995**, *11*, 3705-3711.

(47) Shukla, A. D.; Strawser, D.; Lucassen, A. C. B.; Freeman, D.; Cohen, H.; et al. *J. Phys. Chem. B* **2004**, *108*, 17505-5-17511.

(48) Nieuwkerk, A. C.; Marcelis, A. T. M.; Sudholter, E. J. R. *Langmuir*, **1997**, *13*, 3325-3330.

(49) Everaars, M. D.; Marcelis, A. T. M.; Sudholter, E. J. R. *Langmuir*, **1996**, *12*, 3964-3968.

(50) Li, X.; Xu, W.; Jia, H.; Wang, X.; Zhao, B.; et al. *Journal of Colloid and Interface Science* **2004**, *274*, 9-15.

(51) Elking, M. D.; He, G.; Xu, Z. J. *Chem. Phys.* **1996**, *105(15)*, 6565-6573.

(52) Scholz. F. *Electroanalytical methods : guide to experiments and applications* **2002,** 167-189.

(53) Rapta, P.; Neudeck, A.; Petr, A.; Dunsch L. *J. Chem. Soc., Faraday Trans.* **1998**, *94*, 3625-3630.

(54) Hu, X.; Wang, Q.; He, P.; Fang. Y. *Analytical Sciences* **2002**, *18*, 645-650.

(55) Lapkowski, M.; Zak, J.; Kolodziej-Sadlok, M.; Guillerez, S.; Bidan, G.

Synthetic Metals **2003**, *135-136*, 251-252.

References from chapter 2:

(1) Anariba, F.; DuVall, S. H.; McCreery, R. L. *Anal. Chem.*, **2003**, *75*, 3837–3844.

(2) Allongue, P.; Delamar, M.; Desbat, B.; Fagebaume, O.; Hitmi, R.; Pinson, J.; Save´ant, J.-M. *J. Am. Chem. Soc.*, **1997**, *119*, 201–207.

(3) Delamar, M.; De´sarmot, G.; Fagebaume, O.; Hitmi, R.; Pinson, J.; Save´ant,

J.-M. *Carbon*, **1997**, *35*, 801–807.

(4) Kariuki, J. K.; McDermott, M. T. *Langmuir*, **2001**, *17*, 5947–5951.

(5) Liu, Y.-C.; McCreery, R. L. *J. Am. Chem. Soc.*, **1995**, *112*, 11254–11259.

(6) Combellas, C.; Kanoufi, F.; Mazouzi, D.; Thie´bault, A.; Bertrand, P.; Me´dard, N. *Polymer*, **2003**, *44*, 19–24.

(7) Cooke, J. M.; Galloway, C. P.; Bissell, M. A.; Adams, C. E.; Yu, M. C.; Belmont, J. A.; Amici, R. M. *US Pat, 6 110 9994 A*, **2003** (to Cabot Corp.) and references therein.

(8) Dyke, C. A.; Tour, J. M. *Nano Lett.*, **2003**, *3*, 1215–1218.

(9) Wang, J.; Firestone, M. A.; Auciello, O.; Carlisle, J. A. *Langmuir*, **2004**, *20*, 11450–11456.

(10) Pinson, J.; Podvorica, F. *Chem. Soc. Rev.* **2005**, *34,* 429-439.

(11) http://stm2.nrl.navy.mil/how-afm/how-afm.html

(12) http://www.chembio.uoguelph.ca/educmat/chm729/afm/introdn.htm

(13) Saby, C.; Ortiz, B.; Champagne, G. Y.; Belanger, D. *Langmuir*, **1997**, *13*, 6805-6813.

(14) Brooksby, P. A.; Downard, A. *Langmuir* **2004**, A-H.

(15) Combellas, C.; Kanoufi, F.; Pinson, J.; Podvorica, F. I. *Langmuir*, **2005**, *21*, 280-286.

(16) Ranganathan, S.; McCreery, R. L.; Majji, S. M.; Madou, M. *J. Electrochem. Soc.* **2000**, *147*, 277 - 282.

(17) Wang, Y.; Alsmeyer, D.; McCreery, R. L. *Chem. Mater.* **1990**, *2*, 557-563.

(18) Dresselhaus M. S.; Dresselhaus G.; Sugihara K.; Spain I. L.; Goldberg M. A. *Graphite Fibers and Filaments, 98,* Springer-Verlag, New York, 1988.

(19) Ranganathan, S.; McCreery, R. L. *Anal. Chem.* **2001**, *73*, 893-900.

References from chapter 3:

(1) Sortino, S.; Petralia, S.; Conoci, S.; Bella, S. D. *J. Mater. Chem.***2004**, *14*, 811-813.

(2) Kalyuzhny, G.; Vaskevich, A.; Ashkenasy G.; Shanzer, A.; Rubinstein, I. *J. Phys.. Chem.* **2000**, *104*, 8238-8244.

(3) Kalyuzhny, G.; Schneeweiss, M. A.; Shanzer, A.; Vaskevich, A.; Rubinstein, I. *J. Am. Chem. Soc.* **2001**, *123*, 3177-3178.

(4) Shukla, A. D.; Strawser, D.; Lucassen, A. C. B.; et al. *J. Phys. Chem. B* **2004**, *108*, 17505-17511.

(5) Blount, H. N.; Winograd, N.; Kuwana, T. *J. Phys. Chem.* **1970**, *74*, 3231-3236.

(6) Hawkridge, F. M.; Kuwana, T. *Anal. Chem.* **1973**, *45*, 1021-1027.

(7) Winograd, N.; Blount, H. N.; Kuwana, T. *J Phys Chem* **1969**, *73*, 3456-3462.

(8) Winograd, N.; Kuwana, T. *J. Electroanal. Chem* **1969**, *23*, 333-342.

(9) Winograd, N.; Kuwana, T. *J Am Chem Soc* **1970**, *92*, 224-226.

(10) Winograd, N.; Kuwana, T. *Anal. Chem.* **1971**, *43*, 252-259.

(11) Barthram A. M.; Ward, M. D. *New J. Chem.* **2000**, *24*, 501-504.

(12) Frapart, Y.-M.; Boussac, A.; Albach, R.; et al. *J. Am. Chem. Soc.* **1996**, *118*, 2669-2678.

(13) Page, S. E.; Gordon, K. C.; Burrell, A. K. *Inorg. Chem.* **1998**, *37*, 4452-4459.

(14) Graf, D. D.; Mann, K. R. *Inorg. Chem.* **1997**, *36*, 141-149.

(15) Berger, S.; Klein, A.; Kaim, W.; Fiedler, J. *Inorg. Chem.* **1998**, *37*, 5664-5671.

(16) Meyer, F.; Winter, R. F.; Kaifer, E. *Inorg. Chem.* **2001**, *40*, 4597-4603.

(17) Hornung, F. M.; Heilmann, O.; Kaim, W.; Zalis, S. Fiedler, J. *Inorg. Chem.* **2000**, *39*, 4052-4058.

(18) Chen, S.-P.; Williams, A.; Ejeh, D.; Hambright, P.; Hosten, C. *Langmuir*, **1999**, *15*, 3998-4004.

(19) Zotti, G.; Schiavon, G.; Zecchin, S.; Morin, J.-F.; Leclerc, M. *Macromolecules*, **2002**, *35*, 2122-2128.

(20) McGale, E. M.; Robinson, B. H.; Simpsom, J. *Organometallics*, **2003**, *22*, 931-939.

(21) Klein, R. A.; Elsevier, C. J.; Hartl, F. *Organomellics*, **1997**, *16*, 1284-1291.

(22) Winter, R. F.; Wolmershauser, G. *J. Organometallic Chem.* **1998**, *570*, 201-218.

(23) Winter, R. F. *Chem. Commun.*, **1998**, *20*, 2009-2210.

(24) Malinauskas, A.; Holze, R. *Synthetic Metals*, **1998**, *97*, 31-36.

(25) Zimmermann, A.; Kunzelmann, U.; Dunsch, L. *Synthetic Metals*, **1998**, 17-25.

(26) Berger, R. M.; Holcombe, J. R.. *Inorganica Chimica Acta*, **1995**, *232*, 217-221.

(27) Tarabek, J.; Rapta, P.; Kalbac, M.; Dunsch, L. *Anal. Chem.* **2004**, *76*, 5918-5923.

(28) Rapta, P.; Kress, L.; Hapiot, P.; Dunsch, L. *Phys. Chem. Chem. Phys.* **2002**, *4*, 4181-4185.

(29) Kaim, W.; Sixt, T.; Weber, M.; Fiedler, J. *J. Organometallic Chem.* **2001**, *637-639*, 167-171.

(30) Farrell, I. R.; Hartl, F.; Zalis, S.; et al. *Inorganica Chimica Acta*, **2001**, *318*, 143-151.

(31) Nikolaou, S.; Toma, H. E. *Polyhedron*, **2001**, *20*, 253-259.

(32) Wen, T.-C.; Sivakumar, C.; Gopalan, A. *Electrochimica Acta*, **2001**, *46*, 1071-1085.

(33) Rapta P.; Faber, R.; Dunsch, L.; Neudeck, A.; Nuyken, O. *Spectrochimica Acta Part A*, **2000**, *56*, 357-362.

(34) Kvarnstrom, C.; Neugebauer, H.; Blomquist, S.; et al. *Electrochimica Acta*, **1999**, *44*, 2739-2750.

(35) Malinauskas, A.; Holze, R. *Electrochimica Acta*, **1999**, *44*, 2613-2623.

(36) Freydank, A.; Janietz, S.; Schulz, B. *J. Electroanalytical Chem.* **1998**, *456*, 61-69.

(37) Chung, C.-Y.; Wen, T.-C.; Gopalan, A. *Spectrochimica Acta Part A*, **2004**, *60*, 585-593.

(38) Hartmann, H.; Sarkar, B.; Kaim, W.; Fiedler, J. *J. Organometallic Chem.* **2003**, *687*, 100-107.

(39) Meunier-Prest, R.; Lamblin, G.; Mailfert, A.; Raveau, S. *J. Electroanalytical Chem.* **2003**, *541*, 175-183.

(40) Lezna, R. O.; Romagnoli, R.; de Tacconi, N.R.; Rajeshwar, K. *J. Electroanalytical Chem.* **2003**, *544*, 101-106.

(41) Hartmann, S.; Winter, R. F.; Brunner, B. M.; et al. *Eur. J. Inorg. Chem.* **2003**, 876-891.

(42) Su, C.-Y.; Liao, S.; Wanner, M.; et al. *Dalton Trans.* **2003**, 189-202.

(43) Abd-Elwahed, A.; Holze, R. *Synthetic Metals*, **2002**, *131*, 61-70.

(44) Dauginet-De Pra, L.; Demoustier-Champagne, S. *Thin Solid Films*, **2005**, *479*, 321-328.

(45) Papiteiro, C.; Sobral, A. *Electrochimica Acta* **2005**, *50*, 2445-2451.

(46) Mason, C. R.; Skabara, P. J.; Cupertino, D.; et al. *J. Mater. Chem.* **2005**, 15, 1446-1453.

(47) Dauginet-De Pra, L.; Demoustier-Champagne, S. *Polymer* **2005**, 46, 1583-1594.

(48) Brisach-Wittmeyer, A.; Lobstein, S.; Gross, M.; Giraudeau, A. *J. Electroanalytical Chem.* **2005**, *576*, 129-137.

(49) Tarabek, J.; Rapta, P.; Jahne, E.; et al. *Electrichimica Acta* **2005**, *50*, 1643-1651.

(50) Frantz, S.; Fiedler, J.; Hartenbach, I.; Schleid, T.; Kaim, W. *J. Organometallic Chem.* **2004**, *689*, 3031-3039.

(51) Damlin, P.; Kvarnstrom, C.; Ivaska, A. *J. Electroanalytical Chem.* **2004**, *570*, 113-122.

(52) Battistuzzi, G.; Bellei, M.; Bortolotti, C. A. *Archives of Biochemistry and Biophysics* **2004**, *423*, 317-331.

(53) Niemz, A.; Imbriglio, J.; Rotello, V. M. *J. Am. Chem. Soc.* **1997**, *119*, 887-892.

(54) Petr, A.; Dunsch, L.; Neudeck, A. *J. Electroanalytical Chem.* **1996**, *412*, 153-158.

(55) Barton, M. T.; Rowley, N. M.; Ashton, P. R.; et al. *New J. Chem.* **2000**, *24*, 555-560.

(56) Wang, Z.; Li, X.; Wu, Y.; Tang, Y.; Ma, S. *J. Electroanalytical Chem.* **1999**, *464*, 181-186.

(57) Zhu, Y.; Cheng, G.; Dong, S. *Electroanalysis* **1998**, *10(14)*, 955-958.

(58) Malinauskas, A.; Holze, R. *J. Electroanalytical Chem.* **1999**, *461*, 184-193.

(59) Sun H.-R.; Yang Y.-X.; Liu, G. F.; Cao, X.-Z. *J. Porphyrins Phthalocyanines* **1999**, *3*, 712-719.

(60) Al-Obaidi, A. H. R.; Gorgon, K. C.; McGarvey, J. J.; Bell, S. E. J.; Grimshaw, J. *J. Phys. Chem.* **1993**, *97*, 10942-10947.

(61) Keyes, T. E.; Forster, R. J.; Jayaweera, P. M.; et al. *Inorg. Chem.* **1998**, *37*, 5925-5932.

(62) Qu, Z.; Kadish, K. M.; Crossley, M. J.; et al. *Inorg. Chem.* **2004**, *43*, 2078-2086.

(63) Bernhard, S.; Takada, K.; Jenkins, D.; Abruna, H. D. *Inorg. Chem.* **2002**, *41*, 765-772.

(64) Liu, X.; Zhang, Z.; Cheng, G.; Dong, S. *Electrolysis* **2003**, *15(2)*, 103-107.

(65) Cifuentes, M. P.; Humphrey, M. G.; Heath, G. A. *Inorganica Chimica Acta* **1997**, *259*, 273-280.

(66) Rapta, P.; Neudeck, A.; Petr, A.; Dunsch, L. *J.Chem. Soc., Faraday Trans.* **1998**, *94*, 3625-3630.

(67) Lapkowski, M.; Zak, J.; Kolodziej-sadlok, M.; Guillerez, S.; Bidan, G. *Synthetic Metals* **2003**, *135-136*, 251-252.

(68) Hu, X.; Wang, Q.; He, P.; Fang, Y. *Analytical Sciences* **2002**, *18*, 645-650.

(69) Scotter, J.; Haymond, S.; Zak, J. K.; et al. *The Electrochemical Society Interface* **2003**, *Spring*, 33-38.

(70) Williams, M. W.; Arakawa, E. T. *J. Appl. Phys.* **1972**, *43(8)*, 3460-3463.

(71) Monti, S.; Flamigni, L. *J. Phys. Chem.* **1986**, *90*, 1179-1184.

(72) Itoh, T.; McCreery, R. *J. Am. Chem. Soc.* **2002**, *124*, 10894-10902.

(73) Neta, P.; Levanon, H. *J. Phys. Chem.* **1977**, *81(24)*, 2288-2292.

(74) Meisel, D.; Neta, P. *J. Am. Chem. Soc.* **1975**, *97(18)*, 5198-5203.

(75) Solak, A. O.; Eichorst, L. R.; Clark, W. J.; McCreery, R. L. *Anal. Chem.* **2003**, 296-305.

(76) McCreery, R.; Dieringer, J.; Solak, A. O.; Snyder, B.; Nowak, A. M.; et. Al. *J. Am. Chem. Soc.* **2003**, *125*, 10748-10758.

(77) Solak, A. O.; Ranganathan, S.; Itoh, T.; McCreery, R. L. *Electrochemical and Solid-State Letters* **2002**, *5(8)*, E43-E46.